Politecnico di Torino

Master of Science in Energy and Nuclear Engineering

MASTER THESIS

Investigation into the water-equivalence of plastic materials in high-energy clinical proton beams

at Paul Scherrer Institute (PSI), Switzerland

Candidate:
Francesca Rosa Coniglio

Supervisors:
Prof. Gianni Coppa
Dr. Michele Togno (PSI)

Academic Year 2019/2020

Every step I take,
you'll be watching me...

Al mio papi, ovunque tu sia!

Acknowledgements

First of all I would like to thank Prof. Gianni Coppa (Politecnico di Torino) for supervising this thesis from Italy and for his personal support in the 'strange' period of Covid-19.
My huge thanks goes to my supervisor Michele Togno (PSI) for all his advices and for having helped me with this thesis. I'm infinitely grateful for his continuous support, patience and availability during these months.
I also would like to thank all the people that shared with me my experience abroad, in such a inspiring research environment and anyone which represented a precious guide for me.

Abstract

In the last decades, cancer treatment modalities have been moved towards high technological developments that indicate in the external beam radiotherapy the primacy of delivering a highly conformal radiation dose to the target volume. In this scenario, proton therapy at Paul Scherrer Institute (PSI) occupies a relevant role because it represents the first clinic capable of applying proton radiotherapy with Spot-Scanning technique by means of dedicated beam delivery system mounted over a Gantry, worldwide.
In this field, a study focused on determining how novel materials behave when traversed by protons has been carried out. The plastic candidates would be an extremely useful advancement in dosimetry for high energy proton beams, due to the lack of experimental or theoretical investigations on this aspect. The advantages of using plastic materials instead of water are better positioning accuracy, less time-consuming work flow in pre-treatment stages of the quality assurance and easier managing with respect to the reference material (water).
Hence, this thesis is aimed to explore the properties of several commercial plastic materials when irradiated by protons. The possibility of using them as substitute of water in patient specific verifications as well as in patient treatments as range compensator, or more in general in dosimetric applications will be investigated.
The explored water equivalence is assessed in terms of energy deposition, non-elastic nuclear interactions and scattering. The final goal is to identify the material, the combination of materials or the chemical composition of a new material, which is closely water-like.
Some experimental measurements have been performed at the Center for Proton Therapy (CPT) to calculate the Relative Proton Stopping Power (RPSP) for each candidate material. Results are then compared with theoretical expectations. The remaining investigations regarding fluence reduction and multiple Coulomb scattering have been explored on a theoretical level.
In conclusion, the analysis showed that a three-layers composed material is the best configuration to minimize the total discrepancy from water. The three layers are Polyethylene (PE), Plexiglass (PMMA) and Tecason PMT XRO. In this way, the energy deposition and inelastic nuclear interaction equivalences with water are always satisfied over the restrict clinical range (70 MeV - 200 MeV) whereas the scattering is estimated to be -40% with respect to water.

Keywords: Proton therapy, water-equivalent materials, proton dosimetry.

Contents

List of Figures

List of Tables

List of Abbreviations

MV	Mega Voltage
RBE	Relative Biological Effectiveness
SOBP	Spread-Out Bragg Peak
IMPT	Intensity Modulated Proton Therapy
PSI	Paul Scherrer Institute
CPT	Center for Proton Therapy
MCS	Multiple Coulomb Scattering
MP	Measuring Plane
WE	Water Equivalence
WET	Water Equivalent Thickness
CT	Computed Tomography
IDD	Integral Depth Dose
IC	Ionization Chamber
RPSP	Relative Proton Stopping Power
CCD	Charge-Coupled Device

Chapter 1

Introduction

Nowadays cancer represents the second most common cause of death after cardiovascular diseases on a global scale. Populations from economically developed nations are much more likely to suffer from cancer and the most hit countries are the United States, followed by Canada, Australia and Europe. [20]
The improvement in cancer survival reflects both the possibility of diagnosis at an early stage and the progresses in effective treatment techniques.
The proper treatment is selected taking into account several factors, e.g. the type and stage of the tumor, its location and the goal of the therapy. Possible treatment procedure can involve surgery, radiotherapy, chemotherapy or a combination of these. [6]
For instance, breast cancers are typically treated with a combination of surgery, radiotherapy and chemotherapy, while for prostate cancers radiotherapy alone is often sufficient.
Radiotherapy with external beams has the primary goal to deliver a certain amount of energy (dose) to the target tumor volume. At the same time, it is important to minimize the dose outside the target volume, to preserve the surrounding healthy tissue from damages induced by radiation.
In order to reach the highest level of precision and dose conformity, radiotherapy with external beams has seen a great technological development over the past decades.
Different types of radiation at different energies can be used to deliver the prescribed dose to the tumor, e.g. photons, electrons, protons and heavy ions. In recent years, the use of high-energy protons in radiotherapy has increased significantly, thanks to the intrinsic characteristics of this type of radiation and to the improvements in the modality of delivery. The physical properties of high-energy protons as results from their interactions with matters are detailed in Chapter 2, and a comparison with Megavoltage (MV) photons used in conventional radiotherapy is outlined in Paragraph 1.1.
The first who discovered the potential benefits of the proton adoption in the cancer cure was Wilson in 1946. Wilson demonstrated massive protons have got the capability to move in a nearly straight path inside the matter, causing the localized energy deposition at the end of the range in a very thin extended region (Bragg peak). [26]
The PSI proton therapy dedicated center gives an important impact to the success of proton therapy. It has the fundamental role to introduce for the first time proton therapy in

Switzerland and the institute is very well renowned thanks to the development of a new powerful application technique (named Spot Scanning) which will be explored more in details later on in this work. [9] For more information, a detailed summary of the history of proton therapy can be found in [10].

1.1 Proton therapy

Proton therapy allows outstanding ballistics to target the tumor area, while substantially decreasing the radiation delivered to the surrounding cells. This causes great advantages typical of the proton therapy over the conventional radiotherapy, basically due to the characteristic depth-dose distribution proper of protons.
Conventional radiotherapy involves photon beams of energies ranging from 4 to 18 MeV and is characterized by a depth-dose distribution shown in Fig. 1.1. The photon dose distribution firstly increases with the distance travelled by the photon inside the human body, up to a maximum and then declines exponentially because of their absorption.

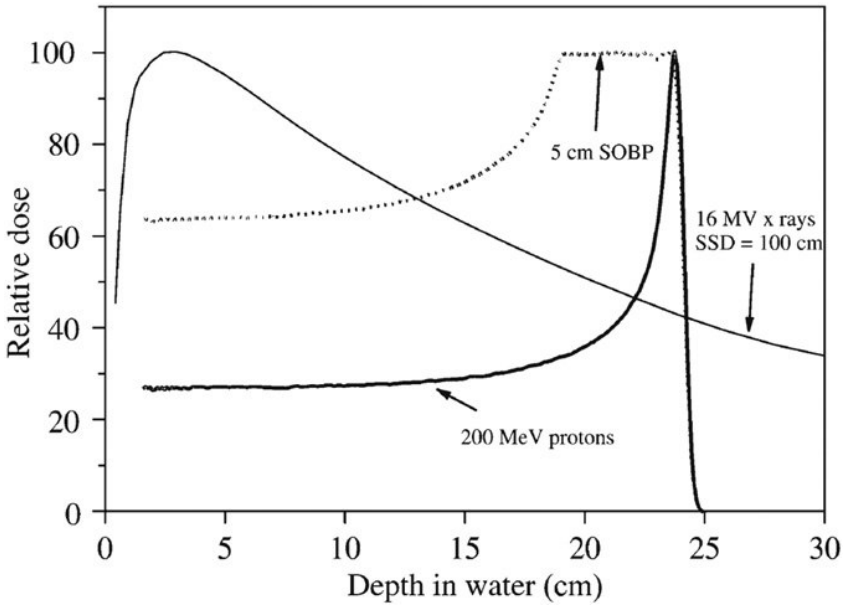

Figure 1.1: Normalized wrt peak depth-dose curves for a 200 MeV proton beam compared with a 16 MV X-ray beam. (Taken from:[16])

On the contrary, protons inside the matter are continuously slowed down, implying the deposited energy inside the human tissues to be inversely proportional to their velocity. Thus, the deposited energy reaches a maximum just before the protons come to a complete stop.
The characteristic proton depth-dose distribution reported in Fig. 1.1 is called *Bragg curve*

and the point where the dose delivered to the tissue reaches his local maximum is the well-known *Bragg peak*.
The depth and the width of the Bragg peak is a function of the beam energy and the material density in the beam path.
The reasons of the different behaviours protons vs photons are related to the intrinsic nature of the particles and their different energy loss processes. The energy deposition mechanisms of protons inside the matter will be deeply described in the Chapter 2 of this work.
As mentioned, one of the great advantages of protons with respect to photons is their well-defined range when they travel inside the human body.
Additional beneficial characteristics are:

- low energy loss at the entrance with the subsequent maximum energy release located at the end of the beam range (Bragg peak);
- very thin shaped lateral and distal doses.

Fig. 1.2, highlights the differences between the dose deposited in water (surrogated for human tissue) by clinical photon and proton beams. The reductions of the deposited dose in the regions which are proximal and distal to the target volume is the rationale for the use of high-energy protons in radiotherapy, specifically their use for treatment of deep-seated solid tumors.

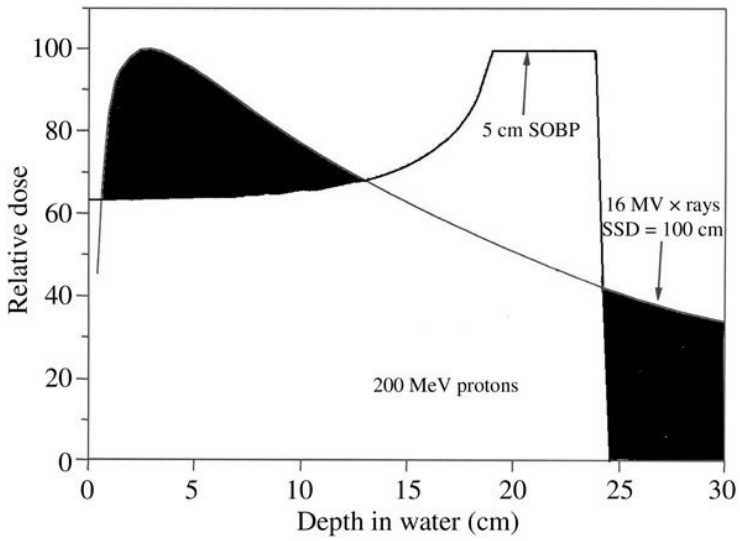

Figure 1.2: Comparison between protons and photons: in black the regions where photon dose drastically overcomes the proton dose. (Taken from:[10])

Another further benefit that lies beyond the use of protons instead of conventional photons is related to protons Relative Biological Effectiveness (RBE), estimated to be 1.1.

This means that protons are capable to be biological effective 10% more than photons. [16]

Furthermore, as it concerns the goals of the proton therapy it should be mentioned the sharper lateral penumbra with respect to conventional photons. If compared with the 'conventional' irradiation, the sharper protons' penumbra is advantageous because the distance from full intensity to zero intensity is smaller. [15] This is not true a priori for protons in every treatment conditions (e.g. especially when high penetrations need to be reached, it is no longer valid).

After having localized the tumor region inside the human body the proton therapy aims to irradiate uniformly the target volume. To reach this the combination of suitable proton beams of different energy content seems to be the best mean. Through an accurate selection of protons energy (range), the resulting superposition is capable to generate the Spread-Out Bragg Peak (SOBP): an almost flat dose region localized in the desired place inside the human body (Fig. 1.3). Thus, with an appropriate energy choice the coincidence with the tumor area defines the strength and the effectiveness of the proton beams applied irradiation procedure.

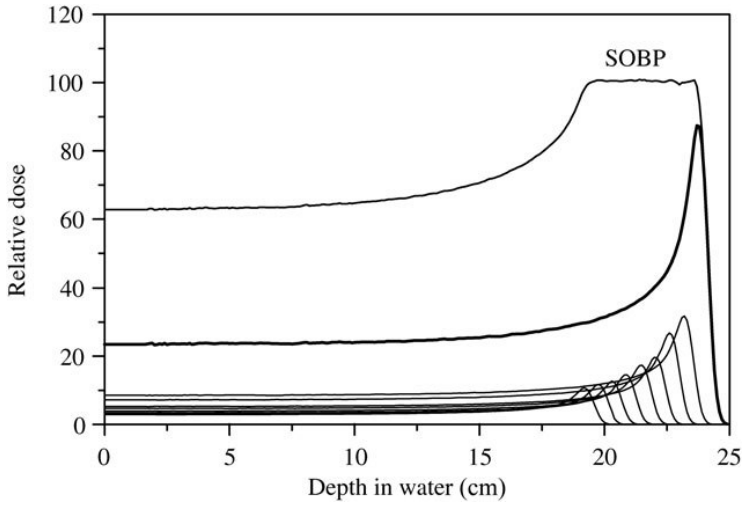

Figure 1.3: Spread-Out Bragg Peak formed by the superposition of apposite weighted proton beams of different ranges. (Taken from:[10])

Again by comparing protons and photons, Fig. 1.4 shows that protons adoption allows to spare surrounding healthy tissues to reach a uniform irradiation of the only target volume, releasing much less dose to non-target regions than photons. Healthy tissue located upstream and downstream of the tumour is less affected by the irradiation.

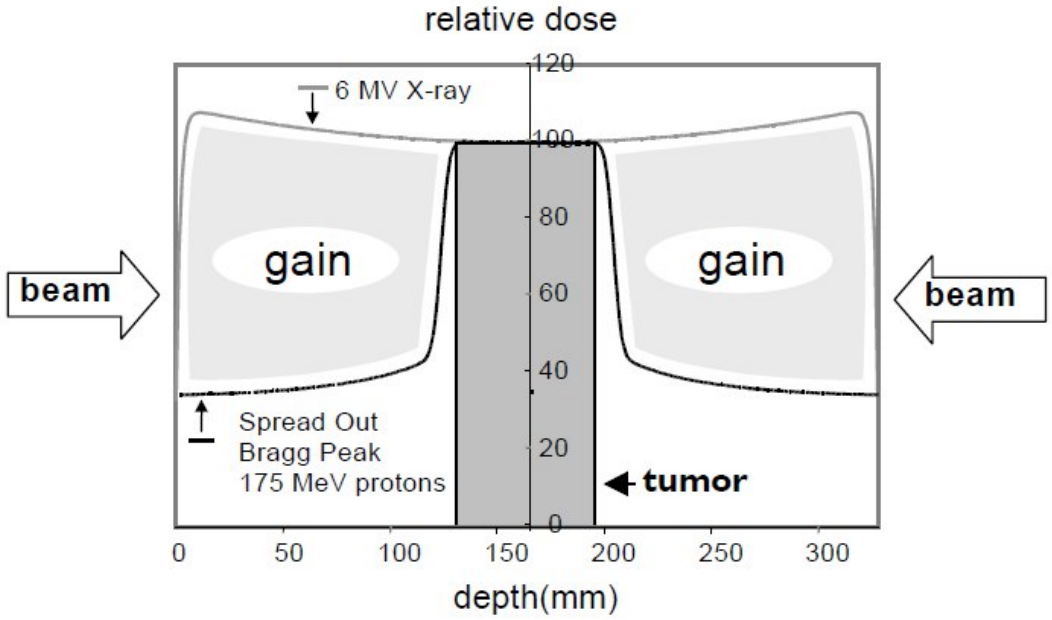

Figure 1.4: Comparison between the two competitive irradiation modes: X-rays and protons. (Taken from: [14])

1.2 Proton therapy facility

A proton therapy facility is a complex apparatus that consists of 3 major sub-systems: an accelerator, a beam transport system and a treatment-delivery system.
Protons originated from the ionization of hydrogen atoms, are accelerated to therapeutic energies typically ranging from 70 to 250 MeV corresponding to penetration ranges in water of 26 cm and 38 cm, respectively. [10] The possibility to scan through a range of energies allows to reach tumors possibly located at different depth inside the human body.

1.2.1 Proton accelerators

Currently, clinical proton therapy facilities are equipped with compact accelerators that can be either a cyclotron or a synchrotron. Other solutions such as linear accelerators ([5]) or laser-driven accelerators ([13]) are in a research phase but still far from their possible clinical implementation.

In a cyclotron (Fig. 1.5 (a)), the particles are accelerated when they pass through the gap between the two pieces of a big magnet, shaped as a 'D' (Dee). Its accelerating working principle can be elementarily explained as follows: a slow neo-ionized particle passes more than once through the empty space left between the two electrodes, increasing each time they cross the velocity content and continuing its semi-circular path with an increasing

radius. The final particle trajectory is a spiral. This procedure is repeated until the desired energy content of the particle has been reached. On this basis, cyclotrons are capable to produce a continuous stream of protons, representing the more compact and with the higher beam intensity acceleration technique.

On the other hand, synchrotrons (Fig. 1.5 (b)) act keeping the batch of protons at a fixed orbit until the end of the acceleration cycle. Once the batch has reached the required energy, it is inserted in the beam line. The positive aspects of synchrotrons are related to the greater energy flexibility, smaller energy spread and lower power consumption.[16] On the contrary, their worst drawback is that they work in a pulsed way (non-continuous beam acceleration as the cyclotron class).

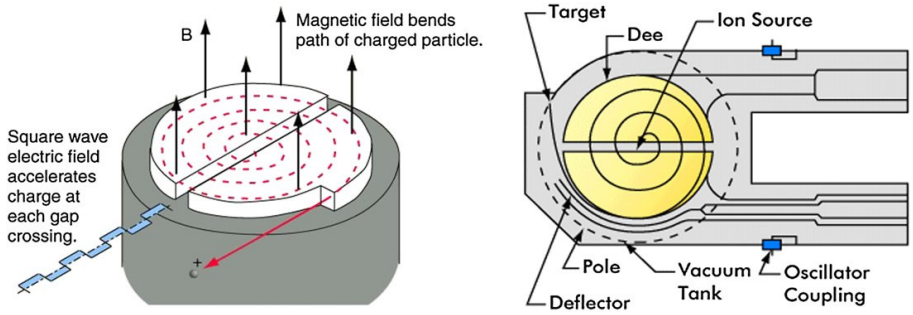

(a) Cyclotron

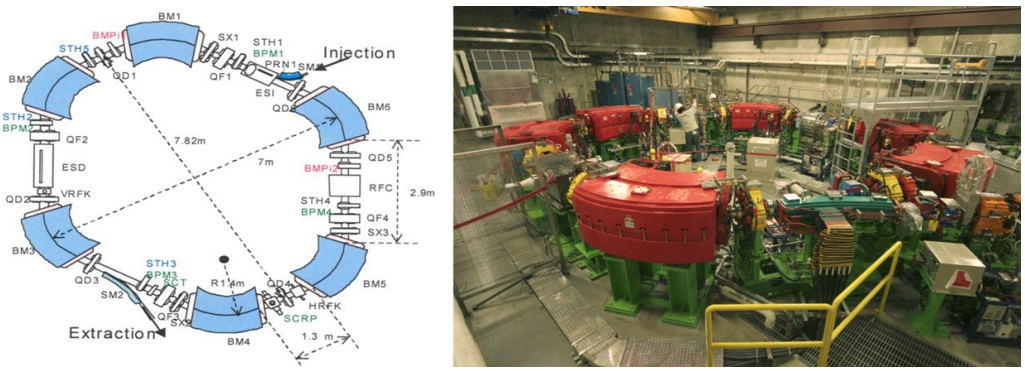

(b) Synchrotron

Figure 1.5: (a): Acceleration process of protons inside a Cyclotron: a fixed magnetic field guides the proton trajectory and everytime they cross the gaps between the two pieces of the Dee magnet, they are accelerated by a square wave electric field. (Taken from:[16]); (b): MD Anderson Proton Therapy Center Synchrotron layout: Each banch of protons is accelerated through an alternating applied electric field, constrained to follow a fixed circular path by the mean of an increasing magnetic field. Only once each banch has got the desired energy content, it is extracted. (Taken from:[16]).

1.2.2 Beam-transport system

After acceleration, protons are injected into the beamline to reach the treatment room. The vacuum condition is strictly guaranteed over the entire beamline length because it is very important to avoid proton-air interactions.
The beamline is made up of several magnets that force the travelling particles to move only in in the desired path. [14] The composition of dipole and quadrupole magnets, vacuum chambers and diagnostic instrumentation gives rise to the so-called *beamline*. [27]

1.2.3 Treatment-delivery system

The treatment delivery system is a complex system that consists of a rotational gantry, a beam nozzle and a patient positioning system. [10]
The delivery system allows for a high conformity of the delivered dose distribution to the target volume.
In proton therapy, two different approaches are typically adopted for beam delivery: the passive beam-delivery technique and the active one (Fig. 1.6).
In the passive technique, a range modulation wheel and scatterers are placed at the exit of

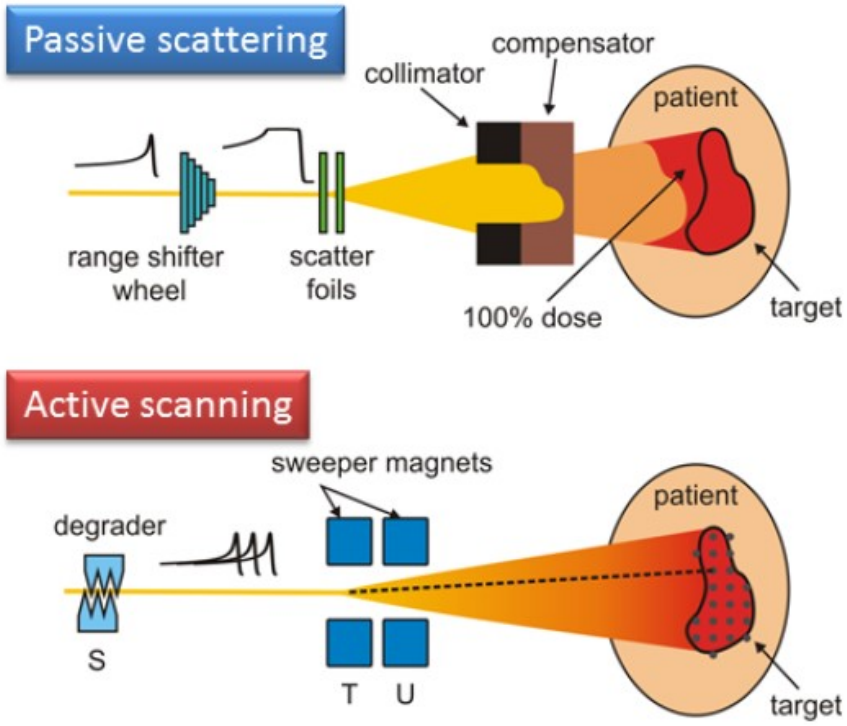

Figure 1.6: Proton therapy treatment-delivery systems: Passive scattering and Active scanning techniques. (Taken from: [28])

the beam from the beamline to degrade the primary proton beam and achieve the wanted spatially uniform dose distribution. [10] The scatterers are not alone to pursue the goal: the adaption of the beam to the target volume is achieved, in addition, by the means of proper collimators and compensators. [4]
A detailed description of the passive methods developed in the past years can be easily found in the work of Ludewigt, Chu and Renner [27].
In active beam scanning the pencil proton beam is magnetically steered in two dimensions across the target volume (Fig. 1.7). The dose conformity in the third dimension is reached by varying the beam energy upstream the delivery system. With active scanning,

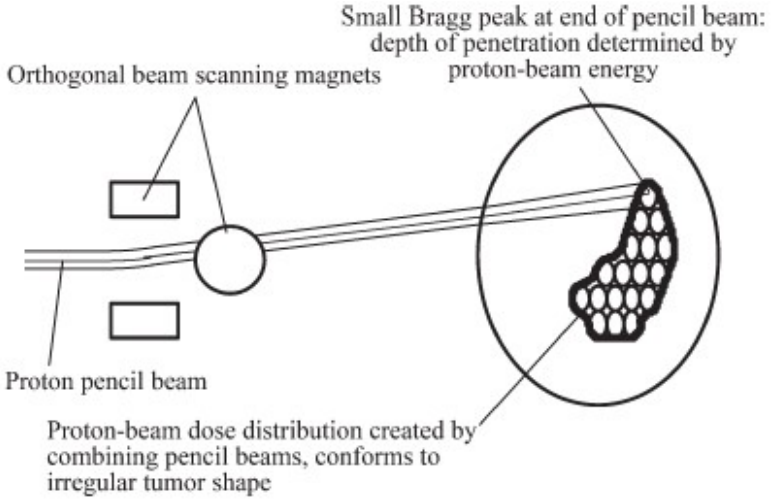

Figure 1.7: Schematic diagram of the active scanning: the pencil beam can perform the spot scanning of the target volume. (Taken from: [10])

the treatment field is delivered spot by spot. Each spot is defined by a point in the beam coordinate system, a beam energy and a dose value. Intensity Modulated Proton Therapy (IMPT) is based on actively scanned beams that combined together generate a uniform dose coverage of the tumor and reduce the dose to healthy tissue and critical structures.
Additional benefits of active scanning are, for instance, a reduced undesired dose to patient due to secondary neutrons and a simplified treatment workflow because of the absence of collimators and compensators. A weakness point of this method is its sensitivity to the organ motion during the dose delivery, revealing especially in moving targets treatment.
Active scanning or pencil beam scanning is the most used technique, spread nowadays among proton therapy centers.

1.3 Proton therapy at PSI

Patient treatment by means of clinical proton beams at Paul Scherrer Institute (PSI) is well established since more than 30 years making the PSI one of the leading centers for

proton therapy worldwide. In total over 1700 patients with deep-seated tumors have been treated at PSI from 1996 to end of 2019.
The spot-scanning technique described in Paragraph 1.2.3 has been developed at PSI and used since 1995 to treat patients. [9] [18]
A short overview on the historical analysis about the facility development at the PSI proton dedicated center is done to give an idea on the pioneering work of the institute in developing the technology of pencil beam scanning with protons on a gantry.

1.3.1 Gantry 1

The first attempt of the scanning gantry rises in the 90's with Gantry 1 at PSI center. [8] It represents one of the branches for the final applications of the PSI proton beam accelerated by COMET accelerator.
For the first time, Gantry 1 (Fig. 1.8) distinguishes for being the first application of pencil beam scanning. The beam scanning reguarded only one direction. In the other direction the shaping of the beam with the target was achieved by moving the patient couch.
Gantry 1 provides the basis for successive high technologically development in the mechanical layout definition of beam delivery systems.

(a) Gantry 1

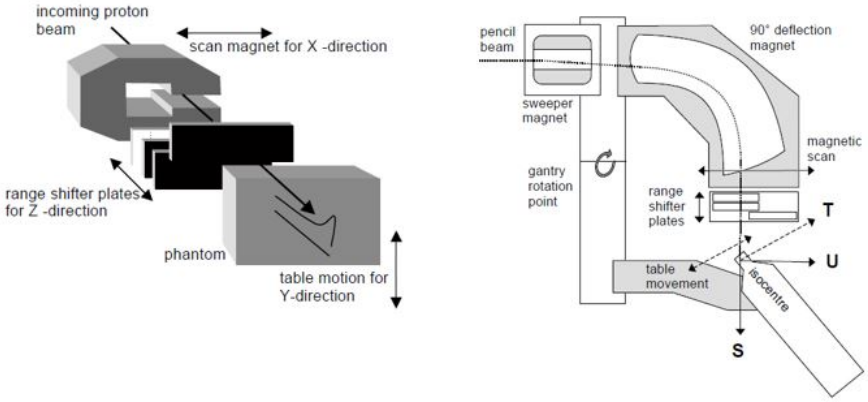

(b) Gantry 1 scheme

Figure 1.8: Gantry 1: first PSI system to treat patients with pencil beam scanning. (Taken from: [22])

1.3.2 Gantry 2

To overcome Gantry 1 limitations, a new concept of rotating gantry rises and the new Gantry 2 has been developed as a part of the PROSCAN project to expand the overall PSI facility. [8]

Gantry 2 aims to better performance: it represents a very compact and robust structure of the beam delivery system with a 210° rotation possibility around the patient.
This time, the beam scanning has been performed in both directions and above a maximum area of $12 * 20\ cm^2$ around the isocenter.

Figure 1.9: Gantry 2 treatment room: patient table and nozzle. (Adapted from: [8])

1.3.3 Gantry 3 and Optis 2

A further improvement of the irradiation is then achieved with the new PSI's treatment unit Gantry 3. It is in operation since July 2008. Gantry 3 is collocated in the technological development path as a Gantry 2 follower, in the sense that its performance in terms of large irradiation fields delivery, fast energy changes and high irradiation dose rates is enhanced. All these aspects keep short the time exposure to radiations of the patients.
As Gantry 2, the beam delivery system is mounted over the rotating structure, capable to reach 360° rotation amplitude. The area that can be covered at the isocenter is enlarged, up to a maximum extension of $30*40\ cm^2$. This fact makes it suitable for treating extended tumors such as cranio-spinal ones.

In the end, a brief mention is given to Optis 2: another application of the PSI clinical accelerated proton beam.
Optis 2 represents the ocular tumors dedicated facility of the PSI institute. It operates starting from 2010 and around 1800 patients have been treated with this facility.
In Optis 2 the beam does not rotate over the gantry but is fixed horizontally and is disposed in front of the patient.

The delivery systems can account on a double scatterers phases: range shifter and 9 scatters foils (each of them dedicated to apposite ranges) are used to pursue the beam shaping objective.
The overall representation of the actual PSI therapy facility roughly described above is shown in Fig.1.10.

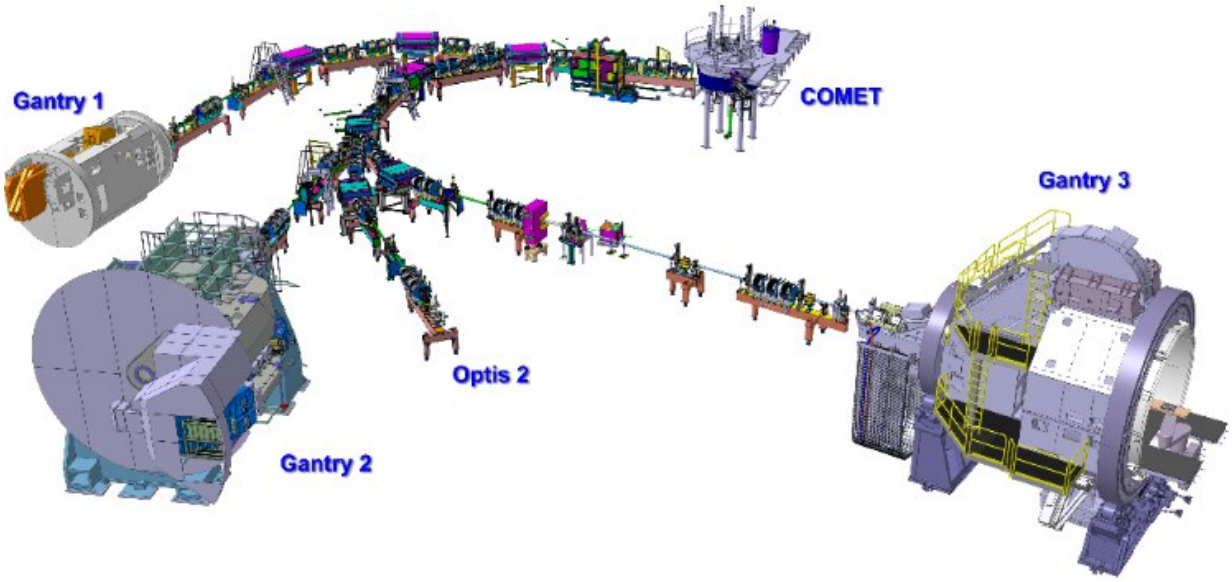

Figure 1.10: The layout of the proton therapy facility at PSI. The system comprises the cyclotron COMET, the Gantry 1, 2 and 3 and Optis 2 with a schematic representation of the entire beam line. (Taken from: [2])

1.4 Aim of the thesis

This project is dedicated to investigate on properties of plastic materials that can be used for dosimetric applications in proton therapy. Plastic materials offer advantages for dosimetry over the reference material, water, such as a more convenient experimental setup and measurement workflow and a better positioning accuracy.
However, protons do interact differently with plastic and water because of the different chemical compositions. The main interactions that clinical protons (energy range 70 – 230 MeV) undergo when travelling in a medium are described in Chapter 2.

At present, most of the water-equivalent plastics -that are commercially available- have been designed for dosimetric applications in X-ray beams (especially in the Mega Voltage energy range). Such materials have physical properties to match the absorption of high energy photons in water. For convenience, these commercial plastics are used in proton

therapy as well.
At present, there are only a few theoretical and experimental studies on novel materials dedicated to dosimetry in proton therapy. [7]

In this work, commercial materials have been evaluated and compared to water in terms of energy deposition (Chapter 3), fluence reduction and elastic scattering (Chapter 4) when traversed by high-energy protons.
The proton energy deposition in the different materials has been investigated both experimentally and theoretically. The selected plastic materials are listed in Tab. 1.1. Among them, some of the most commonly used plastics in radiotherapy applications: Plexiglass (PMMA) and Solid Water (RW3).
The weight fraction of the filller of Barium sulfate (reported in Tab.1.1) inside the candidate material Tecason PMT XRO has been theoretically estimated as:

$$w_{BaSO_4} = \frac{\rho_{BaSO_4} V_{filler}}{M_{tot}} \tag{1.1}$$

where $M_{tot} = \rho_{TECASONPMTXRO} V_{TECASONPMTXRO}$ represents the total mass of the including filler material. The filler volume V_{filler} has been derived, once knowing all the material densities and sample volumes, applying the following equation:

$$\rho_{TECASONPMTXRO} = \frac{V_{filler}}{V_{TECASONPMTXRO}} \rho_{BaSO_4} + \frac{V_{TECASONPMT}}{V_{TECASONPMTXRO}} \rho_{TECASONPMT} \tag{1.2}$$

Table 1.1: Candidate materials.

Material	Acronym	Commercial name	Chemical formula	Material density
Polystyrene	PS	-	C_8H_8	1.060 g/cm^3
Solid Water	RW3	-	98% PS + 2% TiO_2	1.066 g/cm^3
High Molecular Weight Polyethylene	PEHMW	-	C_2H_4	0.95 g/cm^3
Polymethylmethacralate	PMMA	Plexiglass	$C_5H_8O_2$	1.18 g/cm^3
Polyoxymethylene	POM	-	CH_2O	1.41 g/cm^3
TECASON P MT	PPSU MT	Radel R	$C_{39}H_{26}O_8S_2$	1.31 g/cm^3
TECASON P MT XRO	PPSU MT XRO	-	78.02% TECASON P MT + 21.98% $BaSO_4$	1.36 g/cm^3
TECAPEEK MT	PEEK MT	Victrex-PEEK	$C_{19}H_{12}O_3$	1.31 g/cm^3
Tecatec PEEK MT CW 50	PEEK MT CW 50	-	-	1.49 g/cm^3

At PSI, and possibly in other proton therapy clinics, a plastic material which is equivalent to water would be extremely useful specifically as:

- substitute of water during patient specific treatment verification.
  Currently, each treatment plan is re-calculated in water and delivered to a water phantom prior to the effective start of the treatment, as part of the quality assurance plan of the clinic. The verification of the treatment dose in water requires a delicate system and a time-consuming workflow, which could be optimized by replacing water with slabs of plastic material.

- pre-absorber for cranio-spinal treatments.
  At the Center for Proton Therapy (CPT) Gantry 3, the large field of irradiation ($30 * 40\ cm^2$) allows for treatment of large-volume diseases such as cranio-spinal tumors. The patient lies on the treatment couch in supine position, and it is irradiated with the proton beam coming from the bottom and passing through the table to avoid unnecessary dose to other organs. Tumors which are confined in the spine are quite close to skin surface, therefore the energy of the impinging beam has to be degraded to reach the best conformity to the tumor. To degrade the protons energy, a pre-absorber is inserted in the beam path, typically in the nozzle of the delivery system. To reduce the broadening of the beam due to scattering in the material (Chapter 4) it would be desirable to have a pre-absorber as close as possible to the patient, ideally sandwiched between the patient and the treatment table. This solution would also require the pre-absorber to be included in the treatment planning and therefore characterized in terms of energy loss.

Chapter 2

Interaction of protons with matter

Protons with a defined energy E will interact with the atoms and the molecules of matter that they penetrate.
Depending on their energy, protons undergo different type of interactions, resulting either in a change of their trajectory or in a change of their kinetic energy. In this chapter, the main interaction mechanisms for protons with clinical kinetic energies, i.e. $E < 250MeV$, are described. Specifically, three aspects will be discussed:

- inelastic collisions with atomic electrons;
- inelastic collisions with atomic nuclei;
- elastic collisions with atomic nuclei.

The effects of these interactions, if summed up, result in the Bragg curve or protons depth-dose distribution (already shown in the introductory chapter).

2.1 Inelastic collisions with atomic electrons

Protons with kinetic energy up to 250 MeV can cause the excitation or the ionization of the atoms of the stopping medium.
To quantify the energy loss (by ionization and excitation) of primary protons the concept of *stopping power* S is used.
The stopping power S is the rate at which a single charged particle loses its kinetic energy and is equal to the loss of energy dE per unit path length dx:

$$S = -\frac{dE}{dx} \qquad \left[\frac{MeV}{cm}\right] \tag{2.1}$$

The total stopping power S is made up of *electronic* stopping power (due to inelastic collision with bound electrons) and *nuclear* stopping power (caused by elastic Coulomb

collision with nuclei). For proton energies higher than 20 KeV the nuclear stopping power can be ignored, therefore the electronic stopping power is the only to consider in the therapeutic regime. Its mathematical expression is described by the *Bethe-Bloch* formula, which gives the mean energy loss per proton:

$$\frac{1}{\rho}S = -\frac{1}{\rho}\frac{dE}{dx} = \frac{K}{\beta^2}z^2\left(\frac{Z}{A}\right)\left[F(\beta) - \ln(I) - \frac{C}{Z} - \frac{\delta}{2} + zL_1(\beta) + z^2L_2(\beta)\right] \tag{2.2}$$

with

$$K = 4\pi r_e^2 m_e c^2 N_A = 0.307075 MeV cm^2 g^{-1} \tag{2.3}$$

where $r_e = e/4\pi\epsilon_0 m_e c^2$ is the classical electron radius, e the electronic charge,ϵ_0 the permittivity of the vacuum, m_e the electron mass, c the speed of light in vacuum, N_A the Avogadro's number, β is the particle velocity in units of the velocity of light and z is the atomic number of the projectile (proton), M is the proton mass, E the proton kinetic energy, Z, A and I are the atomic number, the relative atomic mass of the target atom and the mean excitation energy (also called mean ionization potential) of the stopping material.

The Bethe-Bloch formula accounts for different phenomena, which are going to be explained more.
The details regarding the energy loss process are hidden in the *energy term* $F(\beta)$ of the equation 2.1, that is, in turn, expressed by

$$F(\beta) = \frac{1}{2}\ln\left(\frac{2m_e c^2\beta^2 E_{max}}{1-\beta^2}\right) - \beta^2 \tag{2.4}$$

in which:

$$E_{max} = \frac{2m_e c^2(\beta\gamma)^2}{1 + 2\gamma\frac{m_e}{M} + \left(\frac{m_e}{M}\right)^2} \tag{2.5}$$

with

$$(\beta\gamma)^2 = \left(\frac{E}{Mc^2}\right)^2 + \frac{2E}{Mc^2} \tag{2.6}$$

and

$$\gamma = 1 + \frac{E}{Mc^2} \tag{2.7}$$

Some correction factors need to be applied to completely describe the interaction mechanism between protons and matter.

The *shell correction term* $\frac{C}{Z}$ is related to the fact that for low projectile velocity the inner-shell electrons do not participate in the interaction. It doesn't play a relevant role in the Bethe-Bloch formulation because its contribute is usually already taken into account by choosing energy dependent mean excitation potential I.
The *density correction term* $\frac{\delta}{2}$ deals with the medium polarization that occurs when the projectile (proton) transverses the matter. The phenomenological analysis of what physically happens reveals a reduction of the projectile energy lost because of the perturbation of the electron field. The entity of this effect is strictly related to the density of the stopping material, hence its denomination (density correction term). For proton energies below 500 MeV the influence of the density correction on the final evaluation is so lower that it can be completely neglected.
The last two terms in the Bethe-Bloch formula L_1 and L_2 represent respectively the *Barkas correction* and the *Block correction*. The *Barkas correction* L_1 accounts for the slightly different stopping power between positive and negative charged particles. This reveals a smaller stopping capability of negative charged particles when compared with the positive ones.
The *Bloch correction* L_2 becomes necessary only with relativistic energies.

The quantity $\frac{S}{\rho} = -\frac{1}{\rho}\frac{dE}{dx}$,whose mathematical expression is given by the Bethe-Bloch formulation, defined as the stopping power divided by the density of the stopping material is called the *mass stopping power* and is expressed in $\left[\frac{MeV}{g/cm^2}\right]$.

2.1.1 The Range

A fundamental strictly energy-related quantity is represented by the *Range R*.
The Range R quantifies the average distance travelled inside the medium by the charged protons with energy E_0 until they reach a null kinetic energy.
Assuming the continuous loss of energy along the protons tracks, the Range (also called Continuous Slowing Down Approximation Range R_{csda}) represents the average path length of protons inside the matter.
Knowing the initial protons kinetic energy E_0 and following the protons energy loss mechanism inside the matter until the point where the energy is nearly zero it is possible to obtain a rough estimation of the Range. It can be calculated by integrating the reciprocal of the stopping power with respect to energy:

$$R_{csda}(E_0) = \int_{E_f}^{E_0} \left(-\frac{1}{\rho}\frac{dE}{dx}\right)^{-1} dE \qquad \left[\frac{g}{cm^2}\right] \tag{2.8}$$

Immediately follows that:

$$R_{csda}(E_0) = R_{csda}(E_f) + \int_{E_f}^{E_0} \left(-\frac{1}{\rho}\frac{dE}{dx}\right)^{-1} dE \tag{2.9}$$

Usually in the practice, in order to associate to each proton energy content value at the inlet of the medium E_0 the correspondent range value $R_{csda}(E_0)$, it is implicitly set the path length $R_{csda}(E_f)$ equal to zero at a final energy E_f of 10 eV.

Furthermore, if the mean travelled distance is projected along a straight line parallel to the original direction of motion of the charged particle entering the medium, the *Projected Range* R_{proj} concept is derived:

$$R_{proj}(E_0) = \int_{E_f}^{E_0} \cos(\chi) \left(-\frac{1}{\rho} \frac{dE}{dx} \right)^{-1} dE \tag{2.10}$$

where $\cos(\chi)$ is the mean value of the cosine of the scattering angle.

2.2 Elastic collisions with atomic nuclei

When a proton comes close to a nucleus, the repulsive elastic Coulomb interaction acts such that the projectile modifies its straight-line trajectory as sketched in Fig.2.1.

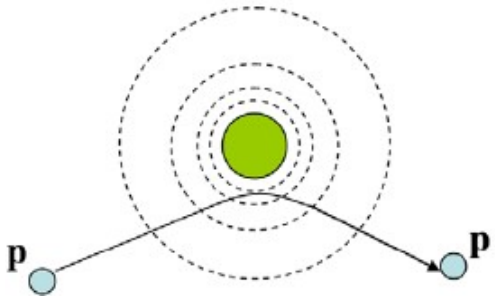

Figure 2.1: Scattering phenomenon between the incoming proton and the nucleus: schematic representation of the deflected proton trajectory by means of repulsive Coulomb forces. (Adapted from: [17])

Since the deflection resulting from a single nucleus-proton interaction is quite small, the modified proton trajectory is in reality the results of many scattering events, called *Multiple Coulomb Scattering (MCS)*.
To analyze from the analytical point of view the proton deflection caused by multiple collisions with atomic nuclei, the statistical approach must be adopted. The MCS theory is the mean used to predict the probability $P(\theta)$ for a proton to be scattered by a net angle of deflection θ.
Theoretical MCS calculations are quite complex and different theories (*Rutherford theory* for single scattering event and *Molière's theory* or *Highland formula* related to MCS) have been proposed to asses probabilistically the scattering phenomenon.

A good approximation of the angular distribution resulting from MCS is given by a Gaussian function (see Fig.2.2):

$$P(\theta) = \frac{2\theta}{\theta^2} \exp\left(\frac{-\theta^2}{\theta^2}\right) d\theta \tag{2.11}$$

where $(\theta^2)^{1/2}$ is the root mean square scattering angle projected on a plane or the width of the Gaussian distribution.

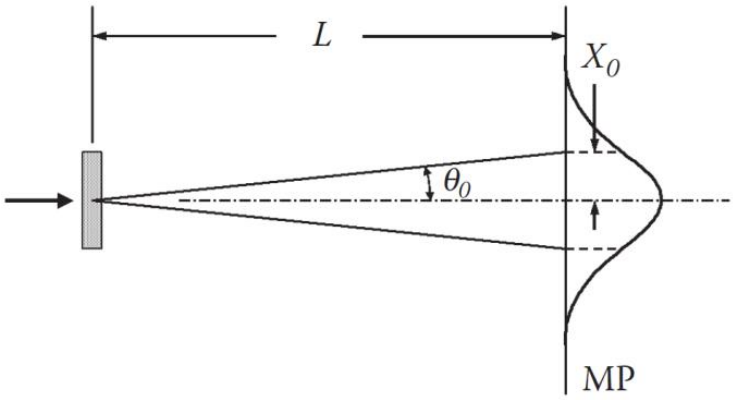

Figure 2.2: Gaussian distribution of the mean squared scattering angle θ_0 projected on a Measuring Plane (MP).

The characteristic width is related to the proton energy content and to the target characteristics. The *Highland's formula* with Lynch and Dahl constants, based on a fitting of the Molière theory gives an estimation of this parameter of interest:

$$\theta_0 = \frac{13.6}{p\beta c} z \left(\frac{r}{X_0}\right)^{1/2} \left[1 + 0.038 ln\left(\frac{r}{X_0}\right)\right] \qquad [rad] \tag{2.12}$$

in which X_0 is the radiation length, r the mass thickness of the scatterer and $p\beta c$ the kinematic factor.
The scattering phenomenon is deeply related to the properties of the absorbing mean and it is directly proportional to the ratio between the atomic number Z and the square root of the atomic mass A of the mean under studied.

2.3 Inelastic collisions with atomic nuclei

Even if less probable, when the proton interacts with atomic nuclei, it can give rise to a nuclear reaction called *inelastic nuclear reaction* in which the nucleus is irreversible transformed (see Fig. 2.3).

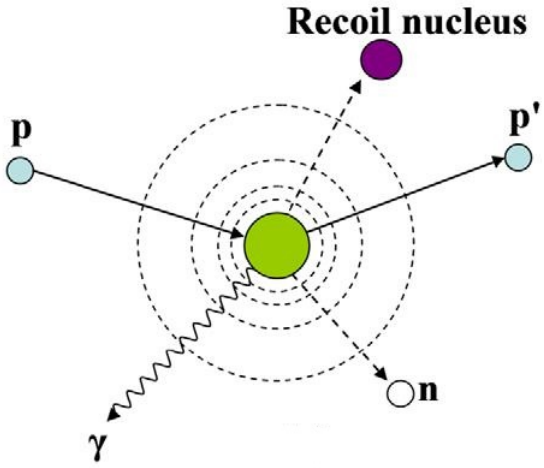

Figure 2.3: Non-elastic nuclear interaction between the incoming proton and the nucleus: generation of secondary particles. (Adapted from: [17])

The adjective *inelastic* stands for the kinetic energy is not preserved between the two scenarios before and after the interaction. The target nucleus may undergo breakup and a particle transfer reaction may occur.
These inelastic collisions cause, in turn, a reduction of the proton flux in depth as a consequence of the removal of part of the primary protons from the beam. At the same time, secondary particle generated from the proton-nuclei interaction (e.g. secondary protons, alpha particle, heavier ions, gamma rays and neutrons) contribute to the locally deposited dose and to the dose deposited outside the primary proton beam.
The condition that must be verified in order to have inelastic nuclear reaction is that the energy content of the impacting proton must overcome the nucleus Coulomb barrier. This is reflected on the energy threshold of the total non-elastic cross-section for proton-induced nuclear reactions, whose value is null until a certain energy.
The probability that a proton undergo a inelastic collision event is given by:

$$P = \sigma * \phi \tag{2.13}$$

where σ is the total nuclear cross section and ϕ the particle fluence. ϕ represents, in turn, the number of particles dN crossing the infinitesimal surface of area dA:

$$\phi = \frac{dN}{dA} \qquad \left[m^{-2}\right] \tag{2.14}$$

The dedicated unit used to express the cross-section values is the *barn* that obeys to the equivalence: $1\ barn = 1 * 10^{-28}\ m^2$.
It is important to underline the energy dependence of the nuclear cross-sections, which is reversed in all the successive calculations or manipulations that involve the need of the cross-section parameter as an input.

If the incident particles are protons, the probability to have a proton induced nuclear interaction over the entire travelled path inside the matter by protons with an energy content E_0 is derived from a particle balance and it assumes the following expression:

$$P_{nuc}(E_0) = 1 - exp\left(-N_A \int_0^{R_{csda}(E_0)} \rho \left(\frac{\sigma}{A}\right) dx\right) \tag{2.15}$$

If an appropriate change of variable is done, the inelastic nuclear interaction probability can be expressed in fuction of the energy and not over the path:

$$P_{nuc}(E_0) = 1 - exp\left(-N_A \int_{E_f}^{E_0} \frac{1}{\frac{1}{\rho}\frac{dE}{dx}} \left(\frac{\sigma}{A}\right) dE\right) \tag{2.16}$$

where E_f is the final energy at which the incoming proton is assumed to be stopped and its value is 10 eV.
In the previous equations, N_A represents the Avogadro's constant and all the other quantities that appear have been already defined above.

In the practice, it is more usefull having a rough estimation of the probability to have an inelastic nuclear probability between two energy values E_1 and E_2, leading to:

$$P_{nuc}(E_1 \rightarrow E_2) = 1 - \frac{1 - P_{nuc}(E_1)}{1 - P_{nuc}(E_2)} \tag{2.17}$$

The two energy values limiting the energy interval over which the integration is performed respect the following inequality: $E_1 > E_2$.

2.4 Medium equivalence

In general, the equivalence of two materials in terms of interactions with protons can be separated into three different aspects, specifically:

- equivalence in terms of energy loss;
- equivalence in terms of nuclear interaction probability;
- equivalence in terms of scattering;

Figure 2.4 schematically illustrates the concept of medium equivalence and helps to understand the relevant parameters that must be compared between two different media in order to conclude about their equivalence.

The equivalence in terms of energy loss is usually the most important aspect, as a direct consequence of the fact that the energy deposition is the most relevant phenomenon during

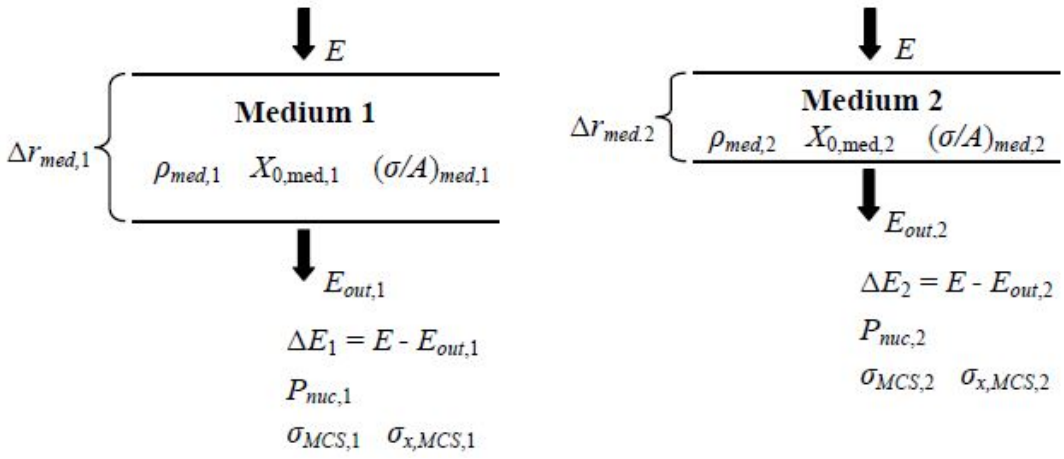

Taken from [21].

Figure 2.4: Energy loss equivalence is assessed if the protons, transversing the media, lose the same energy amount ($\Delta E_1 = \Delta E_2$); nuclear interaction equivalence is verified if the media have the same total nuclear interaction probability ($P_{nuc,1} = P_{nuc,2}$) and the scattering equivalence is satisfied if both the characteristic scattering angles $\sigma_{MCS,i}$ and the characteristic widths $\sigma_{x,MCS,i}$ of the beam are the same.

the passage of protons through matter.
The equivalence $\Delta E_1 = \Delta E_2$ for Medium 1 and Medium 2 is satisfied only for a specific combination of mass thicknesses $\Delta r_{med,1}$ and $\Delta r_{med,2}$. The mass thicknesses for which $\Delta E_1 = \Delta E_2$ are related by the following equation:

$$\left(\frac{\Delta r_{med,1}}{\Delta r_{med,2}}\right)_{\Delta_E} = \frac{\int_{E-\Delta E}^{E} \left(-\frac{1}{\rho}\frac{dE}{dx}\right)^{-1}_{med1} dE}{\int_{E-\Delta E}^{E} \left(-\frac{1}{\rho}\frac{dE}{dx}\right)^{-1}_{med2} dE} = \frac{R_{csda,med1}(E) - R_{csda,med1}(E-\Delta E)}{R_{csda,med2}(E) - R_{csda,med2}(E-\Delta E)} \quad (2.18)$$

where $R_{csda,med1}(E)$ is the range in continuous slowing down approximation as introduced in paragraph 2.2.1, for the medium 1 at a given energy E.

When Δr_{med} is small, ΔE is also small and Eq. 2.18 can be written as the ratio of mass stopping powers at the energy E:

$$\lim_{\Delta E \to 0} \left(\frac{\Delta r_{med,1}}{\Delta r_{med,2}}\right)_{\Delta_E} = \frac{\left(-\frac{1}{\rho}\frac{dE}{dx}\right)_{med,2}}{\left(-\frac{1}{\rho}\frac{dE}{dx}\right)_{med,1}} \quad (2.19)$$

To satisfy the equivalence in terms of nuclear interactions, the total probability for inelastic collisions in $\Delta r_{med,1}$ must be equal to the total probability for inelastic collisions in $\Delta r_{med,2}$. This can be expressed as follows:

$$\int_{R_{csda,med,1(E)-\Delta r_{med,1}}}^{R_{csda,med,1(E)}} (\sigma/A)_{med,1}\ dr = \int_{R_{csda,med,2(E)-\Delta r_{med,2}}}^{R_{csda,med,2(E)}} (\sigma/A)_{med,2}\ dr \tag{2.20}$$

where $(\sigma/\mathrm{A})_{med}$ is the ratio between the total inelastic cross section and the atomic weight of the medium.

Lastly, the equivalence in terms of scattering is satisfied when $\Delta r_{med,1}$ and $\Delta r_{med,2}$ produce the same scattering angle distribution and the same scattering spatial distribution. This is true when the following equations are satisfied:

$$\sigma^2_{x,MCS,1}(\Delta r_{med,1}) = \sigma^2_{x,MCS,2}(\Delta r_{med,2}) \tag{2.21}$$

$$\begin{aligned}&\left[1 + 0.0038 \ln\left(\frac{\Delta r_{med,1}}{X_{0,med,1}}\right)\right]^2 \frac{1}{X_{0,med,1}\rho^2_{med,1}} \int_0^{\Delta r_{med,1}} \left(\frac{1}{p\beta c}\right)^2_{med,1} (\Delta r_{med,1} - r)^2\ dr = \\ &= \left[1 + 0.0038 \ln\left(\frac{\Delta r_{med,2}}{X_{0,med,2}}\right)\right]^2 \frac{1}{X_{0,med,2}\rho^2_{med,2}} \int_0^{\Delta r_{med,2}} \left(\frac{1}{p\beta c}\right)^2_{med,2} (\Delta r_{med,2} - r)^2\ dr\end{aligned} \tag{2.22}$$

in which $X_{0,med}$ is the radiation length, a property of the medium related to the energy loss of high energy particles electromagnetically interacting with it. It is defined as the mean distance, usually measured in $[g\ cm^{-2}]$, over which a high-energy electron loses energy by Bremsstrahlung and by pair production.

2.5 Water equivalence

From what explained above, it follows that the *Water Equivalence* (WE) of a medium is satisfied when the medium and water produce the same energy loss, nuclear interactions and scatter of the beam.
In this case, equations from 2.18 to 2.22 will then assume either med,1 or med,2 to be water, with respective density, stopping power, radiation length and total nuclear cross section.
Since water is the reference material for dosimetric measurements and for dose calculations in treatment plan algorithms, many materials are often converted into an equivalent amount of water in terms of energy loss.
As we will see in Chapter 3, and following from Eq. 2.18, it is useful to define the *Water Equivalent Thickness (WET)* for energy loss as:

$$WET = \rho_s \Delta x_{med} \tag{2.23}$$

where WET and Δx_{med} are geometrical thicknesses and ρ_s is the relative stopping power medium to water.

Chapter 3

Investigations on energy deposition

As discussed in Chapter 2, water equivalence of substitute materials in terms of energy loss is of paramount importance in dosimetric applications. As a matter of fact, this is often the only aspect considered when assessing the medium equivalence to water.
Equation 2.23 defines the proton water equivalent thickness of a medium in terms of energy loss. The proton relative stopping power (medium to water) has been experimentally determined for the materials listed in Chapter 1 and results are presented in the first part of this Chapter.
Furthermore, the experimental values of the relative stopping power are compared to the values extracted from the calibration curve of the Computed Tomography (CT) which is used routinely to image patients for treatment planning.
At the end of the Chapter, conclusions on the energy dependence of the proton relative stopping power are drawn following an analytical approach.

3.1 Experimental determination of proton relative stopping power

Measurements to determine the relative proton stopping power of the candidate materials have been conducted at the Gantry 2 beam line of the Center for Proton Therapy. For different materials, the specimen comes with a different shape and dimensions. The thickness of each specimen is reported in Table 3.1. The beam energy and current are set respectively at 150 MeV and 120 nA at the cyclotron, which means approximately 0.5 nA at the isocenter. The snout of the beam delivery system is 22 cm.

3.1.1 Experimental setup

The energy absorption of the different materials can be determined experimentally by measuring the residual proton range in water.

Table 3.1: Complete geometrical definition of material probes.

Materials	Thickness [mm]
PS	42.3
POM	41.7
RW3	35
PEHMW	20.2
Tecatec PEEK MT CW50	16.9
TECAPEEK MT	40
TECASON PMT	40
TECASON PMT XRO	40

To measure the range of a proton beam in water, an instrument named *'Range Scanner'* was used. The 'Range Scanner' is an in-house built system that allows for precise measurements of Integral Depth Dose (IDD) curves in water. In other terms, with this system is possible to measure the Bragg curve distribution described in Chapter 1 for protons at different energies.
The Range Scanner consists in a tank made of PMMA and in a drive coupled with a stepper motor that allows for precise, sub-millimetric movements. The tank is normally filled with de-mineralized water.
A holder to host an Ionization Chamber (IC) is mounted on the drive. The chamber can then be moved at different positions in water while the proton beam is delivered to the tank. The IC working principle is simply summarized as follows: when the proton beam enters the detector, it generates electrons both because protons are directly ionizing particles and from the interaction with the chamber wall, entering the sensitive part of the IC. The electrons, in turn, interact with the gas filler (usually air) giving rise to positive ions and low-energetic electrons. The latter, combining with the oxigen of the air, generate in addition negative ions. In this way, positive and negative ions will be collected at the electrode and an electric current, a strictly dose-related quantity, can be measured by means of an electrometer.
The pecularities of the parallel-plate IC stay in its shape. As enhanced from the name, a parallel-plate IC is made up of two parallel plates representing the two electrodes (polarizing electrode and collecting electrode). Usually the collecting wall is in a conducting material or non-conducting one coupled with a thin layer of graphite. [19]
The IC used for this experiment is a parallel-plate chamber, with large electrode (8 cm diameter) to collect all secondary particles produced by the primary proton beam. The chamber was biased with a potential of 500 V.

3.1.2 Irradiation procedure

Each time, the material probe has been positioned in front of the water tank at the isocenter of the treatment room, holded by apposite supports. Once the positioning phase has

been terminated, the Range Scanner is remotely activated from the Gantry 2 control room. Then, thanks to the drive motion inside the water phantom, each position is scanned and the resulting deposited dose has been measured. The final result is the measured depth-dose curve of each configurations.
IDD curves have been measured with material specimens in front of the water tank (Fig. 3.1) as well as without material (Fig. 3.2). The latter configuration is necessary to calculate the proton stopping power of each material relative to pure water and also to verify that the overall setup is correct (range of the pristine curve at 150 MeV was compared to tabulated data from NIST [3]).

Figure 3.1: Experimental setup:*"with materials in front"* configurations.

The systematic relationship between the position detected by the Range Scanner and the actual position in water where the dose is measured, is estimated by interposing a material (of a known thickness T) between the water tank's inner wall and the ionization chamber's plate. The representation reported in Fig.3.3 helps to understand the link between the interposed material T and the Range Scanner position P_{drive}:

$$T + WET_{wall} + WET_{chamber} = P_{drive} \tag{3.1}$$

where, more specifically, $WET_{wall} = 2.338\ mm$ and $WET_{chamber} = 8.76\ mm$.

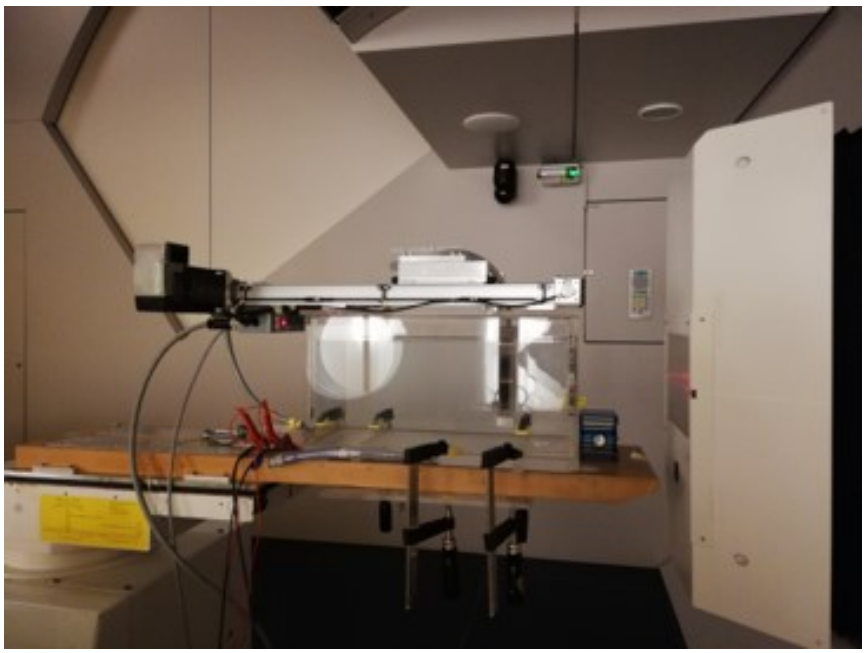

Figure 3.2: Experimental setup:*"only water"* configuration.

Hence, after some manipulations that take into account the relation between the drive position and the effective in-water scanned position, the depth-dose distributions reveal the characteristic Bragg-Peak shape (see Fig. 3.4 and Fig. 3.5) proper of protons, as already said in Chapter 1.

According to the stopping capacity of its own material towards radiation, the Bragg peak is located at a different depth.
Three Bragg peak graphics of three example materials, among those analyzed, have been reported. The others matched the same behavior. The fundamental thing to notice is that for material in front configurations the Bragg peak is moved to minor depth.

3.1.3 Quantification of the Relative Proton Stopping Power and its accuracy

On the basis of the collected data it is possible to derive the *measured* Relative Proton Stopping Power (RPSP) values for each candidate materials. The RPSP gives an idea about the mean capability to stop the radiation with respect to water. Its theoretical definition can be easily found in the following equation:

$$RPSP = \frac{PSP_{material}}{PSP_{water}} \tag{3.2}$$

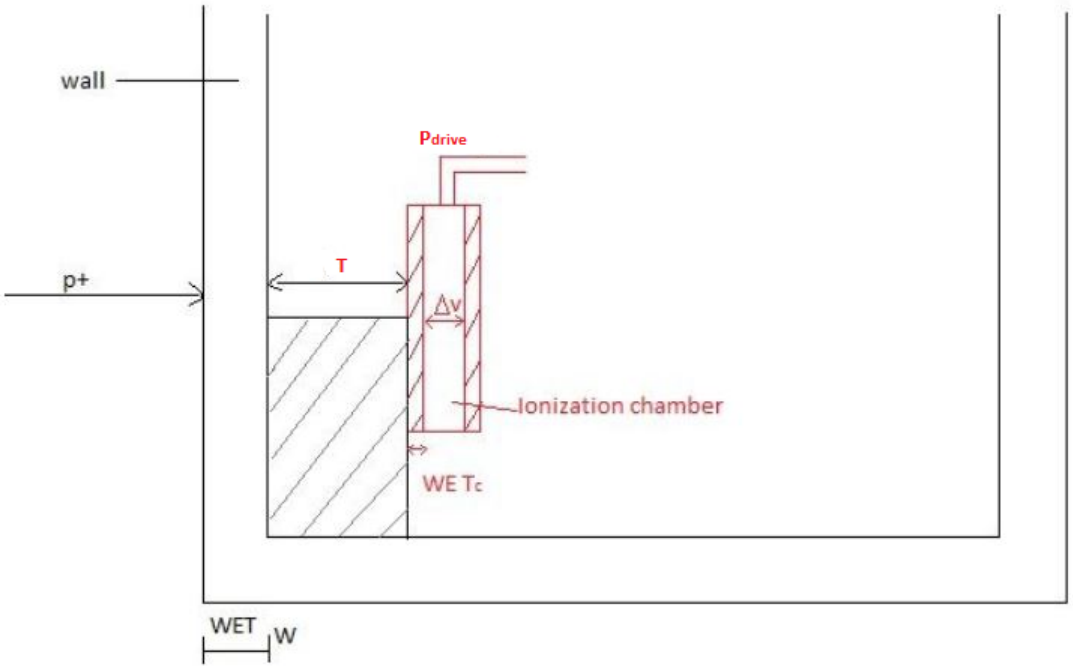

Figure 3.3: Schematic representation of the experimental development.

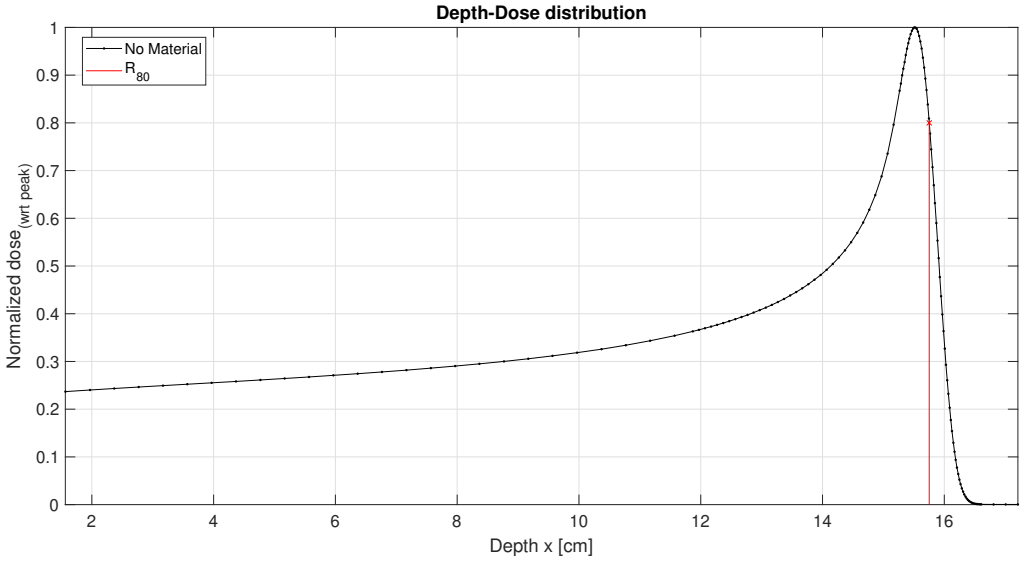

Figure 3.4: Depth-Dose distribution:*"only water"* configuration.

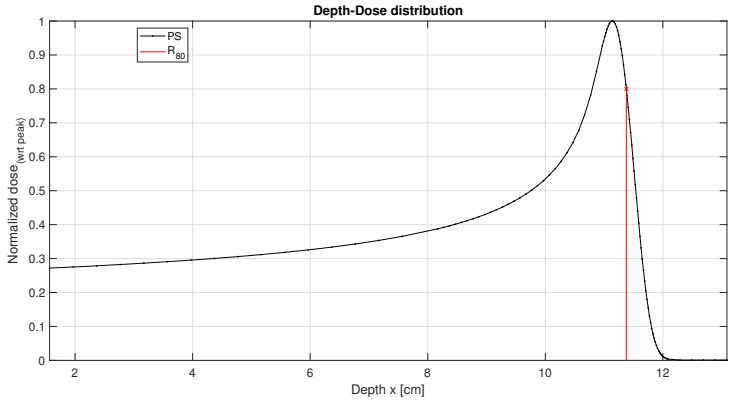

(a) "With PS probe in front"

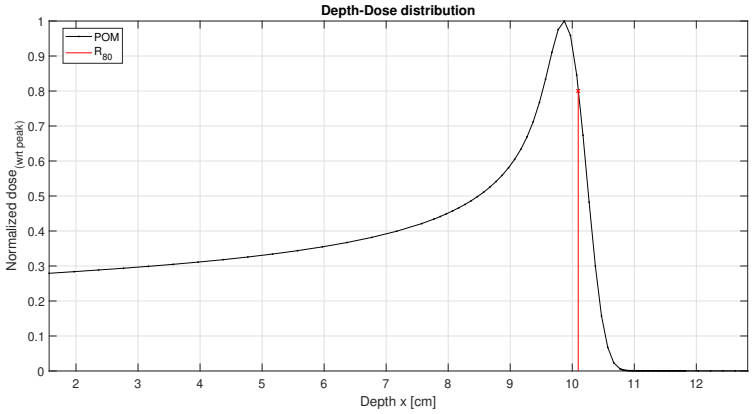

(b) "With POM probe in front"

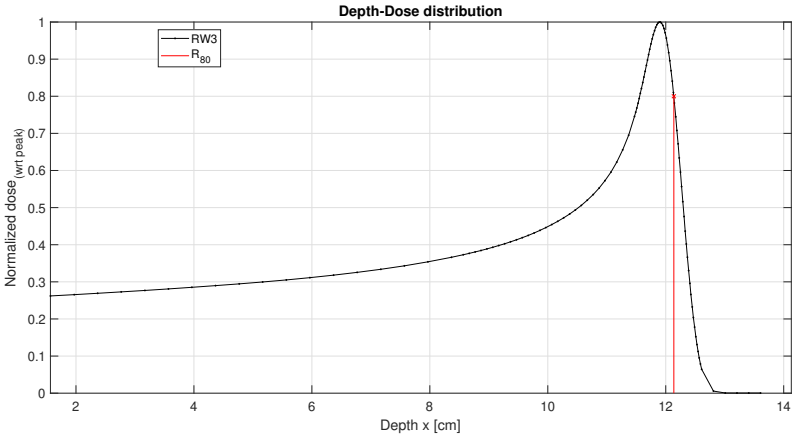

(c) "With RW3 probe in front"

Figure 3.5: Depth-Dose distribution: (a) *"with PS probe in front"*, (b) "with POM probe in front", (c) "with RW3 probe in front" .

where $PSP_{material}$ and PSP_{water} represent the rates at which a single charged particle (in this case a proton) loses kinetic energy, respectively in the mean under study or in water.

Since the difference in the range between the two analysed scenarios corresponds exactly to the material WET (defined as in Eq. 2.23), the *measured* RPSP is calculated for all the candidate materials according to the formula (3.3), as a ratio between the difference of the ranges ($R_{80,w} - R_{80,m}$) and the material thickness t_m:

$$RPSP_{measured} = \frac{R_{80,w} - R_{80,m}}{t_m} \tag{3.3}$$

where $R_{80,w}$ and $R_{80,m}$ are respectively the range measured in pure water and the range measured with the material specimen in the beam path.

Also the RPSP accuracy $dRPSP$ is estimated only for candidate materials whose experimental procedures have been repeated more than once, according to the following expression:

$$dRPSP = \frac{dR_{80,w}}{t_m} + \frac{dR_{80,m}}{t_m} + \frac{(R_{80,w} - R_{80,m})dt_m}{{t_m}^2} \tag{3.4}$$

The calculated RSP accuracy values takes into account the uncertainty related to the thickness measure dt_m and the uncertainties on the range locations of all the examined configurations $dR_{80,w}$,$dR_{80,m}$ (*"only water"* and *"with materials in front"*).

3.2 Comparison between the "measured" RSP and the RSP "derived from the Computed Tomography" of the preabsorber probes

The RSP values derived form Range Scanner measurement associated to each candidate materials have been compared to the RSP values calculated from a CT scan of the probes. The CT fundamental principle is that it relates HU with material electronic density. This is well suited for conventional radiotherapy because the calculated dose within a material lies on electronic density. For protons the calculated dose in a material is based on the material stopping power, so the CT has to relate HU and stopping power. Since the dose is usually calculated inside water, the CT is calibrated in RPSP directly. [24]

The CT scanner adopted is a part of the PSI CPT clinical equipment and it is shown in Figure 3.6.
Once having disposed all the plastic probes on the short couch the Head and Neck CT image is derived.

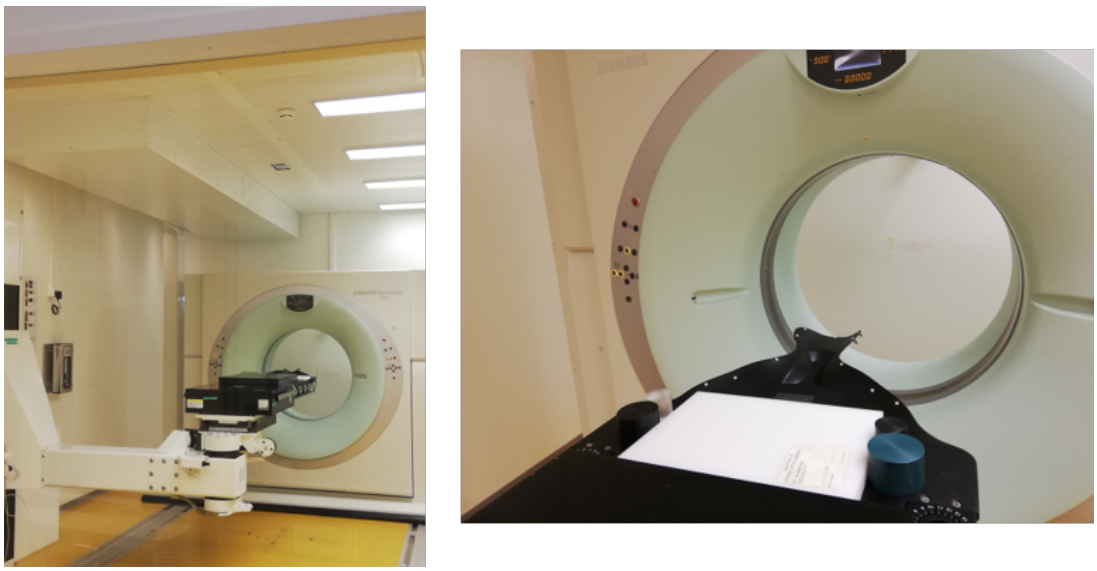

Figure 3.6: *On the left*: PSI Computed Tomography imaging system; *On the right*: Pre-absorber probes placed on the short couch.

The CT scan for all the probes under consideration has allowed the derivation of the *Scaled Hounsfield Unit (HU)* value (also called *CT unit*) corresponding to each material. The scaled Hounsfield number derived from the CT is defined as it follows:

$$HU_{Scaled} = 1000 * \frac{(\mu_m - \mu_w)}{\mu_w} \tag{3.5}$$

where μ_m and μ_w are respectively the attenuation coefficients of the material under consideration and of water.
The deducted HU value from the scan is an average value, obtained eliminating as much as possible edge effects and image noise.
Then, thanks to the calibration curve it has been possible to pass from the HU value to the corresponding RSP.
The adopted calibration curve has been built thanks to clinical data collected during the past year (2019) and it represents the reference clinical curve inserted in the PSI Treatment System. This curve is periodically updated thanks to clinical activity of the center and if no significative differences are remarked, its shape is confirmed, with no modifications.

The result of the comparison between *RSP measured*, resulting from the Range Scanner measurement and *RSP assigned* (extracted from the clinical calibration curve) is shown in Figure 3.7.

A RPSP for each water-substitute material has been assigned by the Treatment Planning System (TPS) using the clinical HU-RPSP calibration curve. The discrepancy between the TPS-assigned RPSP and the measured RPSP is quantitatively assessed through their

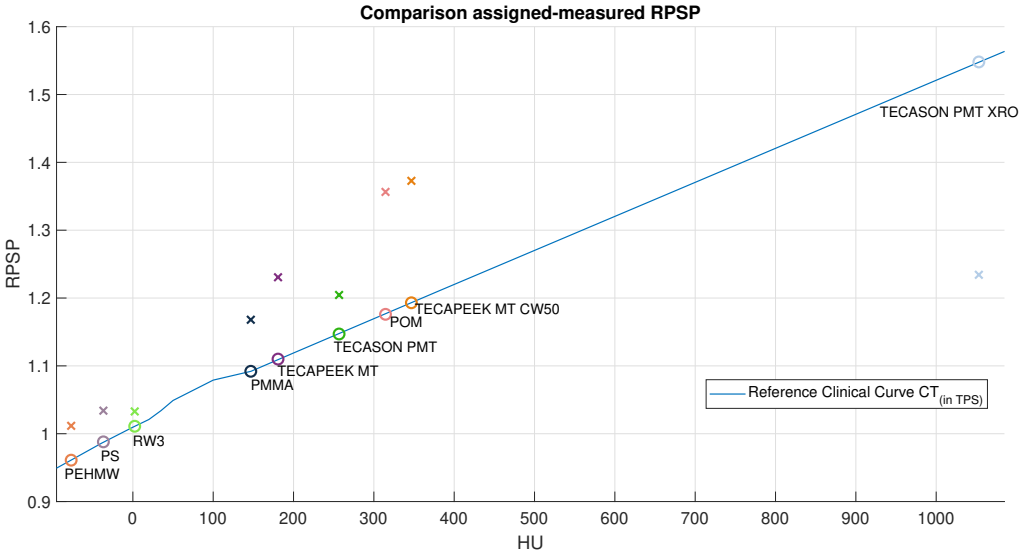

Figure 3.7: Calibration curve for the transformation of Hounsfield values into Relative Proton Stopping Power. For each plastic material, the circled values represent the *assigned RPSP* and the thin crosses are the *measured RSP*. A rough idea of their discrepancy is immediate.

percentage difference, calculated as shown in Eq 3.6:

$$\%\ difference = \frac{RPSP_{Assigned} - RPSP_{Measured}}{RPSP_{Assigned}} * 100 \tag{3.6}$$

The RPSP values calculated according to the method described in Section 3.1.3, those assigned by the TPS and the HU values transferred from the CT scanner to the TPS for each tested material are listed in Table 3.2. The percent difference is also listed in the final column for each material.

3.2.1 Collected results

The obtained results are grouped in Tables 3.3 and 3.4, associating for each pre-absorber materials the corresponding *measured* RPSP and, if calculated, the *RSP Accuracy*. For the materials whose irradiation has been performed only once, it can be assumed the outcomes are affected by the same accuracy level.

Table 3.2: Materials evaluated for the study, mean HU values transferred from the CT scanner to the TPS, measured RPSP, assigned RSP and the percent difference between the two are recorded for each material probes.

Materials	*HU*	**Measured RPSP**	**Assigned RPSP**	**% Difference**
PS	-36.7	1.034	0.988	-4.6 %
POM	314.5	1.356	1.176	-15.3 %
RW3	2	1.033	1.012	-2.1 %
PEHMW	-76.8	1.012	0.961	-5.3 %
TECATEC	346.7	1.373	1.193	-15.1 %
TECAPEEK	180.7	1.231	1.110	-10.9 %
TECASON PMT	256.7	1.204	1.147	-4.9 %
TECASON PMT XRO	1053.1	1.234	1.548	20.3 %
PMMA	146.78	1.168	1.092	-6.9 %

Table 3.3: Measured Relative Proton Stopping Power for each material probes.

Materials	*Measured RPSP*
PS	1.034
POM	1.356
RW3	1.033
PEHMW	1.012
TECATEC	1.373
TECAPEEK	1.231
TECASON PMT	1.204
TECASON PMT XRO	1.234

Table 3.4: Relative Proton Stopping Power accuracy for each material probes.

Materials	*RPSP Accuracy (dRPSP)*
PS	$1.897 * 10^{-4}$
POM	$9.889 * 10^{-4}$
RW3	$5.039 * 10^{-4}$

3.3 Energy dependence of the Relative Proton Stopping Power

A further theoretical analysis regarded the study of the energy dependence of the RSP. Therefore, an in-house developed software has been used, allowing to calculate the mass stopping power and the range associated to each beam entrance energy expressed in MeV. A discretization step of 1 MeV for energy has been selected and thanks to the help of the computational tool, a *Look Up Table* for each candidate material has been built.
The software algorithm repetitively solves the Bethe-Bloch formula (2.1), assigning to each proton energy the material mass stopping power $dE/dx[\frac{MeVcm^2}{g}]$ and the associated range $R\ \ [\frac{g}{cm^2}]$.
The computation requires the user to specify the chemical composition, inserting the chemical formula of each material taken into account, and the density (specified on the material data sheet).
The Ionization Potential is retrieved from 'PStar-NIST' website ([3]) for the already available materials or calculated by the same software if the material is not already scheduled.
Finally the Radiation Length X_0 is computed using the *Bragg Additivity Rule* ([25]) for compounds and mixtures:

$$\left(\frac{1}{X_0}\right)_{compounds,mixtures} = \sum_i w_i \left(\frac{1}{X_0}\right)_i \tag{3.7}$$

where w_i represents the weight fraction of the i-th constituent in the considered compound or mixture and the elemental radiation length is taken from literature ([23]).
The calculated data - obtained through Matlab codes appositely written to perform every specific theoretical investigation - has been grouped in Look Up Tables (LUTs) to be easily accessible for the following analytical analyses.

The calculated values of RPSP for different materials, over the energy range 1-250 MeV, are displayed in Fig. 3.8.

For POM-C, Plexiglass, Solid Water, Tecapeek MT, Tecason PMT and Polystyrene the relative stopping power is almost energy independent over the entire energy range. For Tecason PMT XRO and for Polyethylene the maximum deviations from the mean value at low energies are about 8% and for Tecason PMT XRO and around 5% for PE.
The values measured at 150 MeV are compared with those calculated at the same energy and the differences are shown in the tables below for both water I-values ($I_{water} = 75\ eV$ and $I_{water} = 78\ eV$).
In general, a material is described by a single value of the average ionization potential that represents the energy amount to provide in order to extract electrons from a neutral atom. Several practical formulas offer its expression as a function of the material atomic number Z but modern tables (e.g. ICRU Report 37 and 49) provide much more accurate results. Concerning the water ionization potential, its standard value is I=75 eV, but it is redefined on the basis of experimental data. Its exact determination is difficult, both theoretically

and experimentally. The last modification comes from ICRU 78 which updated the value to I=78 eV. The variation of this parameter greatly influences the deposited dose and therefore has a direct impact in the calculation of stopping power (it is of interest to note the dependence on this parameter in the Bethe-Bloch formula (Eq. 2.1)).

The updated value of 78 eV underlines a 0.5 % general improvement of the percentage difference evaluation, which is calculated as percentage difference between RSP derived and RSP measured, divided by RSP derived, as reported in Eq. 3.8:

$$\% \; difference = \frac{RPSP_{Derived} - RPSP_{Measured}}{RPSP_{Derived}} * 100 \tag{3.8}$$

Final results concerning the derived RPSP, the measured RPSP and the percentage discrepancy between each couple of values are displayed in Tables 3.5 and 3.6. The same information types are sampled in the two tables, where the water ionization potential is the only diversification element.

Table 3.5: Measured RPSP, RPSP derived from LUT in correspondence of 150 MeV energetic content and the percent difference between the two are recorded for each material probes. For Tecatec PEEK MT CW 50 it was impossible to associate the analytical RPSP because theoretical calculation requires the material chemical formula as an input and in this case it is unknown. Calculations are done assuming *Water I-value = 75 eV*.

Materials	**Measured RPSP**	**Derived RPSP**	**% Difference**
PS	1.034	1.028	-0.58 %
POM	1.356	1.348	-0.59 %
RW3	1.033	1.039	0.58 %
PEHMW	1.012	1.008	-0.37 %
TECATEC	1.373	/	/ %
TECAPEEK	1.231	1.227	-0.33 %
TECASON PMT	1.204	1.208	0.33 %
TECASON PMT XRO	1.234	1.1784	-4.72 %
PMMA	1.168	1.1486	-1.69 %

Table 3.6: Measured RPSP, RPSP derived from LUT in correspondence of 150 MeV energetic content and the percent difference between the two are recorded for each material probes. For Tecatec PEEK MT CW 50 it was impossible to associate the analytical RPSP because theoretical calculation requires the material chemical formula as an input and in this case it is unknown. Calculations are done assuming *Water I-value = 78 eV*.

Materials	**Measured RPSP**	**Derived RPSP**	**% Difference**
PS	1.034	1.033	-0.097 %
POM	1.356	1.355	-0.074 %
RW3	1.033	1.044	1.05 %
PEHMW	1.012	1.013	0.099 %
TECATEC	1.373	/	/ %
TECAPEEK	1.231	1.233	0.16 %
TECASON PMT	1.204	1.214	0.82 %
TECASON PMT XRO	1.234	1.184	-4.22 %
PMMA	1.168	1.1541	-1.21 %

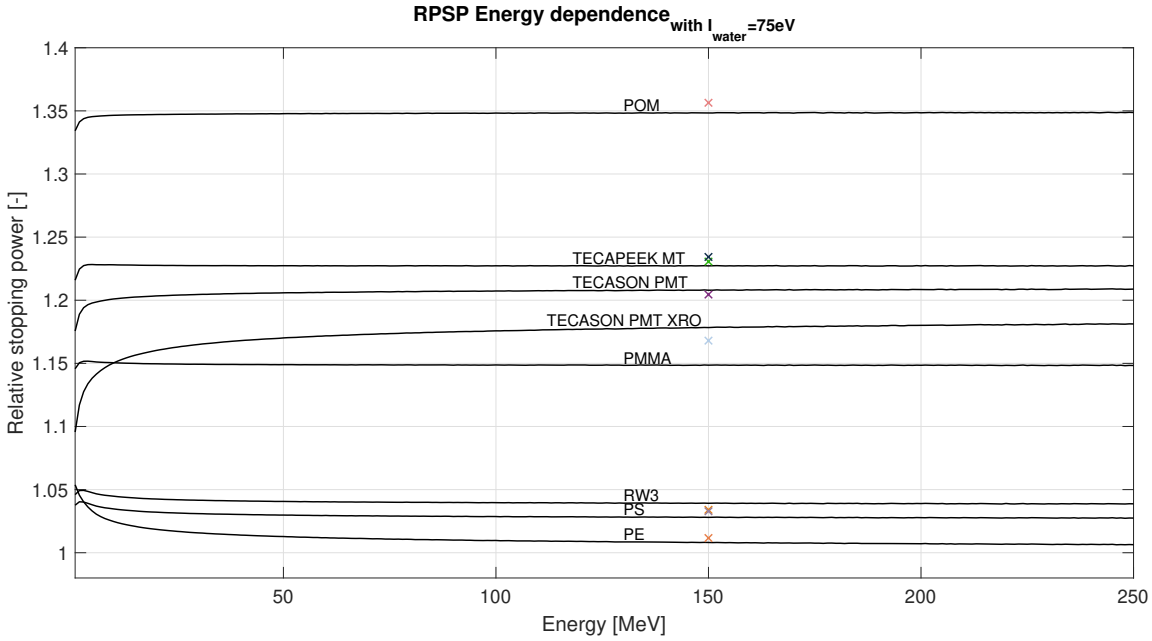

(a) $I_{water} = 75\ eV$

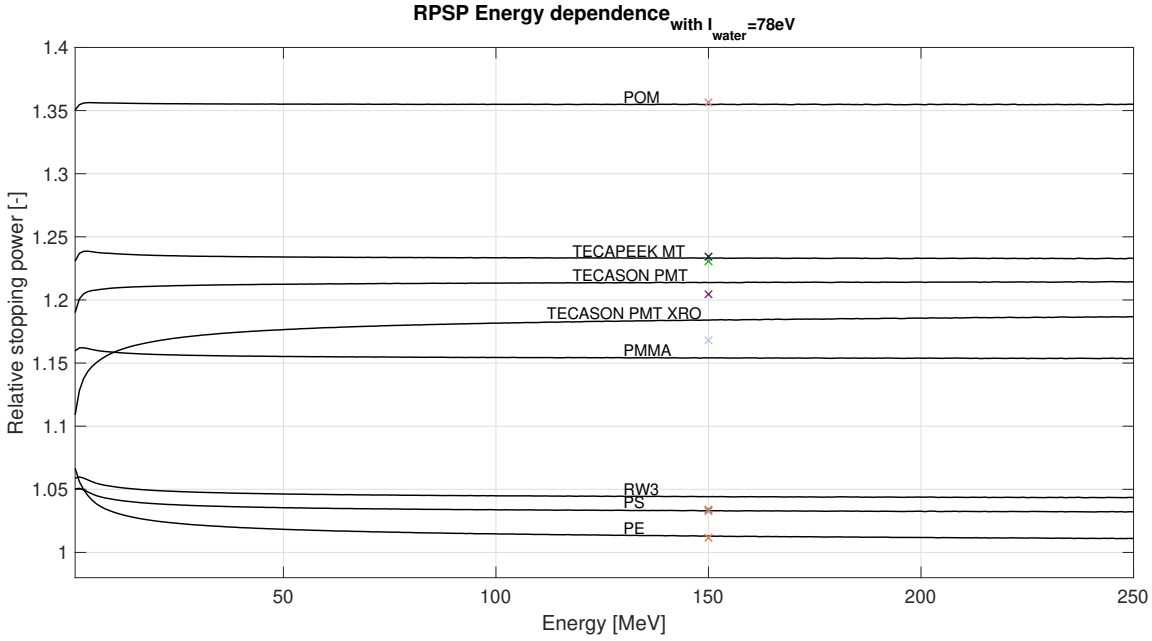

(b) $I_{water} = 78\ eV$

Figure 3.8: Energy dependence of the relative stopping power $\left(\frac{dE}{dx}\right)_{rel}$ for each plastics. The stopping powers have been calculated using the experimental I-values taken from P-Star or obtained with the Bragg additivity rule applied to the constituents of the mixtures. The water Ionization potential is set equal to 75 eV in (a) and to 78 eV in (b). The continuous lines represent the values calculated analytically, while the crosses are those measured at 150 MeV.

3.4 Discussion

From the investigations mentioned above some considerations can be drawn:

1. the fact that the RPSP calculated is almost constant over the energy range is a valid confirmation that assuming a single value is a good approximation;

2. the adoption of the updated water I-value determines the measured and deduced values come closer to each other. This is especially true for PMMA, which is one of the most used materials in dosimetric applications, and it brings the percentage discrepancy difference to lie within 1.5 %;

3. the largest difference between measured and calculated values is recorded for Tecason PMT XRO. Since the producer did not divulge data on its composition, the amount of $BaSO_4$ in the material is an estimation, which is probably the reason of such a great difference;

4. concerning the pre-absorber for Gantry 3 dedicated to cranio-spinal treatments, it can be easily seen from Fig.3.7 that for the singular case of Tecason PMT XRO the CT associates a RSP value greater than the measured one. The special behaviour of this unique material is due to the presence of a filler of Barium sulfate, which enhances the photons absorption. That's why the CT associates an high value of HU.
   For the pre-absorber of Gantry 3 we suggest an assembly of two materials with proper chosen thicknesses, such that the actual (experimental) total RSPS is equal to those calculated by the CT. In this way, during the treatment plan definition stage since the pre-absorber has to be positioned between the patient and the couch, it is scanned together with patient in the CT scan. It implies that the CT assigns to the pre-absorber a RPSP value based on its measured HU. Hence, if the composite material is properly designed such that the RPSP differences are exactly compensated by the actual RPSP differences, it can be avoided to make the material contouring because the CT associated RPSP value matches perfectly with the real situation and no manual adjustment from doctors is necessary.
   In conclusion, taking into account the plot shown in Fig. 3.7 and according to the measured RPSPs some possible material combinations result to be:

   (a) PMMA + Tecason PMTXRO;
   (b) PEHMW + Tecason PMTXRO;
   (c) PS + Tecason PMTXRO;
   (d) RW3 + Tecason PMTXRO;

   also knowing that the final thickness of the above-mentioned composed material has to be equivalent to 3.5 cm of water.

Chapter 4

Investigations on fluence reduction and multiple Coulomb scattering

The water equivalence of substitute materials in terms of both inelastic and elastic scattering with atomic nuclei has been introduced in Chapter 2 with equations 2.20 and 2.21-2.22. In this Chapter, the investigation on these aspects is carried out at a theoretical level, since it was not possible to perform experimental activities at the clinic.

4.1 Investigation on fluence reduction

As discussed in Chapter 2, the reduction of the fluence of the primary proton beam traversing a medium is caused by the inelastic nuclear interactions with the nuclei of the medium.

First of all, the total nuclear interaction probability $P_{nuc,mat}$ has been calculated through Eq. 2.16, from the mass stopping power (calculated as explained in Chapter 3), the inelastic nuclear cross-sections and taking into account the Bragg additivity rule to find out the compounds-related quantities starting from single elements. Specifically the Bragg additivity rule has been used to calculate the ratio σ/A between the total nuclear inelastic cross-section and the atomic mass of the medium, assuming as known the right proportions of the pure elements w_i constituting the compound, as follows:

$$\left(\frac{\sigma}{A}\right)_{compounds,mixtures} = \sum_i w_i \left(\frac{\sigma}{A}\right)_i \tag{4.1}$$

The total inelastic nuclear cross-sections have been taken from tabulated values, listed in the 'Janis Nuclear Database' ([1]) that offers a furnished library for all the nuclear related quantities. Then the calculated total nuclear interaction probability has been compared with the available data reported in literature [11] [12].

When the available data did not cover the entire energy spectrum, interpolated values have been recovered. The interpolation is performed on the probability of non-elastic

nuclear interactions using a second order polynomial fitting to reconstruct the complete description of the investigated parameter over the entire clinical energy range with a discretization step of $1MeV$. Then, the obtained values of $P_{nuc,mat}$ are added to every material LUT, forming an additional column of the table. The built LUT reports mass stopping power, the range in the continuous slowing down approximation and the just added non-elastic nuclear interaction probability for each value of the initial energy from 1 MeV up to 250 MeV. After the coming analysis about the MCS (Chapter 4) the LUT is going to be enriched with the amplitude of the gaussian angular MCS distribution.

Then, assuming the same amount of energy loss ΔE in the medium and in water, the relative difference for the inelastic nuclear interaction probability ΔP can be expressed as:

$$\Delta P = \frac{P_{nuc,mat}(E \to E - \Delta E) - P_{nuc,water}(E \to E - \Delta E)}{P_{nuc,water}(E \to E - \Delta E)} \tag{4.2}$$

where $P_{nuc,mat}$ is the nuclear interaction probability obtained for each considered material and $P_{nuc,water}$ is the probability for an equivalent amount of water that generate the same energy loss ΔE.
Knowing the initial energy E and the energy lost traversing the material ΔE, the investigated parameter can be calculated from the Look Up Tables through Eq. 2.3.
It is also important to notice that the nuclear interaction probability P_{nuc} is a function of both the entrance beam energy E and the thickness of the absorber Δr_{med}. Both the dependencies are singularly explored.

4.1.1 Nuclear interaction probability as a function of the initial energy

The obtained results of the first explored aspect ($\Delta P(E)$) for all materials are reported in Fig.4.1. The comparison in terms of nuclear interaction probability with water has been done assuming having protons with a certain initial energy E, travelling through their range, until they completely stopped. Calculations have been done considering both water I-values.

At high energies Tecapeek MT, Tecason PMT and Tecason PMTXRO behave in a similar way. The same behavior can be observed for PMMA, RW3 and PS too.

The updated ionization water potential reveals a slight improvements of the outcomes in the sense that the discrepancies towards the reference material are smaller if an I-value of 78 eV is used. For each considered material the percentage difference between the mean value of $\Delta P(E)$ over an energy interval ranging from 50 MeV up to 250 MeV is reported for both the analysed cases in Tab. 4.1. The last column of the table shows the difference between the corresponding two associated mean values, taken in absolute value. For TECASON PMT XRO and RW3 the compared values are averaged over a different energy

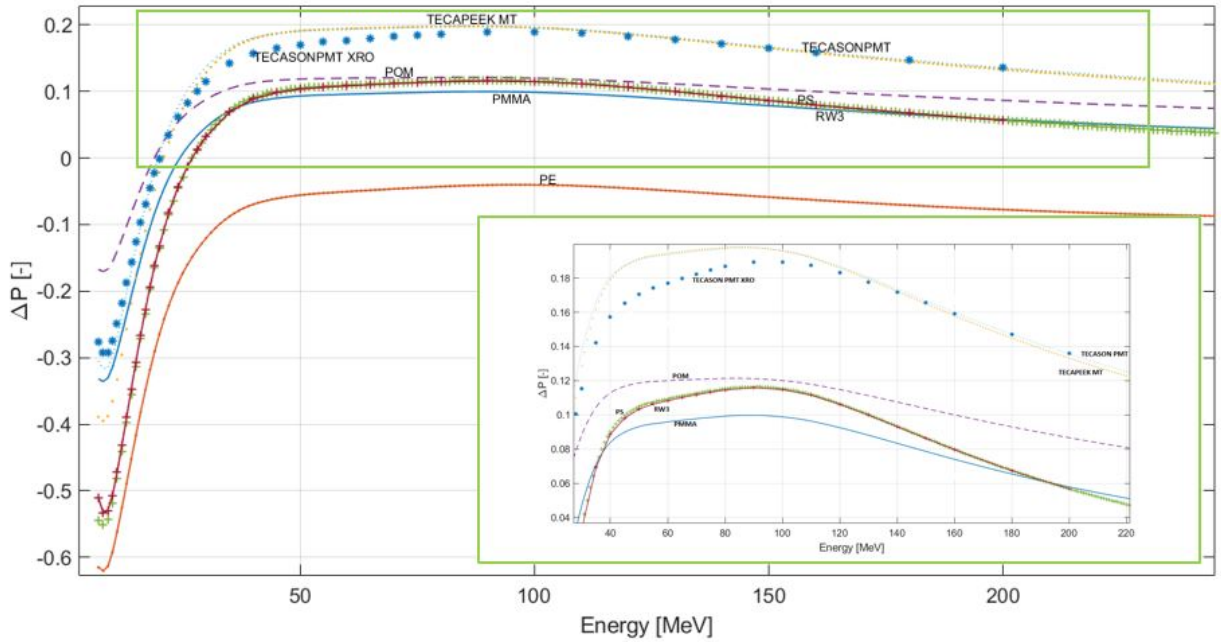

(a) $I_{water} = 75\ eV$

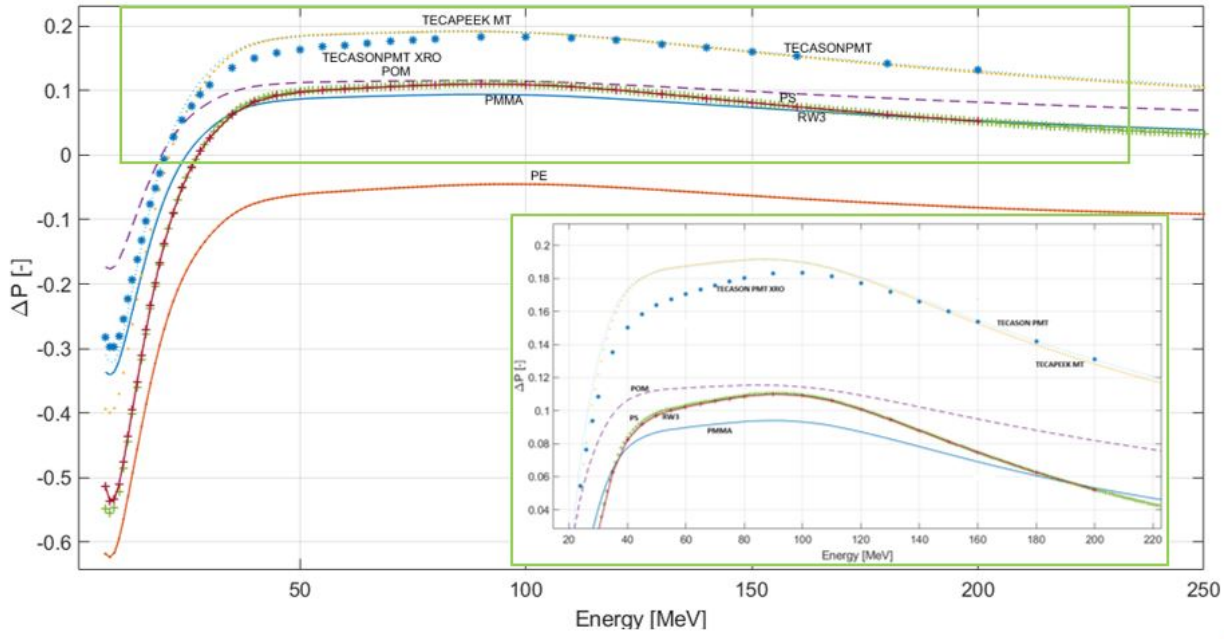

(b) $I_{water} = 78\ eV$

Figure 4.1: Nuclear interaction probability difference ΔP between materials and water. The water Ionization potential is set equal to 75 eV in (a) and to 78 eV in (b).

interval that has its upper limit to 200 MeV. This limitation is justified by the fact that 200 MeV represents the last available energy value reported in the cross-section library for Barium (TECASON PMT XRO constituent) and Titanium (RW3 constituent).
The only material for which the use of $I_{water} = 78\ eV$ reveals a worsening is PE.

Table 4.1: Nuclear interaction probability difference ΔP between materials and water at high energies.

Material	ΔP $(I_{water} = 75\ eV)$	ΔP $(I_{water} = 78\ eV)$	**% Difference**
PMMA	0.0763	0.0712	0.51 %
PEHMW	-0.0615	-0.066	-0.45%
TECAPEEK MT	0.1617	0.1562	0.55%
POM	0.1019	0.0967	0.52%
PS	0.083	0.0778	0.52%
TECASON PMT	0.1630	0.1575	0.55%
RW3	0.0999	0.0943	0.56%
TECASON PMT XRO	0.1742	0.1682	0.6%

It is of interest to investigate the difference in the nuclear interaction probability between water and the pre-absorber for Gantry 3 treatments. The possible configurations and materials, based on the evaluation of the relative stopping power, are those listed in the conclusions of Chapter 3. Each material thickness has been determined thanks to the calculated RPSPs and in compliance with the constraint of 3.5 cm equivalent total WET. The results are shown in Fig. 4.2 for PE, PS, PMMA and TECASON PMT XRO for the specified thicknesses.
In this analysis RW3 has not been considered because, in this case, the availability of the total inelastic nuclear cross-section of Titanium (fundamental input data for the performed calculation) did not completely match the explored energy interval. Similarly with what done previously for Tecason PMT XRO, an interpolation has been tried but results were not acceptable and consistent.

All the curves present the same shape, the amplitude of the deviation from water is the major point of this analysis. As already shown above, again PE is the only material for which -when considered as water- nuclear interaction probabilities are overestimated. It follows that the combination of PE with other materials (e.g. PE with TECASON PMT XRO) could be suitable in the pre-absorber design because these materials, when combined, could reach at least a partial compensation between their ΔP.
The mean discrepancies from water (mean over the energy interval from 100 MeV up to 250 MeV) for PE and for TECASON PMT XRO are respectively -11.7 % and 13.1 %. This could represent an appreciable example of compensation between two opposite behaving materials in terms of nuclear interactions.

The curve describing the TECASON PMT XRO behavior is affected by major imperfections because an interpolation has been revealed necessary due to cross-section availability data with a different energy discretization step towards the other materials.

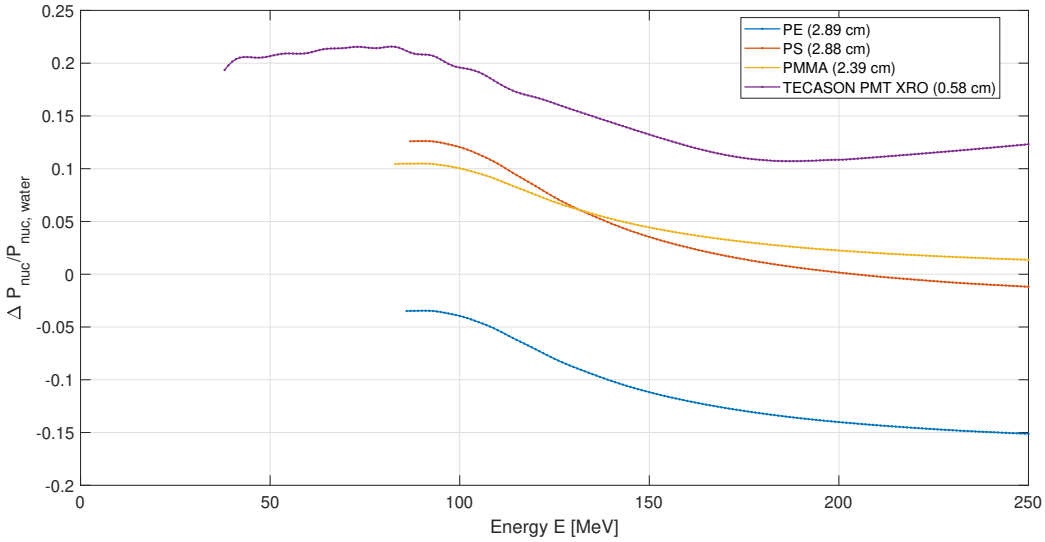

Figure 4.2: Nuclear interaction probability as a function of the entrance energy, once fixed the material thickness. The procedure is conducted for Polyethylene (PE), Polystyrene (PS), Polymethyl methacrylate (PMMA) and TECASON PMT XRO. The lower energy bound for all the materials is justified because the investigation has been stopped when the 97 % of the csda-Range (E_{out}) of protons becomes lower than the material mass thickness (below the lower energy limit the protons are stopped by each material and no calculations were performed).

4.1.2 Nuclear interaction probability as a function of the material thickness

Once fixed the beam entrance energy to an arbitrary value of 180 MeV, the dependency of the nuclear interaction probability from the material thickness has been investigated. Results obtained for each material are shown in Fig. 4.3, exploring all the possible material thickness values. The maximum analysed material thickness is the one that corresponds to the initial protons' range $R_{csda}(E)$.

Every curves present the same shape and a P_{nuc} tendency increasing along the material thickness. It is again important to underline the different deviation from water: PS seems to be the least diversified from water and PE is the only one subjected to a negative variation. From the point of view of nuclear interactions the above mentioned means that in this latter material less proton-nucleus interactions take place than in water.

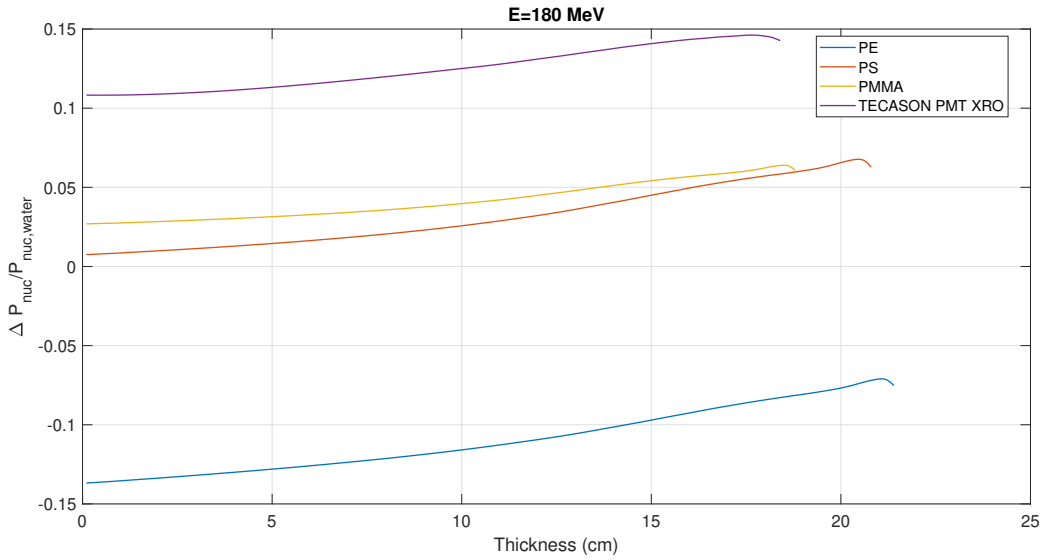

Figure 4.3: Nuclear interaction probability as a function of the material thickness, once fixed the Beam Energy to 180 MeV. The procedure is conducted for Polyethylene (PE), Polystyrene (PS), Polymethyl methacrylate (PMMA) and TECASON PMT XRO.

4.2 Investigation on the Multiple Coulomb Scattering (MCS)

The equivalence between two media in terms of multiple Coulomb scattering is satisfied when both the spatial distribution and the angular distribution of the beam after the media are equivalent. Both aspects will be analyzed in the two subsequent sections.

4.2.1 MCS spatial distribution

First of all, for each investigated material the beam width of the spatial distribution has been calculated.
In the following, the "beam width" indicates the standard deviation of the Gaussian spatial distribution $\sigma_{x,MCS}$. That quantity derives directly from the transport equation with monoenergetic and unidimensional beam, that is orthogonally directed toward the absorber material, assumed, in turn, to be homogeneous. With these assumptions, the width of the MCS spatial distribution can be expressed as:

$$\sigma_{x,MCS}(\Delta r, E_n) = \sqrt{\frac{A_x(\Delta r, E_n)}{2}} \tag{4.3}$$

where A_x describes the propagation of the multiple scattering for a system consisting of laterally infinite layers orthogonal to the beam direction. [21]

The expression for A_x is reported in Eq. 4.4:

$$\begin{aligned} A_x(\Delta r, E_n) = \left[1 + 0.038 \ln\left(\frac{\Delta r}{X_0}\right)\right]^2 \left(\frac{13.6}{\rho}\right)^2 \frac{2}{X_0} * \\ \left[\left(\frac{1}{p\beta c}\right)_m^2 \int_{R_{csda}(E_n)-R_{csda}(E_m)}^{\Delta r} (\Delta r - r)^2 dr + \right. \\ \left. + \sum_{i=m+1}^{n} \left(\frac{1}{p\beta c}\right)_i^2 * \int_{R_{csda}(E_n)-R_{csda}(E_i)}^{R_{csda}(E_n)-R_{csda}(E_{i-1})} (\Delta r - r)^2 dr \right. \end{aligned} \tag{4.4}$$

in which X_0 represents the radiation length and the quantity $1/p\beta c$ is the kinematic term defined as:

$$\frac{1}{p\beta c} = \frac{E + Mc^2}{E(E + 2Mc^2)} \tag{4.5}$$

with $Mc^2 = 938.27MeV$ and $r = \rho z$ symbolizes the mass thickness (product between the material mass density and the geometrical thickness). The indexes n and m of the Eq. 4.4 scan respectively all the possible beam entering condition (when the beam enters the medium) and the exit one (at the end of the traversed material). It directly follows that $m \leq n$.

The integral in Eq. 4.4 can be explicitly solved, leading to the following expression:

$$\begin{aligned} A_x(\Delta r, E_n) = \left[1 + 0.038 \ln\left(\frac{\Delta r}{X_0}\right)\right]^2 \left(\frac{13.6}{\rho}\right)^2 \frac{2}{X_0} * \\ \left[\left(\frac{1}{p\beta c}\right)_m^2 \frac{(\Delta r - r)^3}{3}\Bigg|_{R_{csda}(E_n)-R_{csda}(E_m)}^{\Delta r} + \right. \\ \left. + \sum_{i=m+1}^{n} \left(\frac{1}{p\beta c}\right)_i^2 \frac{(\Delta r - r)^3}{3}\Bigg|_{R_{csda}(E_n)-R_{csda}(E_i)}^{R_{csda}(E_n)-R_{csda}(E_{i-1})} \right. \end{aligned} \tag{4.6}$$

Hence, the integration has been performed using the energy-range LUTs through a structured algorithm appositely written, to compute A_x as expressed above.

The water discrepancy for each material has been quantified by means of parameter $P_{MCS,x}$, again assuming the energy deposition is the same in water and in the medium:

$$P_{MCS,x} = \frac{\Delta\sigma_{MCS,x}}{\sigma_{MCS,x}} = \frac{\sigma_{MCS,x,med}(E \to E - \Delta E) - \sigma_{MCS,x,water}(E \to E - \Delta E)}{\sigma_{MCS,x,water}(E \to E - \Delta E)} \tag{4.7}$$

where $\sigma_{MCS,x,med}$ is the width of the Gaussian approximation for the spacial MCS distribution obtained with Eq. 4.3 and $\sigma_{MCS,x,water}$ is the width for the equivalent amount of

water that produce the same energy loss ΔE.

$P_{MCS,x}$ has been estimated for the possible combinations of materials listed at the end of Chapter 3.
Table 4.2 summarizes the values calculated assuming an initial proton beam energy of 100 MeV.

Table 4.2: Relative deviation $\frac{\Delta\sigma_{MCS,x}}{\sigma_{MCS,x}}$ in % for 100 MeV energetic proton beam, once thickness has been fixed.

	PMMA	**Tecason PMT XRO**	**PS**	**Tecason PMT XRO**	**PEHMW**	**Tecason PMT XRO**	**RW3**	**Tecason PMT XRO**
Thickness [cm]	2.39	0.58	2.88	0.42	2.89	0.47	3.13	0.21
$\frac{\Delta\sigma_{MCS,x}}{\sigma_{MCS,x}}$ *[%]*	-19.2	4.01	-11.7	4.05	-15.0	4.03	-10.2	4.13

The complete set of results correspondent to the entire allowed energy spectrum is graphically reported in Fig. 4.4 for each singular candidate displaying directly the parameter $P_{MCS,x}$. The investigated energy interval has been taken coincident with the one belonging to angular MCS analysis for 'thick absorber' case (see paragraph 4.2.2). It has been decided to investigate always the same energy interval for both the MCS aspects. For simplicity, the curve of Tecason PMT XRO has been plotted just for one representative value of material thickness, arbitrarily chosen among all the values corresponding to Gantry 3 candidate configurations. In fact, the impact of the material thickness choice on the investigated parameter is very small, as it can be seen from Table 4.2.

The energy dependence is almost negligible: the material Tecason PMT XRO shows an increase of the investigated parameter at low energies. Its deviation from the mean value at low energies is about 60%. There is a small tendency to decrease at low energies for PMMA, instead for all the other considered materials the tendency is a slightly increase of very small entity.
The most important conclusion concerns the amplitude of the deviation from water: every scanned materials except the Tecason PMT XRO behave with a negative deviations, which means that the scattering phenomenon is less present in these materials than in water. This is not true form Tecason PMT XR0. Hence the opposite behavior should recommend a combination between opposite behaving materials.

Further theoretical investigation regarded the exploration at a fixed beam energy of 180 MeV of the MCS spatial discrepancy with respect water as a function of the material thickness. Again, for each candidate material, the upper limit of the explored material thicknesses has been set equal to the value that corresponds to 97% of the initial protons range. Results are shown in Fig. 4.5.

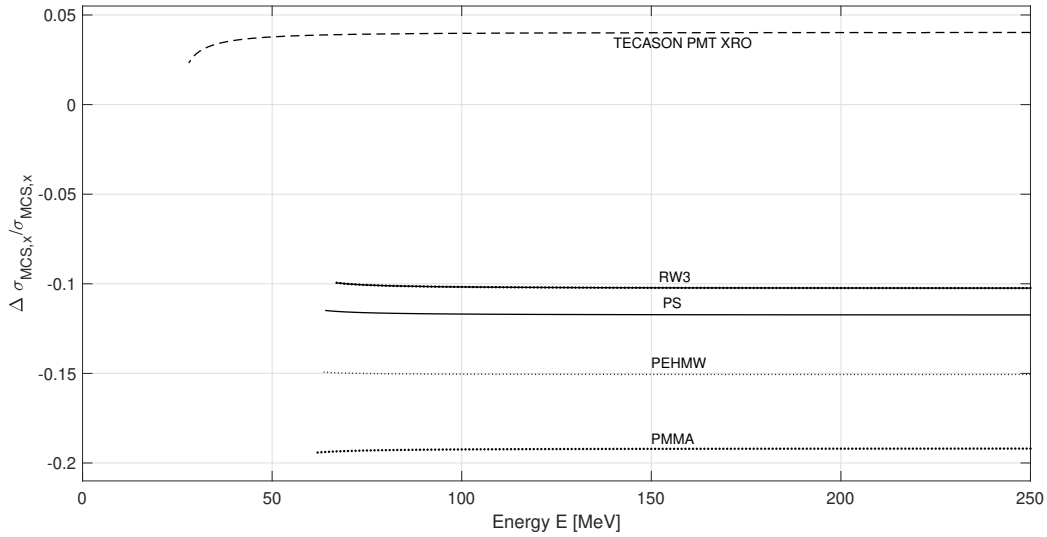

Figure 4.4: Relative deviation $\Delta\sigma_{MCS,x}/\sigma_{MCS,x}$ between the beam width referred to the material $\sigma_{MCS,x,med}$ and the water equivalent beam width $\sigma_{MCS,x,water}$, when the equivalence in terms of energy loss is satisfied for TECASON PMT XRO, Solid Water (RW3), Polystyrene (PS), Polyethylene (PEHMW) and Polymethylmethacrylate (PMMA).

A general trend can be revealed: the discrepancy from water tends to decrease when the material quantity is gradually added. Plexiglass (PMMA) behaves differently: the curve reaches the maximum for a PMMA block thickness of 1.9 cm and then starts to decrease.

4.2.2 MCS angular distribution

For the angular distribution two configurations have been analyzed: the *real absorber* and the *thick absorber* one. The *thick absorber* represents an absorber that completely stops the protons and therefore its thickness has been set to the 97% of the $R_{csda}(E)$ for each entering beam energy value.
As previously said, the *real absorbers* remain the ones designed with a thickness determined in the investigations for the Gantry 3 applications.
For both the examined configurations the parameter P_{MCS} standing as the error approximation for the angular distribution of the MCS has been computed and plotted, as it follows:

$$P_{MCS} = \frac{\Delta\sigma_{MCS}}{\sigma_{MCS}} = \frac{\sigma_{MCS,med}(E \to E - \Delta E) - \sigma_{MCS,water}(E \to E - \Delta E)}{\sigma_{MCS,water}(E \to E - \Delta E)} \tag{4.8}$$

Given E, ΔE as a direct consequence of having fixed the thickness material every time,

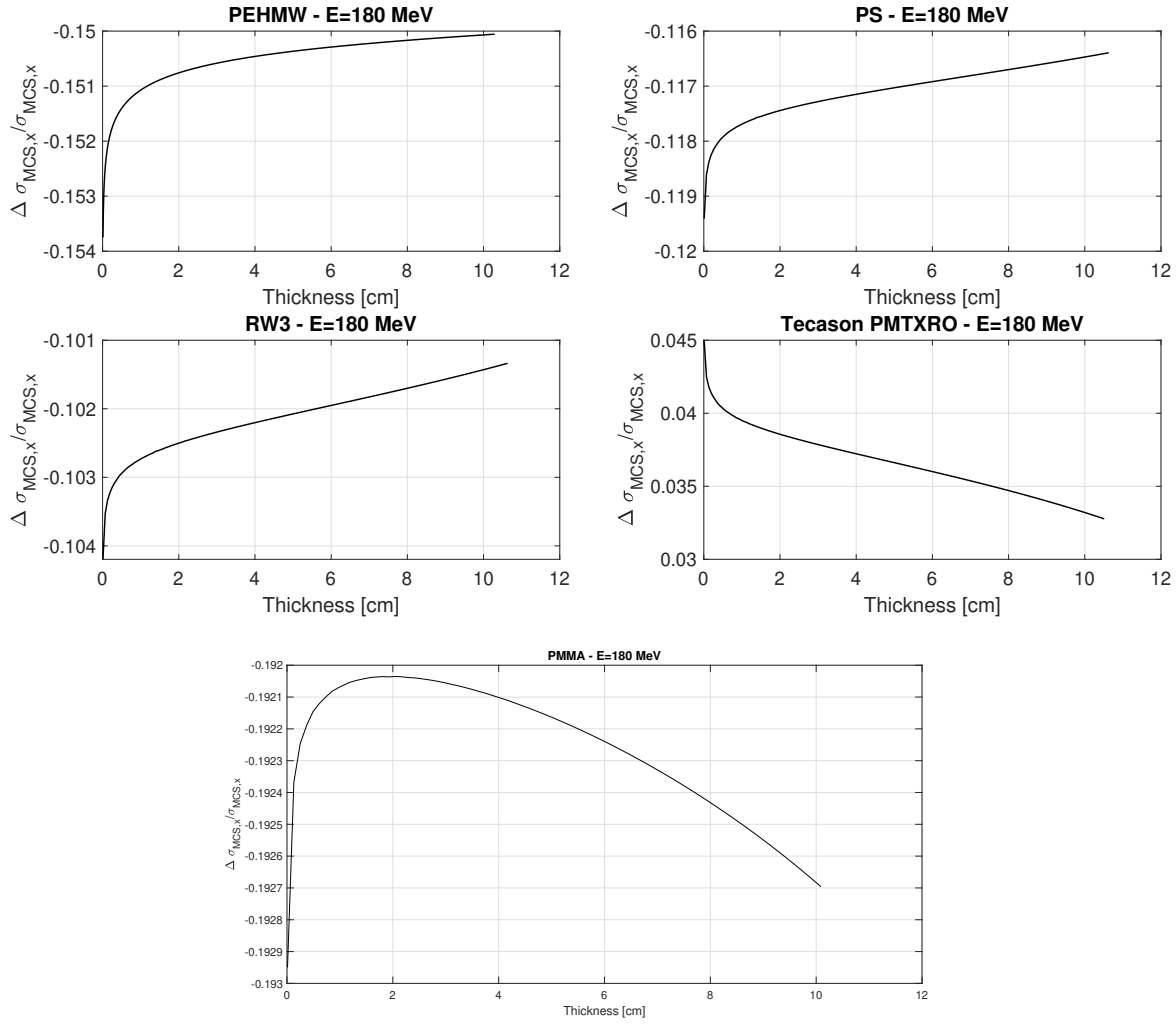

Figure 4.5: $\Delta\sigma_{MCS,x}/\sigma_{MCS,x}$ between the beam width referred to the material $\sigma_{MCS,x,med}$ and the water equivalent beam width $\sigma_{MCS,x,water}$ plotted against the changed material thickness. The beam energy is now fixed (E=180 MeV). Each subplot refers to a specific material.

σ_{MCS} is derived by applying the square root to the variance of the angular MCS distribution expressed in Formula 4.9.

$$\sigma^2_{MCS}(E_n \to E_m) = \left[1 + 0.038\ ln\left(\frac{R_{csda}(E_n) - R_{csda}(E_m)}{X_0}\right)\right]^2 \frac{13.6^2}{X_0} * \sum_{i=m}^{n} \frac{R_{csda}(E_i) - R_{csda}(E_{i-1})}{(p\beta c)^2_i} \qquad for E_n > E_m \tag{4.9}$$

This time, the kinematic term is evaluated at the mean energy between each (i-1)-th and

i-th energy steps as $(E_i + E_{i-1})/2$.

Thanks to the added column in the LUTs containing σ^2_{MCS} as a function of the energy E, it has been possible to avoid any integration, just using the following expression for $\sigma^2_{MCS}(E \to E - \Delta E)$:

$$\sigma^2_{MCS}(E \to E - \Delta E) = \left[1 + 0.038\ ln\left(\frac{R_{csda}(E) - R_{csda}(E - \Delta E)}{X_0}\right)\right]^2 * \left[\frac{\sigma^2_{MCS}(E)}{[1 + 0.038 ln(R_{csda}(E)/X_0)]^2} - \frac{\sigma^2_{MCS}(E - \Delta E)}{[1 + 0.038 ln(R_{csda}(E - \Delta E)/X_0)]^2}\right] \tag{4.10}$$

This is now possible to find out the width of the Gaussian MCS angular distribution $\sigma_{MCS} = \sqrt{\sigma^2_{MCS}}$ determined using the only LUT and the radiation length.

There will follow in Fig. 4.6 the data resulting from the comparison with water concerning the angular MCS for both the examined cases but singularly for each candidate material. The two explored configurations reveal a similar behavior and the energy dependence for both the curves is almost the same. Even if having a material with a great thickness means that the proton beam loses a significant amount of energy traversing the mean, the MCS angular distribution is not too much affected (in comparison with a target of smaller thickness that represents a more realistic case).

Similarly with what done in the previous paragraph also for the angular MCS distribution it has been investigated the general dependency of the $\Delta\sigma_{MCS}/\sigma_{MCS}$ from the beam energy. The calculation is simply done applying the definition reported in Eq. 4.10 both to the material and to the equivalent amount of water.

Eq. 4.10 is derived from the general formulation reported in Eq. 2.12, so that the scattering angle can be calculated using the data in the LUTs, together with the radiation length X_0, the entrance beam energy E and the energy loss ΔE. Results are shown in Fig. 4.7. Again, the investigated energy interval has been taken coincident with the one belonging to previous angular MCS analysis for 'thick absorber' case. The curves' shapes remain similar to those reported for spacial MCS in Fig. 4.4, hence the energy dependence is almost negligible also in this case. Again, it is important to notice the different deviations from the reference material (water). The interesting aspect is again the positive sign of the Tecason PMT XRO discrepancy from water, opposite to those for RW3, PS, PEHMW and PMMA.

Table 4.3 reports the relative deviations from water for the selected materials, both for characteristic beam width and scattering angle.

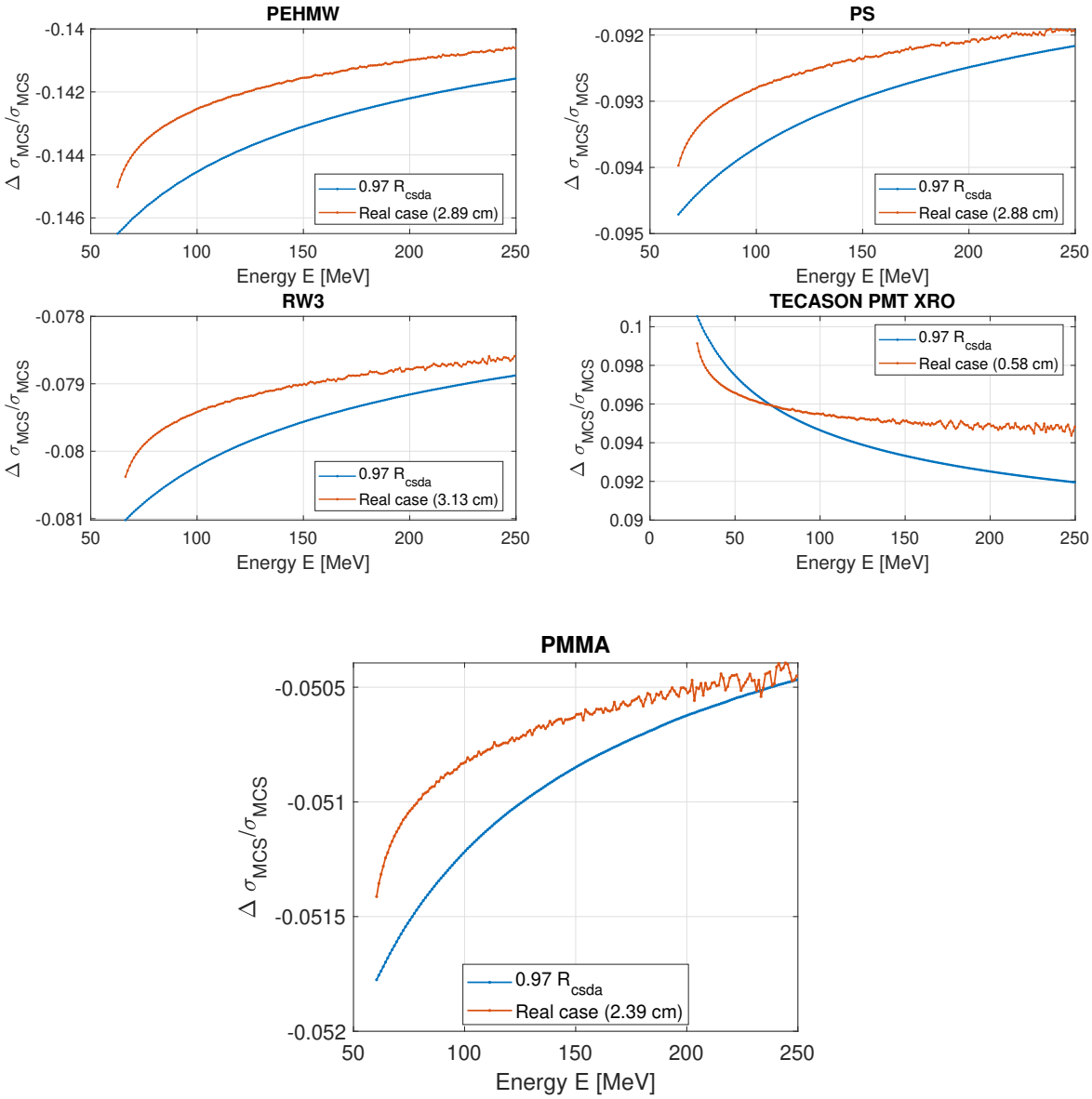

Figure 4.6: Exploration of the energy dependence of the relative deviation $\Delta\sigma_{MCS}/\sigma MCS$. Both the configurations are examined: *real absorber* and *thick absorber*. For *real* absorbers the thickness is supposed to be the same at each entrance energy E and equal to the designed G3 absorber. For *thick* absorbers (in red) the target thickness varies at each beam energy E and is set equal to the 97 % of the csda-Range of the protons at the considered energy. Each subplot refers to a specific material.

For PE and PS the deviations are similar to those for spacial MCS distribution. RW3 and Tecason PMT XRO behave slightly different, but keeping the difference small. It is interesting to note the peculiarity of Tecason PMT XRO: if treated as water, both the

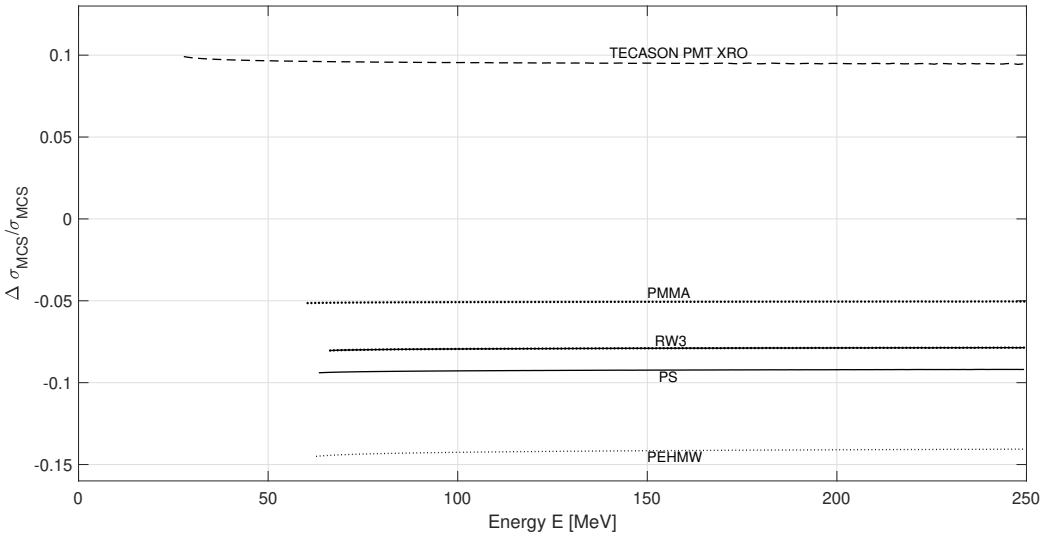

Figure 4.7: Relative deviation $\Delta\sigma_{MCS}/\sigma_{MCS}$ between the width of the Gaussian MCS angular distribution referred to the material $\sigma_{MCS,med}$ and to water $\sigma_{MCS,water}$, when the equivalence in terms of energy loss is satisfied for TECASON PMT XRO, Solid Water (RW3), Polystyrene (PS), Polyethylene (PEHMW) and Polymethylmethacrylate (PMMA).

Table 4.3: Percentage relative deviation for 100 MeV energetic proton beam for both spatial and angular MCS distributions, once thickness has been fixed to "real" values.

	PMMA	**Tecason PMT XRO**	**PS**	**Tecason PMT XRO**	**PEHMW**	**Tecason PMT XRO**	**RW3**	**Tecason PMT XRO**
Thickness [cm]	2.39	0.58	2.88	0.42	2.89	0.47	3.13	0.21
$\frac{\Delta\sigma_{MCS,x}}{\sigma_{MCS,x}}$ *[%]*	-19.2	4.01	-11.7	4.05	-15.0	4.03	-10.2	4.13
$\frac{\Delta\sigma_{MCS}}{\sigma_{MCS}}$ *[%]*	-5.1	9.51	-9.3	9.54	-14.2	9.53	-7.3	9.61

angular scattering and the characteristic beam width are underestimated. In principle, it can partially compensate the behaviour of the other materials.

4.3 Discussion

The studied aspects concerned the fluence reduction and MCS lead to summarize all the previous considerations in a concise way, as follows:

- PEHMW is the only material among the analyzed ones for which the nuclear interaction is underestimated, when considered as water-like, while PS is the less diversified from water;
- regarding the beam broadening effects induced by MCS phenomenon, Tecason PMT XRO is the material for which an overestimation of the beam broadening for both spacial and angular MCS is registered.

The above considerations concerning flux reduction and beam broadening can be used to quantitatively predict the effects on protons beam when it crosses water or a system consisting of layers of different materials treated as water-like. The two-layered composed material compared with water is made up of 2.39 cm of PMMA and 0.58 cm of Tecason PMT XRO. The proton energy at the entrance of both analyzed configurations is 100 MeV. Obtained results show an absolute angular deviation from water of 6.2 mrad for 100 MeV protons and 0.67 mm for the spatial deviation (again with respect water). Thus, calculated differences for the beam width and for the protons angular deviation affect very little the dose distribution at a certain depth.

Chapter 5

Conclusions

In this study the water-equivalence of different plastic materials was evaluated for high energy clinical proton beams. Water-equivalence was evaluated for different aspects, specifically for energy deposition, fluence reduction and multiple Coulomb scattering.
The conducted measurements, added to the additional theoretical investigations, indicate that Polyethylene (PE), Plexiglass (PMMA) and Tecason PMT XRO, when combined, are the most suitable water-substitute in dosimetry applications with clinical proton beams.
This conclusion is drawn taking into account the possibility to combine different materials in order to compensate their relative deviations from water in terms of energy deposition, inelastic nuclear interactions and multiple Coulomb scattering.
According to this idea, a minimization algorithm has been developed. The implemented Matlab script applies an iterative process, aiming to select optimal materials' thicknesses that minimize the total discrepancy from water.

5.1 Minimization problem

The process to identify the best configuration result from a minimization problem mathematically formulated as following:

$$\begin{cases} x_A\ \rho_A(E) + x_B\ \rho_B(E) + x_C\ \rho_C(E) = x_W\ \rho_W(E) \\ \\ P^A_{nuc}(E, x_A) + P^B_{nuc}(E, x_B) + P^C_{nuc}(E, x_C) = P^W_{nuc}(E, x_W) \\ \\ \sigma^A_{MCS,x}(E, x_A) + \sigma^B_{MCS,x}(E, x_B) + \sigma^C_{MCS,x}(E, x_C) = \sigma^W_{MCS,x}(E, x_W) \end{cases} \tag{5.1}$$

where $x_A,\ x_B\ and\ x_C$ represent the three materials mass thicknesses that are the unknowns in the minimization problem, and x_W is the water mass thickness. The terms $\rho_A,\ \rho_B\ and\ \rho_C$ are the mass stopping powers respectively of material A, material B and material C of the studied configuration.
Each equation of the system represents the water-equivalence respectively for energy deposition, nuclear interaction and scattering.

In the following, when it will be talked about the 'total' behavior it is intended the satisfaction of the three aspects of the water-equivalence at the same time.
The solutions of the problem described with equations 5.1, i.e. the mass thicknesses of the three materials, are searched for each energy value of the restricted clinical range (from 70 MeV up to 200 MeV). The reasons of this energy restriction are due to the unavailability for some candidate materials of the total inelastic nuclear cross-sections at energies greater than the upper limit of the interval.
More details on the implemented Matlab routine are given in the following.
For each value of initial energy, the total water thickness x_W is fixed to 97% of the proton range in water for that energy. Deviations from water for each material, for each aspect of the equivalence to water (e.g. energy deposition, nuclear interactions and scattering), are calculated and compared to a fixed set of thresholds. The solutions of the problem are iteratively changed until the deviations from water are smaller than the fixed thresholds. These thresholds were arbitrarily defined to give a tighter constraint on the minimization of errors for the energy deposition equivalence, and a more relaxed constraint on the minimization of errors for the other aspects.
Additionally, among the different iterations over the energy range, the ratios of the materials' thickness are forced to be as much constant as possible. This goal is reached by introducing a further arbitrary constraint to be matched at each iteration. This constraint was chosen taking into account computational time and accuracy of the outcomes.
Figure 5.1 (a) shows the ratios of the materials' thickness versus the beam energy, for the 3-layers configuration.
Figure 5.1 (b) shows the corresponding deviations from water at each energy, assuming a set of materials with thicknesses ratios as in (a). While the deviations from water are kept small for energy deposition and inelastic nuclear interactions, the multiple coulomb scattering is overestimated by 40% when the combined materials are considered to be water.

Again, considering a proton beam with initial energy of 100 MeV, 150 MeV and 200 MeV the MCS spatial deviations from water have been assessed in absolute terms. Results are reported in Tab.5.1 for the prescribed three-materials configuration dimensioned with thicknesses extrapolated form Fig. 5.1 (a) in correspondence of those beam initial energies. The absolute error with respect water is therefore small, remaining in the worst case below 2.5 mm deviation. Thus, relative differences of about 40% in the MCS spatial distribution affect very little the dose prediction.

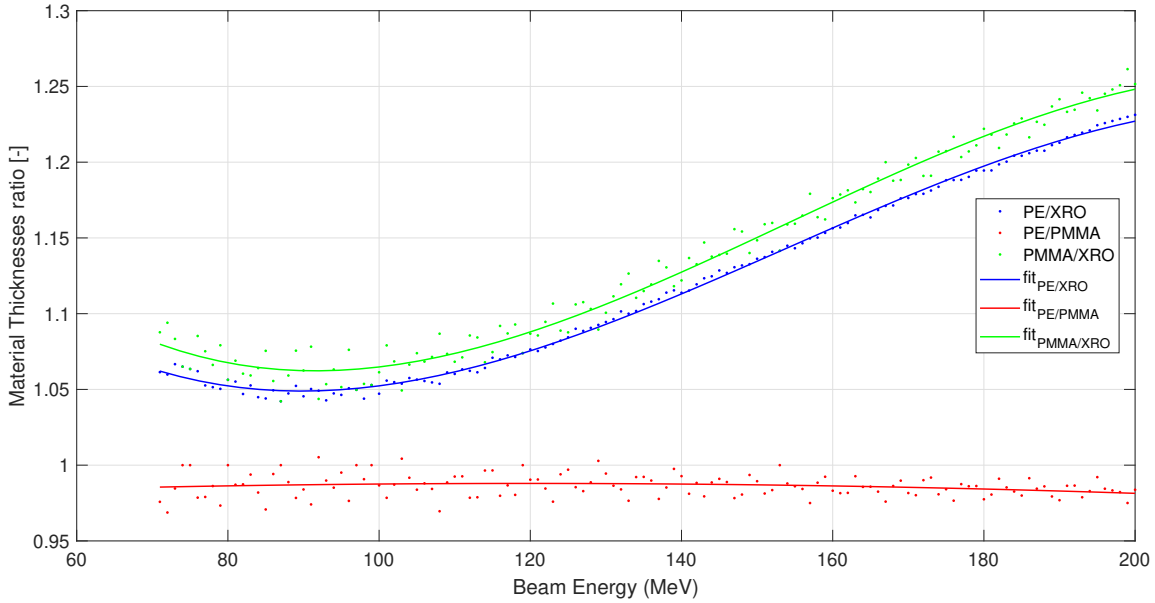

(a) Thicknesses

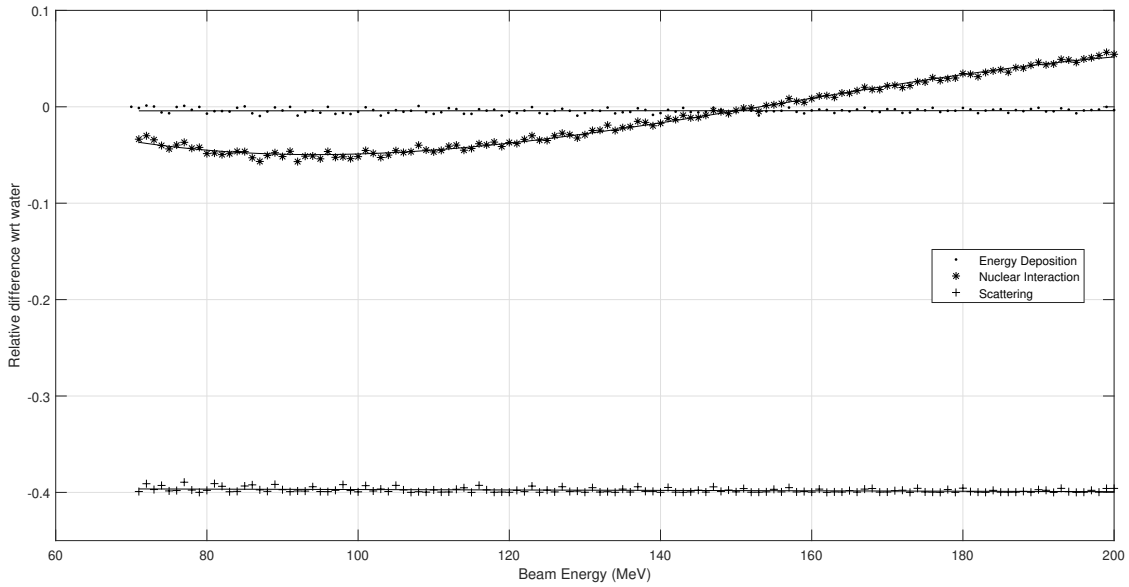

(b) Discrepancies from water

Figure 5.1: Best found materials' configuration *PEHMW + PMMA + Tecason PMT XTRO*: (a) represents its composition in terms of thicknesses ratio and (b) the minimum discrepancy level achieved from water for each aspect of the WE concept.

Table 5.1: Comparison in absolute terms between the 3-layers material configuration and water. The comparison is done for different beam energy values and for the spatial distribution of the multiple Coulomb scattering. The compared amount of water has every time a thickness equal to the 97% of the proton range in water linked to that specified beam energy.

Investigated MCS distribution	**Beam Energy [MeV]**	**97% Range in Water** $[g/cm^2]$	**Absolute difference wrt water**
Spatial	100	7.530	-0.656 mm
Spatial	150	15.386	-1.342 mm
Spatial	200	25.315	-2.191 mm

5.2 Future improvements

The first improvement at the existing investigation could be, as soon as new data on the total inelastic nuclear cross-section will be available, the review and the characterization of the nuclear interaction probabilities also at energies higher than 200 MeV.
Then, further improvements concern the experimental validation of the results from the theoretical analysis. More in details, the conclusions that have been presented in this work should be verified through:

- absolute dose measurements by means of a calibrated ionization chamber, at different depths in the material. This test would be useful to confirm the estimated fluence reduction.
- measurements of beam dimensions by means of an imaging system consisting of a scintillating foil coupled with a CCD (Charge-Coupled Device) camera. This test would be useful to confirm the scattering occurred to the primary proton beam after traversing the material.

The mentioned experimental validations could be performed for single materials alone, and for the layered configuration as presented in section 5.1, and results compared to water.
Finally, considering the Gantry 3 pre-absorber for cranio-spinal treatments, it would be useful to explore the impact of the Barium sulfate concentration on the overall material behavior. By changing the concentration of this filler in the plastic it is possible to greatly change the HU measured by the CT, without affecting significantly the relative stopping power of the compound. Thus, several combinations with different materials could be tried to best match the requirements for the pre-absorber discussed at the end of Chapter 3.

Bibliography

[1] JANIS Nuclear Database. http://www.oecd-nea.org/janisweb/.

[2] Paul Scherrer Institut - Website. https://www.psi.ch/en/protontherapy/therapy-facilities.

[3] PSTAR-NIST. https://.nist.gov/PhysRefData/Star/Text/PSTAR.html.

[4] S. Braccini A. Ereditato et al. A. Ariga, T. Ariga. Characterization of the dose distribution in the halo region of a clinical proton pencil beam using emulsion film detectors. *JINST*, 10(P01007):2080 – 2093, 2015.

[5] P. Stabile A. Degiovanni and D. Ungaro. LIGHT: A linear accelerator for proton therapy. ("NAPAC-2016-FRB1IO02"):"FRB1IO02. 5 p", "2017".

[6] C.Alapetite C.Carrie et al. A. Laprie, Y. Hu. Paediatric brain tumours:a review of radiotherapy,state of the art and challenges for the future regarding protontherapy and carbontherapy. *Cancer/Radiothérapie*, 19:775 – 789, 2015.

[7] N. Wellock et al. A. Lourenço, D. Shipley. Evaluation of the water-equivalence of plastic materials in low- and high-energy clinical proton beams. *in Medicine and Biology*, 62, 2017.

[8] C. Bula S.Safai E. Pedroni, D. Meer and S. Zenklusen. Pencil beam characteristics of the next-generation proton scanning gantry of psi: design issues and initial commissioning results. *The European Physical Journal Plus*, 126(66), 2011.

[9] H. Blattmann A. Lomax et al. E. Pedroni, R. Bacher. The 200 - mev proton therapy project at the paul scherrer institute: Conceptual design and practical realization. *Medical*, 22:37 – 53, 1995.

[10] ICRU78. *Journal of the ICRU*, 7(2), 2007.

[11] J. F. Janni. Proton rage-energy tables - Part 1. *Atomic data and nuclear data tables*, 27:147–339, 1982.

[12] J. F. Janni. Proton rage-energy tables - Part 2. *Atomic data and nuclear data tables*, 27:341–529, 1982.

[13] N. Shikazono K.W.D. Ledingham, P.R. Bolton and C-M. Ma. Towards laser driven hadron cancer radiotherapy: A review of progress. *Applied Sciences*, 4, 2014.

[14] M.W. McDonald and M.M. Fitzek. Proton therapy. *Current Problems in Cancer*, 34(4):257 – 296, 2010.

[15] A.M. Koehler M. Goitein et al. M.M. Urie, J.M. Sisterson. Proton beam penumbra: Effects of separation between patient and beam bodifying devices. *Medical*, 13(5):735 – 741, 1986.

[16] R. Mohan and D. Grosshans. Proton therapy - present and future. *Advanced Drug Delivery Reviews*, 109:26 – 44, 2017.

[17] W.D. Newhauser and R. Zhang. The physics of proton therapy. *Physics in Medicine Biology*, 60:R155–R209, 2015.

[18] E. Pedroni and H. Enge. Beam optics design of compact gantry for proton therapy. *Med. Biol. Eng. Comput.*, 33:271 – 277, 1995.

[19] E.B. Podgorsak. Radiation oncology : A handbook for teachers and students. *International Atomic Energy Agency*, 2005.

[20] H. Ritchie and M. Roser. Causes of death. *Our World in Data*, 2018. https://ourworldindata.org/causes-of-death.

[21] S. Safai. Development of a dosimetric phantom with 400 pointlike scintillators coupled to optical light guides for 3d verification dosimetry for scanned proton beam. 2005.

[22] D. Schardt Th. Haberer, W. Becher and G. Kraft. Magnetic scanning system for heavy ion therapy. *Nuclear Instruments and Methods in Research*, A330:296 – 305, 1993.

[23] Y.S. Tsai. Pair production and Bremsstrahlung of charged leptons. *Review of Modern*, 46(4), 1974.

[24] E. Pedroni U. Schneider and A. Lomax. The calibration of CT Hounsfield Units for radiotherapy treatment planning. *Phys. Med. Biol.*, 41:111 – 124, 1996.

[25] W.H.Bragg and R.Kleeman. On the particles of Radium, and their loss of range in passing through various atoms and molecules. *The London, Edinburgh, and Dublin Philosophical Magazine and Journal of Science*, 10(57):318–340, 1905.

[26] R.R. Wilson. Radiological use of fast protons. *Radiology*, pages 487 – 491, 1946.

[27] B.A. Ludewigt W.T. Chu and T.R. Renner. Instrumentation for treatment of cancer using proton and light-ion beams. *Review of Scientific Instruments*, 64(2055):2080 – 2093, 1993.

[28] S.M. Zenklusen. Exploring the Potential of Advanced Pencil Beam Scanning for Treating Moving Targets with the New Gantry 2 at the Paul Scherrer Institut. 2010.

Appendix A

Look Up Tables

This appendix contains the constructed Look Up Tables of some candidate materials developed to obtain the results described in this thesis.
Energy dependence of the stopping powers, the csda-range, the nuclear interactions probability and the variance of the characteristic scattering angle up to 250 MeV for constant energy step of 1 MeV are represented in the Look Up Tables of this appendix. For Tecason PMT XRO and RW3 data have been displayed with a different energy discretization step. In addition, material mass density ρ, radiation length X_0, mean ionization energy I and details about elemental composition are reported for each analysed material.
The materials for which these kind of information have been reported are listed below:

- Polyethylene (PE);
- Plexiglass (PMMA);
- Polystyrene (PS);
- Solid water (RW3);
- Tecason PMT XRO;
- Water ($I = 78eV$);

PROTONS IN POLYETYLENE

Density ρ [g cm^{-3}]: 0.95
Radiation Length X_0 [g cm^{-2}] 44.7736
Mean ionization energy I [eV] 57.40

COMPOSITION:

Element	H	C
Z	1	6
A	1.00794	12.01070
% by weight	0. 143711	0.856289
I [eV]	19.20	81.00

ENERGY MeV	STOPPING POWER MeV g^{-1}cm^2	CSDA RANGE g cm^{-2}	P_{nuc}	σ^2_{MCS} rad^2	ENERGY MeV	STOPPING POWER MeV g^{-1}cm^2	CSDA RANGE g cm^{-2}	P_{nuc}	σ^2_{MCS} rad^2
1	2.891E+02	2.001E-03	0.000E+00	3.173E-03	34	1.811E+01	1.035E+00	1.584E-02	1.228E-02
2	1.745E+02	6.631E-03	0.000E+00	4.598E-03	35	1.769E+01	1.091E+00	1.677E-02	1.237E-02
3	1.282E+02	1.341E-02	0.000E+00	5.513E-03	36	1.729E+01	1.148E+00	1.772E-02	1.246E-02
4	1.025E+02	2.220E-02	0.000E+00	6.198E-03	37	1.691E+01	1.206E+00	1.867E-02	1.255E-02
5	8.598E+01	3.290E-02	0.000E+00	6.750E-03	38	1.654E+01	1.266E+00	1.963E-02	1.264E-02
6	7.435E+01	4.545E-02	0.000E+00	7.215E-03	39	1.620E+01	1.327E+00	2.060E-02	1.273E-02
7	6.571E+01	5.978E-02	2.205E-05	7.618E-03	40	1.587E+01	1.390E+00	2.157E-02	1.281E-02
8	5.900E+01	7.587E-02	7.933E-05	7.975E-03	41	1.556E+01	1.453E+00	2.254E-02	1.289E-02
9	5.364E+01	9.367E-02	1.667E-04	8.295E-03	42	1.526E+01	1.518E+00	2.352E-02	1.297E-02
10	4.924E+01	1.132E-01	2.916E-04	8.585E-03	43	1.497E+01	1.584E+00	2.451E-02	1.305E-02
11	4.556E+01	1.343E-01	4.604E-04	8.852E-03	44	1.470E+01	1.652E+00	2.550E-02	1.313E-02
12	4.244E+01	1.570E-01	6.784E-04	9.099E-03	45	1.443E+01	1.720E+00	2.649E-02	1.320E-02
13	3.975E+01	1.814E-01	9.490E-04	9.328E-03	46	1.418E+01	1.790E+00	2.749E-02	1.328E-02
14	3.742E+01	2.073E-01	1.274E-03	9.543E-03	47	1.394E+01	1.861E+00	2.848E-02	1.335E-02
15	3.536E+01	2.349E-01	1.654E-03	9.745E-03	48	1.371E+01	1.934E+00	2.949E-02	1.342E-02
16	3.354E+01	2.639E-01	2.088E-03	9.935E-03	49	1.348E+01	2.007E+00	3.049E-02	1.349E-02
17	3.192E+01	2.945E-01	2.573E-03	1.012E-02	50	1.327E+01	2.082E+00	3.150E-02	1.356E-02
18	3.045E+01	3.266E-01	3.108E-03	1.029E-02	51	1.306E+01	2.158E+00	3.251E-02	1.363E-02
19	2.913E+01	3.601E-01	3.688E-03	1.045E-02	52	1.286E+01	2.235E+00	3.353E-02	1.369E-02
20	2.793E+01	3.952E-01	4.311E-03	1.061E-02	53	1.266E+01	2.314E+00	3.455E-02	1.376E-02
21	2.684E+01	4.317E-01	4.973E-03	1.076E-02	54	1.248E+01	2.393E+00	3.557E-02	1.382E-02
22	2.584E+01	4.697E-01	5.670E-03	1.090E-02	55	1.230E+01	2.474E+00	3.659E-02	1.388E-02
23	2.491E+01	5.091E-01	6.400E-03	1.104E-02	56	1.212E+01	2.556E+00	3.762E-02	1.395E-02
24	2.406E+01	5.500E-01	7.160E-03	1.117E-02	57	1.195E+01	2.639E+00	3.865E-02	1.401E-02
25	2.327E+01	5.923E-01	7.945E-03	1.130E-02	58	1.179E+01	2.723E+00	3.968E-02	1.407E-02
26	2.253E+01	6.360E-01	8.755E-03	1.142E-02	59	1.163E+01	2.809E+00	4.071E-02	1.413E-02
27	2.185E+01	6.810E-01	9.585E-03	1.154E-02	60	1.148E+01	2.895E+00	4.175E-02	1.418E-02
28	2.121E+01	7.275E-01	1.044E-02	1.165E-02	61	1.133E+01	2.983E+00	4.279E-02	1.424E-02
29	2.061E+01	7.753E-01	1.130E-02	1.177E-02	62	1.118E+01	3.072E+00	4.384E-02	1.430E-02
30	2.005E+01	8.245E-01	1.218E-02	1.187E-02	63	1.104E+01	3.162E+00	4.488E-02	1.435E-02
31	1.952E+01	8.751E-01	1.308E-02	1.198E-02	64	1.091E+01	3.253E+00	4.594E-02	1.441E-02
32	1.902E+01	9.270E-01	1.399E-02	1.208E-02	65	1.078E+01	3.345E+00	4.699E-02	1.446E-02
33	1.855E+01	9.802E-01	1.491E-02	1.218E-02	66	1.065E+01	3.438E+00	4.805E-02	1.451E-02

ENERGY MeV	STOPPING POWER MeV g^{-1}cm^2	CSDA RANGE g cm^{-2}	P_{nuc}	σ^2_{MCS} rad^2
67	1.052E+01	3.533E+00	4.911E-02	1.457E-02
68	1.040E+01	3.628E+00	5.017E-02	1.462E-02
69	1.029E+01	3.725E+00	5.124E-02	1.467E-02
70	1.017E+01	3.823E+00	5.231E-02	1.472E-02
71	1.006E+01	3.922E+00	5.338E-02	1.477E-02
72	9.950E+00	4.022E+00	5.446E-02	1.482E-02
73	9.844E+00	4.123E+00	5.554E-02	1.487E-02
74	9.740E+00	4.225E+00	5.662E-02	1.491E-02
75	9.640E+00	4.328E+00	5.771E-02	1.496E-02
76	9.541E+00	4.432E+00	5.880E-02	1.501E-02
77	9.446E+00	4.538E+00	5.990E-02	1.505E-02
78	9.352E+00	4.644E+00	6.099E-02	1.510E-02
79	9.261E+00	4.752E+00	6.210E-02	1.515E-02
80	9.172E+00	4.860E+00	6.320E-02	1.519E-02
81	9.084E+00	4.970E+00	6.431E-02	1.523E-02
82	8.999E+00	5.080E+00	6.542E-02	1.528E-02
83	8.916E+00	5.192E+00	6.654E-02	1.532E-02
84	8.835E+00	5.305E+00	6.766E-02	1.536E-02
85	8.755E+00	5.418E+00	6.879E-02	1.540E-02
86	8.678E+00	5.533E+00	6.992E-02	1.545E-02
87	8.602E+00	5.649E+00	7.105E-02	1.549E-02
88	8.527E+00	5.766E+00	7.218E-02	1.553E-02
89	8.454E+00	5.883E+00	7.332E-02	1.557E-02
90	8.383E+00	6.002E+00	7.447E-02	1.561E-02
91	8.313E+00	6.122E+00	7.562E-02	1.565E-02
92	8.245E+00	6.243E+00	7.677E-02	1.569E-02
93	8.177E+00	6.364E+00	7.792E-02	1.573E-02
94	8.112E+00	6.487E+00	7.908E-02	1.576E-02
95	8.047E+00	6.611E+00	8.025E-02	1.580E-02
96	7.984E+00	6.736E+00	8.141E-02	1.584E-02
97	7.922E+00	6.862E+00	8.258E-02	1.588E-02
98	7.862E+00	6.988E+00	8.376E-02	1.591E-02
99	7.802E+00	7.116E+00	8.494E-02	1.595E-02
100	7.744E+00	7.245E+00	8.612E-02	1.599E-02
101	7.686E+00	7.374E+00	8.731E-02	1.602E-02
102	7.630E+00	7.505E+00	8.850E-02	1.606E-02
103	7.575E+00	7.636E+00	8.970E-02	1.609E-02
104	7.521E+00	7.769E+00	9.089E-02	1.613E-02
105	7.467E+00	7.902E+00	9.210E-02	1.616E-02
106	7.415E+00	8.037E+00	9.330E-02	1.620E-02
107	7.364E+00	8.172E+00	9.451E-02	1.623E-02
108	7.313E+00	8.308E+00	9.573E-02	1.626E-02
109	7.263E+00	8.445E+00	9.695E-02	1.630E-02
110	7.215E+00	8.584E+00	9.817E-02	1.633E-02
111	7.167E+00	8.723E+00	9.939E-02	1.636E-02
112	7.120E+00	8.863E+00	1.006E-01	1.640E-02
113	7.073E+00	9.004E+00	1.019E-01	1.643E-02
114	7.028E+00	9.145E+00	1.031E-01	1.646E-02
115	6.983E+00	9.288E+00	1.043E-01	1.649E-02
116	6.939E+00	9.432E+00	1.056E-01	1.652E-02
117	6.896E+00	9.576E+00	1.068E-01	1.656E-02
118	6.853E+00	9.722E+00	1.081E-01	1.659E-02
119	6.811E+00	9.868E+00	1.093E-01	1.662E-02
120	6.770E+00	1.002E+01	1.106E-01	1.665E-02
121	6.729E+00	1.016E+01	1.119E-01	1.668E-02
122	6.689E+00	1.031E+01	1.131E-01	1.671E-02
123	6.650E+00	1.046E+01	1.144E-01	1.674E-02
124	6.611E+00	1.061E+01	1.157E-01	1.677E-02
125	6.573E+00	1.077E+01	1.170E-01	1.680E-02
126	6.535E+00	1.092E+01	1.182E-01	1.683E-02
127	6.498E+00	1.107E+01	1.195E-01	1.685E-02
128	6.461E+00	1.123E+01	1.208E-01	1.688E-02
129	6.425E+00	1.138E+01	1.221E-01	1.691E-02
130	6.390E+00	1.154E+01	1.234E-01	1.694E-02
131	6.355E+00	1.169E+01	1.247E-01	1.697E-02
132	6.321E+00	1.185E+01	1.260E-01	1.700E-02
133	6.287E+00	1.201E+01	1.273E-01	1.702E-02
134	6.253E+00	1.217E+01	1.286E-01	1.705E-02
135	6.220E+00	1.233E+01	1.299E-01	1.708E-02
136	6.188E+00	1.249E+01	1.312E-01	1.711E-02
137	6.156E+00	1.265E+01	1.326E-01	1.713E-02
138	6.124E+00	1.282E+01	1.339E-01	1.716E-02
139	6.093E+00	1.298E+01	1.352E-01	1.719E-02
140	6.062E+00	1.314E+01	1.365E-01	1.721E-02
141	6.032E+00	1.331E+01	1.379E-01	1.724E-02
142	6.002E+00	1.348E+01	1.392E-01	1.726E-02
143	5.972E+00	1.364E+01	1.405E-01	1.729E-02
144	5.943E+00	1.381E+01	1.419E-01	1.732E-02
145	5.914E+00	1.398E+01	1.432E-01	1.734E-02
146	5.886E+00	1.415E+01	1.446E-01	1.737E-02
147	5.858E+00	1.432E+01	1.459E-01	1.739E-02
148	5.830E+00	1.449E+01	1.473E-01	1.742E-02
149	5.803E+00	1.466E+01	1.486E-01	1.744E-02
150	5.776E+00	1.484E+01	1.500E-01	1.747E-02
151	5.749E+00	1.501E+01	1.514E-01	1.749E-02
152	5.723E+00	1.518E+01	1.527E-01	1.751E-02
153	5.697E+00	1.536E+01	1.541E-01	1.754E-02
154	5.671E+00	1.553E+01	1.555E-01	1.756E-02

ENERGY MeV	STOPPING POWER MeV g^{-1}cm^2	CSDA RANGE g cm^{-2}	P_{nuc}	σ^2_{MCS} rad^2
155	5.646E+00	1.571E+01	1.568E-01	1.759E-02
156	5.621E+00	1.589E+01	1.582E-01	1.761E-02
157	5.596E+00	1.607E+01	1.596E-01	1.763E-02
158	5.572E+00	1.625E+01	1.610E-01	1.766E-02
159	5.548E+00	1.643E+01	1.624E-01	1.768E-02
160	5.524E+00	1.661E+01	1.638E-01	1.770E-02
161	5.501E+00	1.679E+01	1.652E-01	1.773E-02
162	5.477E+00	1.697E+01	1.665E-01	1.775E-02
163	5.454E+00	1.715E+01	1.679E-01	1.777E-02
164	5.432E+00	1.734E+01	1.693E-01	1.780E-02
165	5.409E+00	1.752E+01	1.707E-01	1.782E-02
166	5.387E+00	1.771E+01	1.721E-01	1.784E-02
167	5.365E+00	1.789E+01	1.735E-01	1.786E-02
168	5.344E+00	1.808E+01	1.750E-01	1.788E-02
169	5.322E+00	1.827E+01	1.764E-01	1.791E-02
170	5.301E+00	1.845E+01	1.778E-01	1.793E-02
171	5.280E+00	1.864E+01	1.792E-01	1.795E-02
172	5.259E+00	1.883E+01	1.806E-01	1.797E-02
173	5.239E+00	1.902E+01	1.820E-01	1.799E-02
174	5.219E+00	1.922E+01	1.835E-01	1.801E-02
175	5.198E+00	1.941E+01	1.849E-01	1.804E-02
176	5.179E+00	1.960E+01	1.863E-01	1.806E-02
177	5.159E+00	1.979E+01	1.877E-01	1.808E-02
178	5.140E+00	1.999E+01	1.892E-01	1.810E-02
179	5.121E+00	2.018E+01	1.906E-01	1.812E-02
180	5.102E+00	2.038E+01	1.920E-01	1.814E-02
181	5.083E+00	2.057E+01	1.935E-01	1.816E-02
182	5.064E+00	2.077E+01	1.949E-01	1.818E-02
183	5.046E+00	2.097E+01	1.964E-01	1.820E-02
184	5.028E+00	2.117E+01	1.978E-01	1.822E-02
185	5.010E+00	2.137E+01	1.992E-01	1.824E-02
186	4.992E+00	2.157E+01	2.007E-01	1.826E-02
187	4.974E+00	2.177E+01	2.021E-01	1.828E-02
188	4.957E+00	2.197E+01	2.036E-01	1.830E-02
189	4.940E+00	2.217E+01	2.050E-01	1.832E-02
190	4.923E+00	2.237E+01	2.065E-01	1.834E-02
191	4.906E+00	2.258E+01	2.079E-01	1.836E-02
192	4.889E+00	2.278E+01	2.094E-01	1.838E-02
193	4.872E+00	2.299E+01	2.109E-01	1.840E-02
194	4.856E+00	2.319E+01	2.123E-01	1.842E-02
195	4.840E+00	2.340E+01	2.138E-01	1.844E-02
196	4.824E+00	2.361E+01	2.153E-01	1.846E-02
197	4.808E+00	2.381E+01	2.167E-01	1.848E-02
198	4.792E+00	2.402E+01	2.182E-01	1.849E-02
199	4.776E+00	2.423E+01	2.197E-01	1.851E-02
200	4.761E+00	2.444E+01	2.211E-01	1.853E-02
201	4.746E+00	2.465E+01	2.226E-01	1.855E-02
202	4.730E+00	2.486E+01	2.241E-01	1.857E-02
203	4.715E+00	2.507E+01	2.255E-01	1.859E-02
204	4.700E+00	2.529E+01	2.270E-01	1.861E-02
205	4.686E+00	2.550E+01	2.285E-01	1.862E-02
206	4.671E+00	2.571E+01	2.300E-01	1.864E-02
207	4.657E+00	2.593E+01	2.315E-01	1.866E-02
208	4.642E+00	2.614E+01	2.329E-01	1.868E-02
209	4.628E+00	2.636E+01	2.344E-01	1.870E-02
210	4.614E+00	2.657E+01	2.359E-01	1.871E-02
211	4.600E+00	2.679E+01	2.374E-01	1.873E-02
212	4.586E+00	2.701E+01	2.389E-01	1.875E-02
213	4.573E+00	2.723E+01	2.404E-01	1.877E-02
214	4.559E+00	2.745E+01	2.418E-01	1.878E-02
215	4.546E+00	2.767E+01	2.433E-01	1.880E-02
216	4.532E+00	2.789E+01	2.448E-01	1.882E-02
217	4.519E+00	2.811E+01	2.463E-01	1.884E-02
218	4.506E+00	2.833E+01	2.478E-01	1.885E-02
219	4.493E+00	2.855E+01	2.493E-01	1.887E-02
220	4.480E+00	2.877E+01	2.508E-01	1.889E-02
221	4.468E+00	2.900E+01	2.523E-01	1.890E-02
222	4.455E+00	2.922E+01	2.538E-01	1.892E-02
223	4.443E+00	2.945E+01	2.553E-01	1.894E-02
224	4.430E+00	2.967E+01	2.568E-01	1.895E-02
225	4.418E+00	2.990E+01	2.583E-01	1.897E-02
226	4.406E+00	3.012E+01	2.598E-01	1.899E-02
227	4.394E+00	3.035E+01	2.613E-01	1.900E-02
228	4.382E+00	3.058E+01	2.628E-01	1.902E-02
229	4.370E+00	3.081E+01	2.643E-01	1.904E-02
230	4.358E+00	3.104E+01	2.658E-01	1.905E-02
231	4.346E+00	3.127E+01	2.673E-01	1.907E-02
232	4.335E+00	3.150E+01	2.688E-01	1.909E-02
233	4.323E+00	3.173E+01	2.703E-01	1.910E-02
234	4.312E+00	3.196E+01	2.718E-01	1.912E-02
235	4.301E+00	3.219E+01	2.733E-01	1.913E-02
236	4.289E+00	3.243E+01	2.748E-01	1.915E-02
237	4.278E+00	3.266E+01	2.763E-01	1.916E-02
238	4.267E+00	3.289E+01	2.778E-01	1.918E-02
239	4.256E+00	3.313E+01	2.793E-01	1.920E-02
240	4.246E+00	3.336E+01	2.808E-01	1.921E-02
241	4.235E+00	3.360E+01	2.823E-01	1.923E-02
242	4.224E+00	3.384E+01	2.838E-01	1.924E-02

ENERGY MeV	STOPPING POWER MeV $g^{-1}cm^2$	CSDA RANGE g cm^{-2}	P_{nuc}	σ^2_{MCS} rad^2
243	4.214E+00	3.407E+01	2.853E-01	1.926E-02
244	4.203E+00	3.431E+01	2.869E-01	1.927E-02
245	4.193E+00	3.455E+01	2.884E-01	1.929E-02
246	4.182E+00	3.479E+01	2.899E-01	1.930E-02
247	4.172E+00	3.503E+01	2.914E-01	1.932E-02
248	4.162E+00	3.527E+01	2.929E-01	1.933E-02
249	4.152E+00	3.551E+01	2.944E-01	1.935E-02
250	4.142E+00	3.575E+01	2.959E-01	1.936E-02

PROTONS IN PLEXIGLASS

Density ρ [g cm^{-3}]:	1.18
Radiation Length X_0 [g cm^{-2}]	40.5491
Mean ionization energy I [eV]	74.0

COMPOSITION:

Element	H	C	O
Z	1	6	8
A	1.00794	12.01070	15.99940
% by weight	0.080542	0.599840	0.319618
I [eV]	19.20	81.00	106.00

ENERGY	STOPPING POWER	CSDA RANGE	P_{nuc}	σ^2_{MCS}	ENERGY	STOPPING POWER	CSDA RANGE	P_{nuc}	σ^2_{MCS}
MeV	MeV g^{-1}cm^2	g cm^{-2}		rad^2	MeV	MeV g^{-1}cm^2	g cm^{-2}		rad^2
1	2.531E+02	2.309E-03	0.000E+00	4.164E-03	33	1.691E+01	1.080E+00	1.757E-02	1.554E-02
2	1.546E+02	7.561E-03	0.000E+00	5.993E-03	34	1.651E+01	1.140E+00	1.862E-02	1.566E-02
3	1.143E+02	1.519E-02	0.000E+00	7.158E-03	35	1.612E+01	1.201E+00	1.969E-02	1.578E-02
4	9.174E+01	2.503E-02	0.000E+00	8.026E-03	36	1.576E+01	1.264E+00	2.076E-02	1.589E-02
5	7.715E+01	3.697E-02	0.000E+00	8.725E-03	37	1.542E+01	1.328E+00	2.184E-02	1.600E-02
6	6.687E+01	5.093E-02	0.000E+00	9.311E-03	38	1.509E+01	1.393E+00	2.293E-02	1.611E-02
7	5.919E+01	6.686E-02	3.829E-05	9.819E-03	39	1.478E+01	1.460E+00	2.402E-02	1.622E-02
8	5.321E+01	8.471E-02	1.387E-04	1.027E-02	40	1.448E+01	1.529E+00	2.513E-02	1.633E-02
9	4.843E+01	1.044E-01	2.887E-04	1.067E-02	41	1.420E+01	1.598E+00	2.624E-02	1.643E-02
10	4.450E+01	1.260E-01	4.902E-04	1.104E-02	42	1.393E+01	1.670E+00	2.736E-02	1.653E-02
11	4.121E+01	1.494E-01	7.443E-04	1.137E-02	43	1.367E+01	1.742E+00	2.848E-02	1.663E-02
12	3.842E+01	1.745E-01	1.054E-03	1.168E-02	44	1.342E+01	1.816E+00	2.961E-02	1.672E-02
13	3.601E+01	2.014E-01	1.421E-03	1.197E-02	45	1.318E+01	1.891E+00	3.074E-02	1.682E-02
14	3.391E+01	2.301E-01	1.846E-03	1.224E-02	46	1.295E+01	1.968E+00	3.188E-02	1.691E-02
15	3.207E+01	2.604E-01	2.327E-03	1.249E-02	47	1.273E+01	2.046E+00	3.302E-02	1.700E-02
16	3.043E+01	2.924E-01	2.862E-03	1.273E-02	48	1.252E+01	2.125E+00	3.417E-02	1.709E-02
17	2.897E+01	3.261E-01	3.449E-03	1.295E-02	49	1.231E+01	2.205E+00	3.532E-02	1.717E-02
18	2.765E+01	3.615E-01	4.085E-03	1.317E-02	50	1.212E+01	2.287E+00	3.647E-02	1.726E-02
19	2.647E+01	3.984E-01	4.768E-03	1.337E-02	51	1.193E+01	2.370E+00	3.762E-02	1.734E-02
20	2.538E+01	4.370E-01	5.494E-03	1.357E-02	52	1.175E+01	2.455E+00	3.878E-02	1.742E-02
21	2.440E+01	4.772E-01	6.261E-03	1.376E-02	53	1.157E+01	2.541E+00	3.995E-02	1.751E-02
22	2.349E+01	5.190E-01	7.065E-03	1.393E-02	54	1.140E+01	2.628E+00	4.112E-02	1.759E-02
23	2.266E+01	5.623E-01	7.904E-03	1.411E-02	55	1.124E+01	2.716E+00	4.229E-02	1.766E-02
24	2.189E+01	6.073E-01	8.774E-03	1.427E-02	56	1.108E+01	2.806E+00	4.346E-02	1.774E-02
25	2.117E+01	6.537E-01	9.672E-03	1.443E-02	57	1.092E+01	2.897E+00	4.464E-02	1.782E-02
26	2.051E+01	7.017E-01	1.060E-02	1.459E-02	58	1.077E+01	2.989E+00	4.582E-02	1.789E-02
27	1.989E+01	7.512E-01	1.154E-02	1.474E-02	59	1.063E+01	3.082E+00	4.700E-02	1.796E-02
28	1.931E+01	8.023E-01	1.251E-02	1.488E-02	60	1.049E+01	3.177E+00	4.819E-02	1.804E-02
29	1.877E+01	8.548E-01	1.349E-02	1.502E-02	61	1.036E+01	3.273E+00	4.937E-02	1.811E-02
30	1.826E+01	9.088E-01	1.449E-02	1.515E-02	62	1.023E+01	3.370E+00	5.057E-02	1.818E-02
31	1.779E+01	9.643E-01	1.551E-02	1.529E-02	63	1.010E+01	3.469E+00	5.176E-02	1.825E-02
32	1.733E+01	1.021E+00	1.653E-02	1.541E-02	64	9.974E+00	3.568E+00	5.296E-02	1.831E-02

ENERGY MeV	STOPPING POWER MeV $g^{-1}cm^2$	CSDA RANGE g cm^{-2}	P_{nuc}	σ^2_{MCS} rad^2	ENERGY MeV	STOPPING POWER MeV $g^{-1}cm^2$	CSDA RANGE g cm^{-2}	P_{nuc}	σ^2_{MCS} rad^2
65	9.854E+00	3.669E+00	5.416E-02	1.838E-02	108	6.700E+00	9.090E+00	1.095E-01	2.063E-02
66	9.738E+00	3.771E+00	5.536E-02	1.845E-02	109	6.655E+00	9.240E+00	1.109E-01	2.067E-02
67	9.624E+00	3.874E+00	5.657E-02	1.851E-02	110	6.611E+00	9.391E+00	1.123E-01	2.071E-02
68	9.514E+00	3.979E+00	5.778E-02	1.858E-02	111	6.567E+00	9.543E+00	1.137E-01	2.075E-02
69	9.407E+00	4.085E+00	5.900E-02	1.864E-02	112	6.524E+00	9.696E+00	1.151E-01	2.079E-02
70	9.303E+00	4.192E+00	6.021E-02	1.870E-02	113	6.482E+00	9.849E+00	1.166E-01	2.083E-02
71	9.201E+00	4.300E+00	6.143E-02	1.877E-02	114	6.440E+00	1.000E+01	1.180E-01	2.087E-02
72	9.102E+00	4.409E+00	6.266E-02	1.883E-02	115	6.399E+00	1.016E+01	1.194E-01	2.091E-02
73	9.006E+00	4.519E+00	6.389E-02	1.889E-02	116	6.359E+00	1.032E+01	1.208E-01	2.095E-02
74	8.912E+00	4.631E+00	6.512E-02	1.895E-02	117	6.320E+00	1.047E+01	1.223E-01	2.099E-02
75	8.820E+00	4.744E+00	6.635E-02	1.901E-02	118	6.281E+00	1.063E+01	1.237E-01	2.103E-02
76	8.730E+00	4.858E+00	6.759E-02	1.906E-02	119	6.243E+00	1.079E+01	1.251E-01	2.107E-02
77	8.643E+00	4.973E+00	6.884E-02	1.912E-02	120	6.205E+00	1.095E+01	1.266E-01	2.110E-02
78	8.558E+00	5.089E+00	7.008E-02	1.918E-02	121	6.168E+00	1.112E+01	1.280E-01	2.114E-02
79	8.475E+00	5.207E+00	7.133E-02	1.923E-02	122	6.131E+00	1.128E+01	1.295E-01	2.118E-02
80	8.394E+00	5.325E+00	7.259E-02	1.929E-02	123	6.095E+00	1.144E+01	1.309E-01	2.122E-02
81	8.314E+00	5.445E+00	7.384E-02	1.934E-02	124	6.060E+00	1.161E+01	1.324E-01	2.125E-02
82	8.237E+00	5.566E+00	7.511E-02	1.940E-02	125	6.025E+00	1.177E+01	1.339E-01	2.129E-02
83	8.161E+00	5.688E+00	7.637E-02	1.945E-02	126	5.991E+00	1.194E+01	1.353E-01	2.133E-02
84	8.087E+00	5.811E+00	7.764E-02	1.951E-02	127	5.957E+00	1.211E+01	1.368E-01	2.136E-02
85	8.015E+00	5.935E+00	7.892E-02	1.956E-02	128	5.924E+00	1.227E+01	1.383E-01	2.140E-02
86	7.944E+00	6.060E+00	8.020E-02	1.961E-02	129	5.891E+00	1.244E+01	1.398E-01	2.143E-02
87	7.875E+00	6.187E+00	8.149E-02	1.966E-02	130	5.858E+00	1.261E+01	1.413E-01	2.147E-02
88	7.807E+00	6.314E+00	8.277E-02	1.971E-02	131	5.826E+00	1.278E+01	1.428E-01	2.150E-02
89	7.740E+00	6.443E+00	8.407E-02	1.976E-02	132	5.795E+00	1.296E+01	1.443E-01	2.154E-02
90	7.675E+00	6.573E+00	8.536E-02	1.981E-02	133	5.764E+00	1.313E+01	1.458E-01	2.157E-02
91	7.612E+00	6.704E+00	8.667E-02	1.986E-02	134	5.734E+00	1.330E+01	1.473E-01	2.161E-02
92	7.549E+00	6.835E+00	8.797E-02	1.991E-02	135	5.703E+00	1.348E+01	1.488E-01	2.164E-02
93	7.488E+00	6.968E+00	8.928E-02	1.996E-02	136	5.674E+00	1.365E+01	1.503E-01	2.167E-02
94	7.428E+00	7.103E+00	9.060E-02	2.001E-02	137	5.645E+00	1.383E+01	1.518E-01	2.171E-02
95	7.370E+00	7.238E+00	9.192E-02	2.005E-02	138	5.616E+00	1.401E+01	1.533E-01	2.174E-02
96	7.312E+00	7.374E+00	9.325E-02	2.010E-02	139	5.587E+00	1.419E+01	1.549E-01	2.177E-02
97	7.256E+00	7.511E+00	9.458E-02	2.015E-02	140	5.559E+00	1.437E+01	1.564E-01	2.181E-02
98	7.200E+00	7.650E+00	9.592E-02	2.019E-02	141	5.531E+00	1.455E+01	1.579E-01	2.184E-02
99	7.146E+00	7.789E+00	9.726E-02	2.024E-02	142	5.504E+00	1.473E+01	1.595E-01	2.187E-02
100	7.093E+00	7.929E+00	9.861E-02	2.028E-02	143	5.477E+00	1.491E+01	1.610E-01	2.190E-02
101	7.041E+00	8.071E+00	9.996E-02	2.033E-02	144	5.450E+00	1.509E+01	1.625E-01	2.194E-02
102	6.989E+00	8.213E+00	1.013E-01	2.037E-02	145	5.424E+00	1.528E+01	1.641E-01	2.197E-02
103	6.939E+00	8.357E+00	1.027E-01	2.042E-02	146	5.398E+00	1.546E+01	1.656E-01	2.200E-02
104	6.890E+00	8.502E+00	1.040E-01	2.046E-02	147	5.373E+00	1.565E+01	1.672E-01	2.203E-02
105	6.841E+00	8.647E+00	1.054E-01	2.050E-02	148	5.347E+00	1.583E+01	1.688E-01	2.206E-02
106	6.793E+00	8.794E+00	1.068E-01	2.054E-02	149	5.323E+00	1.602E+01	1.703E-01	2.209E-02
107	6.746E+00	8.942E+00	1.082E-01	2.059E-02	150	5.298E+00	1.621E+01	1.719E-01	2.212E-02

ENERGY MeV	STOPPING POWER MeV $g^{-1}cm^2$	CSDA RANGE g cm^{-2}	P_{nuc}	σ^2_{MCS} rad^2	ENERGY MeV	STOPPING POWER MeV $g^{-1}cm^2$	CSDA RANGE g cm^{-2}	P_{nuc}	σ^2_{MCS} rad^2
151	5.274E+00	1.640E+01	1.735E-01	2.215E-02	194	4.458E+00	2.532E+01	2.435E-01	2.331E-02
152	5.250E+00	1.659E+01	1.750E-01	2.218E-02	195	4.443E+00	2.554E+01	2.452E-01	2.333E-02
153	5.226E+00	1.678E+01	1.766E-01	2.221E-02	196	4.428E+00	2.577E+01	2.469E-01	2.335E-02
154	5.203E+00	1.697E+01	1.782E-01	2.224E-02	197	4.414E+00	2.599E+01	2.485E-01	2.338E-02
155	5.179E+00	1.716E+01	1.798E-01	2.227E-02	198	4.399E+00	2.622E+01	2.502E-01	2.340E-02
156	5.157E+00	1.736E+01	1.814E-01	2.230E-02	199	4.385E+00	2.645E+01	2.519E-01	2.342E-02
157	5.134E+00	1.755E+01	1.829E-01	2.233E-02	200	4.371E+00	2.668E+01	2.536E-01	2.345E-02
158	5.112E+00	1.775E+01	1.845E-01	2.236E-02	201	4.357E+00	2.691E+01	2.553E-01	2.347E-02
159	5.090E+00	1.794E+01	1.861E-01	2.239E-02	202	4.343E+00	2.714E+01	2.569E-01	2.349E-02
160	5.068E+00	1.814E+01	1.877E-01	2.242E-02	203	4.329E+00	2.737E+01	2.586E-01	2.352E-02
161	5.047E+00	1.834E+01	1.893E-01	2.245E-02	204	4.316E+00	2.760E+01	2.603E-01	2.354E-02
162	5.025E+00	1.854E+01	1.909E-01	2.248E-02	205	4.302E+00	2.783E+01	2.620E-01	2.356E-02
163	5.004E+00	1.874E+01	1.925E-01	2.250E-02	206	4.289E+00	2.806E+01	2.637E-01	2.358E-02
164	4.984E+00	1.894E+01	1.941E-01	2.253E-02	207	4.276E+00	2.830E+01	2.654E-01	2.361E-02
165	4.963E+00	1.914E+01	1.958E-01	2.256E-02	208	4.263E+00	2.853E+01	2.671E-01	2.363E-02
166	4.943E+00	1.934E+01	1.974E-01	2.259E-02	209	4.250E+00	2.876E+01	2.687E-01	2.365E-02
167	4.923E+00	1.954E+01	1.990E-01	2.262E-02	210	4.237E+00	2.900E+01	2.704E-01	2.367E-02
168	4.903E+00	1.975E+01	2.006E-01	2.264E-02	211	4.224E+00	2.924E+01	2.721E-01	2.370E-02
169	4.884E+00	1.995E+01	2.022E-01	2.267E-02	212	4.211E+00	2.947E+01	2.738E-01	2.372E-02
170	4.864E+00	2.015E+01	2.039E-01	2.270E-02	213	4.199E+00	2.971E+01	2.755E-01	2.374E-02
171	4.845E+00	2.036E+01	2.055E-01	2.272E-02	214	4.186E+00	2.995E+01	2.772E-01	2.376E-02
172	4.826E+00	2.057E+01	2.071E-01	2.275E-02	215	4.174E+00	3.019E+01	2.789E-01	2.378E-02
173	4.807E+00	2.078E+01	2.087E-01	2.278E-02	216	4.162E+00	3.043E+01	2.806E-01	2.380E-02
174	4.789E+00	2.098E+01	2.104E-01	2.280E-02	217	4.150E+00	3.067E+01	2.823E-01	2.383E-02
175	4.771E+00	2.119E+01	2.120E-01	2.283E-02	218	4.138E+00	3.091E+01	2.840E-01	2.385E-02
176	4.753E+00	2.140E+01	2.137E-01	2.286E-02	219	4.126E+00	3.115E+01	2.857E-01	2.387E-02
177	4.735E+00	2.161E+01	2.153E-01	2.288E-02	220	4.114E+00	3.140E+01	2.874E-01	2.389E-02
178	4.717E+00	2.183E+01	2.169E-01	2.291E-02	221	4.103E+00	3.164E+01	2.891E-01	2.391E-02
179	4.699E+00	2.204E+01	2.186E-01	2.294E-02	222	4.091E+00	3.188E+01	2.908E-01	2.393E-02
180	4.682E+00	2.225E+01	2.202E-01	2.296E-02	223	4.080E+00	3.213E+01	2.925E-01	2.395E-02
181	4.665E+00	2.246E+01	2.219E-01	2.299E-02	224	4.069E+00	3.237E+01	2.942E-01	2.397E-02
182	4.648E+00	2.268E+01	2.235E-01	2.301E-02	225	4.057E+00	3.262E+01	2.959E-01	2.399E-02
183	4.631E+00	2.290E+01	2.252E-01	2.304E-02	226	4.046E+00	3.287E+01	2.976E-01	2.401E-02
184	4.615E+00	2.311E+01	2.268E-01	2.306E-02	227	4.035E+00	3.311E+01	2.993E-01	2.403E-02
185	4.598E+00	2.333E+01	2.285E-01	2.309E-02	228	4.024E+00	3.336E+01	3.010E-01	2.405E-02
186	4.582E+00	2.355E+01	2.302E-01	2.311E-02	229	4.013E+00	3.361E+01	3.027E-01	2.407E-02
187	4.566E+00	2.377E+01	2.318E-01	2.314E-02	230	4.003E+00	3.386E+01	3.044E-01	2.409E-02
188	4.550E+00	2.398E+01	2.335E-01	2.316E-02	231	3.992E+00	3.411E+01	3.061E-01	2.411E-02
189	4.534E+00	2.420E+01	2.352E-01	2.319E-02	232	3.981E+00	3.436E+01	3.078E-01	2.413E-02
190	4.519E+00	2.443E+01	2.368E-01	2.321E-02	233	3.971E+00	3.461E+01	3.095E-01	2.415E-02
191	4.503E+00	2.465E+01	2.385E-01	2.323E-02	234	3.960E+00	3.487E+01	3.112E-01	2.417E-02
192	4.488E+00	2.487E+01	2.402E-01	2.326E-02	235	3.950E+00	3.512E+01	3.129E-01	2.419E-02
193	4.473E+00	2.509E+01	2.418E-01	2.328E-02	236	3.940E+00	3.537E+01	3.146E-01	2.421E-02

ENERGY MeV	STOPPING POWER MeV $g^{-1}cm^2$	CSDA RANGE g cm^{-2}	P_{nuc}	σ^2_{MCS} rad^2	ENERGY MeV	STOPPING POWER MeV $g^{-1}cm^2$	CSDA RANGE g cm^{-2}	P_{nuc}	σ^2_{MCS} rad^2
237	3.930E+00	3.563E+01	3.163E-01	2.423E-02	244	3.861E+00	3.742E+01	3.282E-01	2.437E-02
238	3.920E+00	3.588E+01	3.180E-01	2.425E-02	245	3.852E+00	3.768E+01	3.299E-01	2.439E-02
239	3.910E+00	3.614E+01	3.197E-01	2.427E-02	246	3.842E+00	3.794E+01	3.316E-01	2.441E-02
240	3.900E+00	3.639E+01	3.214E-01	2.429E-02	247	3.833E+00	3.820E+01	3.333E-01	2.442E-02
241	3.890E+00	3.665E+01	3.231E-01	2.431E-02	248	3.823E+00	3.846E+01	3.350E-01	2.444E-02
242	3.880E+00	3.691E+01	3.248E-01	2.433E-02	249	3.814E+00	3.873E+01	3.367E-01	2.446E-02
243	3.871E+00	3.716E+01	3.265E-01	2.435E-02	250	3.805E+00	3.899E+01	3.384E-01	2.448E-02

PROTONS IN POLYSTYRENE

Density ρ [g cm^{-3}]: 1.060
Radiation Length X_0 [g cm^{-2}] 43.7911
Mean ionization energy I [eV] 68.70

COMPOSITION:

Element	H	C
Z	1	6
A	1.00794	12.01070
% by weight	0. 077418	0. 922582
I [eV]	19.20	81.00

ENERGY MeV	STOPPING POWER MeV g^{-1}cm^2	CSDA RANGE g cm^{-2}	P_{nuc}	σ^2_{MCS} rad^2	ENERGY MeV	STOPPING POWER MeV g^{-1}cm^2	CSDA RANGE g cm^{-2}	P_{nuc}	σ^2_{MCS} rad^2
1	2.576E+02	2.265E-03	0.000E+00	3.738E-03	31	1.793E+01	9.554E-01	1.535E-02	1.382E-02
2	1.571E+02	7.431E-03	0.000E+00	5.388E-03	32	1.747E+01	1.012E+00	1.641E-02	1.394E-02
3	1.160E+02	1.494E-02	0.000E+00	6.442E-03	33	1.704E+01	1.070E+00	1.749E-02	1.405E-02
4	9.302E+01	2.464E-02	0.000E+00	7.227E-03	34	1.664E+01	1.129E+00	1.857E-02	1.416E-02
5	7.816E+01	3.642E-02	0.000E+00	7.860E-03	35	1.625E+01	1.190E+00	1.967E-02	1.427E-02
6	6.769E+01	5.021E-02	0.000E+00	8.392E-03	36	1.588E+01	1.252E+00	2.078E-02	1.437E-02
7	5.989E+01	6.595E-02	2.607E-05	8.852E-03	37	1.554E+01	1.316E+00	2.189E-02	1.447E-02
8	5.382E+01	8.360E-02	9.374E-05	9.259E-03	38	1.521E+01	1.381E+00	2.301E-02	1.457E-02
9	4.897E+01	1.031E-01	1.969E-04	9.624E-03	39	1.489E+01	1.447E+00	2.414E-02	1.467E-02
10	4.498E+01	1.244E-01	3.442E-04	9.956E-03	40	1.459E+01	1.515E+00	2.527E-02	1.477E-02
11	4.164E+01	1.476E-01	5.432E-04	1.026E-02	41	1.430E+01	1.585E+00	2.641E-02	1.486E-02
12	3.881E+01	1.725E-01	8.001E-04	1.054E-02	42	1.403E+01	1.655E+00	2.755E-02	1.495E-02
13	3.637E+01	1.991E-01	1.119E-03	1.080E-02	43	1.377E+01	1.727E+00	2.870E-02	1.504E-02
14	3.424E+01	2.274E-01	1.502E-03	1.105E-02	44	1.352E+01	1.800E+00	2.986E-02	1.513E-02
15	3.238E+01	2.575E-01	1.949E-03	1.128E-02	45	1.328E+01	1.875E+00	3.101E-02	1.521E-02
16	3.072E+01	2.892E-01	2.459E-03	1.149E-02	46	1.304E+01	1.951E+00	3.218E-02	1.530E-02
17	2.924E+01	3.226E-01	3.030E-03	1.170E-02	47	1.282E+01	2.028E+00	3.334E-02	1.538E-02
18	2.791E+01	3.576E-01	3.658E-03	1.189E-02	48	1.261E+01	2.107E+00	3.451E-02	1.546E-02
19	2.670E+01	3.942E-01	4.339E-03	1.208E-02	49	1.240E+01	2.187E+00	3.568E-02	1.554E-02
20	2.561E+01	4.325E-01	5.071E-03	1.226E-02	50	1.220E+01	2.268E+00	3.685E-02	1.562E-02
21	2.461E+01	4.723E-01	5.848E-03	1.243E-02	51	1.201E+01	2.351E+00	3.803E-02	1.569E-02
22	2.370E+01	5.137E-01	6.667E-03	1.259E-02	52	1.183E+01	2.435E+00	3.921E-02	1.577E-02
23	2.285E+01	5.567E-01	7.523E-03	1.275E-02	53	1.165E+01	2.520E+00	4.040E-02	1.584E-02
24	2.208E+01	6.013E-01	8.414E-03	1.290E-02	54	1.148E+01	2.606E+00	4.159E-02	1.591E-02
25	2.135E+01	6.473E-01	9.335E-03	1.304E-02	55	1.132E+01	2.694E+00	4.278E-02	1.598E-02
26	2.068E+01	6.949E-01	1.028E-02	1.318E-02	56	1.116E+01	2.783E+00	4.397E-02	1.605E-02
27	2.006E+01	7.440E-01	1.126E-02	1.332E-02	57	1.100E+01	2.873E+00	4.517E-02	1.612E-02
28	1.947E+01	7.946E-01	1.225E-02	1.345E-02	58	1.085E+01	2.965E+00	4.637E-02	1.619E-02
29	1.893E+01	8.467E-01	1.327E-02	1.358E-02	59	1.071E+01	3.058E+00	4.757E-02	1.626E-02
30	1.841E+01	9.003E-01	1.430E-02	1.370E-02	60	1.057E+01	3.152E+00	4.878E-02	1.632E-02

ENERGY MeV	STOPPING POWER MeV g^{-1}cm^2	CSDA RANGE g cm^{-2}	P_{nuc}	σ^2_{MCS} rad^2	ENERGY MeV	STOPPING POWER MeV g^{-1}cm^2	CSDA RANGE g cm^{-2}	P_{nuc}	σ^2_{MCS} rad^2
61	1.043E+01	3.247E+00	4.999E-02	1.639E-02	103	6.983E+00	8.298E+00	1.042E-01	1.849E-02
62	1.030E+01	3.344E+00	5.120E-02	1.645E-02	104	6.933E+00	8.442E+00	1.056E-01	1.853E-02
63	1.017E+01	3.441E+00	5.242E-02	1.651E-02	105	6.884E+00	8.586E+00	1.070E-01	1.857E-02
64	1.004E+01	3.540E+00	5.364E-02	1.658E-02	106	6.836E+00	8.732E+00	1.083E-01	1.861E-02
65	9.922E+00	3.640E+00	5.486E-02	1.664E-02	107	6.789E+00	8.879E+00	1.097E-01	1.865E-02
66	9.805E+00	3.742E+00	5.609E-02	1.670E-02	108	6.743E+00	9.027E+00	1.111E-01	1.868E-02
67	9.690E+00	3.844E+00	5.732E-02	1.676E-02	109	6.697E+00	9.175E+00	1.125E-01	1.872E-02
68	9.579E+00	3.948E+00	5.855E-02	1.682E-02	110	6.652E+00	9.325E+00	1.139E-01	1.876E-02
69	9.471E+00	4.053E+00	5.979E-02	1.687E-02	111	6.608E+00	9.476E+00	1.153E-01	1.880E-02
70	9.366E+00	4.159E+00	6.103E-02	1.693E-02	112	6.565E+00	9.628E+00	1.168E-01	1.883E-02
71	9.263E+00	4.267E+00	6.227E-02	1.699E-02	113	6.522E+00	9.781E+00	1.182E-01	1.887E-02
72	9.164E+00	4.375E+00	6.352E-02	1.704E-02	114	6.480E+00	9.935E+00	1.196E-01	1.891E-02
73	9.066E+00	4.485E+00	6.477E-02	1.710E-02	115	6.439E+00	1.009E+01	1.210E-01	1.894E-02
74	8.972E+00	4.596E+00	6.603E-02	1.715E-02	116	6.399E+00	1.025E+01	1.224E-01	1.898E-02
75	8.879E+00	4.708E+00	6.729E-02	1.721E-02	117	6.359E+00	1.040E+01	1.239E-01	1.901E-02
76	8.789E+00	4.821E+00	6.855E-02	1.726E-02	118	6.320E+00	1.056E+01	1.253E-01	1.905E-02
77	8.701E+00	4.936E+00	6.982E-02	1.731E-02	119	6.281E+00	1.072E+01	1.267E-01	1.908E-02
78	8.615E+00	5.051E+00	7.109E-02	1.736E-02	120	6.243E+00	1.088E+01	1.282E-01	1.912E-02
79	8.531E+00	5.168E+00	7.236E-02	1.741E-02	121	6.206E+00	1.104E+01	1.296E-01	1.915E-02
80	8.449E+00	5.285E+00	7.364E-02	1.746E-02	122	6.169E+00	1.120E+01	1.311E-01	1.919E-02
81	8.370E+00	5.404E+00	7.493E-02	1.751E-02	123	6.133E+00	1.136E+01	1.325E-01	1.922E-02
82	8.291E+00	5.524E+00	7.621E-02	1.756E-02	124	6.097E+00	1.153E+01	1.340E-01	1.925E-02
83	8.215E+00	5.646E+00	7.750E-02	1.761E-02	125	6.062E+00	1.169E+01	1.355E-01	1.929E-02
84	8.140E+00	5.768E+00	7.880E-02	1.766E-02	126	6.027E+00	1.186E+01	1.369E-01	1.932E-02
85	8.067E+00	5.891E+00	8.010E-02	1.771E-02	127	5.993E+00	1.202E+01	1.384E-01	1.935E-02
86	7.996E+00	6.016E+00	8.140E-02	1.776E-02	128	5.960E+00	1.219E+01	1.399E-01	1.939E-02
87	7.926E+00	6.141E+00	8.271E-02	1.780E-02	129	5.927E+00	1.236E+01	1.413E-01	1.942E-02
88	7.858E+00	6.268E+00	8.402E-02	1.785E-02	130	5.894E+00	1.253E+01	1.428E-01	1.945E-02
89	7.791E+00	6.396E+00	8.534E-02	1.789E-02	131	5.862E+00	1.270E+01	1.443E-01	1.948E-02
90	7.725E+00	6.525E+00	8.666E-02	1.794E-02	132	5.830E+00	1.287E+01	1.458E-01	1.951E-02
91	7.661E+00	6.655E+00	8.798E-02	1.799E-02	133	5.799E+00	1.304E+01	1.473E-01	1.954E-02
92	7.598E+00	6.786E+00	8.931E-02	1.803E-02	134	5.768E+00	1.321E+01	1.488E-01	1.958E-02
93	7.537E+00	6.918E+00	9.064E-02	1.807E-02	135	5.738E+00	1.339E+01	1.503E-01	1.961E-02
94	7.476E+00	7.051E+00	9.198E-02	1.812E-02	136	5.708E+00	1.356E+01	1.518E-01	1.964E-02
95	7.417E+00	7.186E+00	9.332E-02	1.816E-02	137	5.679E+00	1.374E+01	1.533E-01	1.967E-02
96	7.359E+00	7.321E+00	9.466E-02	1.820E-02	138	5.649E+00	1.391E+01	1.548E-01	1.970E-02
97	7.302E+00	7.457E+00	9.601E-02	1.824E-02	139	5.621E+00	1.409E+01	1.563E-01	1.973E-02
98	7.247E+00	7.595E+00	9.737E-02	1.829E-02	140	5.593E+00	1.427E+01	1.578E-01	1.976E-02
99	7.192E+00	7.733E+00	9.872E-02	1.833E-02	141	5.565E+00	1.445E+01	1.593E-01	1.979E-02
100	7.138E+00	7.873E+00	1.001E-01	1.837E-02	142	5.537E+00	1.463E+01	1.609E-01	1.982E-02
101	7.085E+00	8.013E+00	1.015E-01	1.841E-02	143	5.510E+00	1.481E+01	1.624E-01	1.985E-02
102	7.034E+00	8.155E+00	1.028E-01	1.845E-02	144	5.483E+00	1.499E+01	1.639E-01	1.987E-02

ENERGY MeV	STOPPING POWER MeV g^{-1}cm^2	CSDA RANGE g cm^{-2}	P_{nuc}	σ^2_{MCS} rad^2	ENERGY MeV	STOPPING POWER MeV g^{-1}cm^2	CSDA RANGE g cm^{-2}	P_{nuc}	σ^2_{MCS} rad^2
145	5.457E+00	1.518E+01	1.654E-01	1.990E-02	187	4.592E+00	2.361E+01	2.320E-01	2.097E-02
146	5.431E+00	1.536E+01	1.670E-01	1.993E-02	188	4.576E+00	2.383E+01	2.337E-01	2.099E-02
147	5.405E+00	1.554E+01	1.685E-01	1.996E-02	189	4.560E+00	2.405E+01	2.353E-01	2.102E-02
148	5.379E+00	1.573E+01	1.700E-01	1.999E-02	190	4.544E+00	2.427E+01	2.369E-01	2.104E-02
149	5.354E+00	1.592E+01	1.716E-01	2.002E-02	191	4.529E+00	2.449E+01	2.385E-01	2.106E-02
150	5.329E+00	1.610E+01	1.731E-01	2.005E-02	192	4.513E+00	2.471E+01	2.402E-01	2.108E-02
151	5.305E+00	1.629E+01	1.747E-01	2.007E-02	193	4.498E+00	2.493E+01	2.418E-01	2.110E-02
152	5.281E+00	1.648E+01	1.762E-01	2.010E-02	194	4.483E+00	2.516E+01	2.435E-01	2.113E-02
153	5.257E+00	1.667E+01	1.778E-01	2.013E-02	195	4.468E+00	2.538E+01	2.451E-01	2.115E-02
154	5.233E+00	1.686E+01	1.793E-01	2.016E-02	196	4.453E+00	2.561E+01	2.467E-01	2.117E-02
155	5.210E+00	1.705E+01	1.809E-01	2.018E-02	197	4.439E+00	2.583E+01	2.484E-01	2.119E-02
156	5.187E+00	1.724E+01	1.825E-01	2.021E-02	198	4.424E+00	2.606E+01	2.500E-01	2.121E-02
157	5.164E+00	1.744E+01	1.840E-01	2.024E-02	199	4.410E+00	2.628E+01	2.517E-01	2.123E-02
158	5.142E+00	1.763E+01	1.856E-01	2.026E-02	200	4.396E+00	2.651E+01	2.533E-01	2.125E-02
159	5.120E+00	1.783E+01	1.872E-01	2.029E-02	201	4.381E+00	2.674E+01	2.550E-01	2.127E-02
160	5.098E+00	1.802E+01	1.887E-01	2.032E-02	202	4.368E+00	2.697E+01	2.566E-01	2.130E-02
161	5.076E+00	1.822E+01	1.903E-01	2.034E-02	203	4.354E+00	2.719E+01	2.583E-01	2.132E-02
162	5.055E+00	1.842E+01	1.919E-01	2.037E-02	204	4.340E+00	2.743E+01	2.599E-01	2.134E-02
163	5.034E+00	1.861E+01	1.935E-01	2.039E-02	205	4.326E+00	2.766E+01	2.616E-01	2.136E-02
164	5.013E+00	1.881E+01	1.950E-01	2.042E-02	206	4.313E+00	2.789E+01	2.632E-01	2.138E-02
165	4.992E+00	1.901E+01	1.966E-01	2.044E-02	207	4.300E+00	2.812E+01	2.649E-01	2.140E-02
166	4.972E+00	1.921E+01	1.982E-01	2.047E-02	208	4.287E+00	2.835E+01	2.665E-01	2.142E-02
167	4.952E+00	1.942E+01	1.998E-01	2.049E-02	209	4.273E+00	2.859E+01	2.682E-01	2.144E-02
168	4.932E+00	1.962E+01	2.014E-01	2.052E-02	210	4.261E+00	2.882E+01	2.698E-01	2.146E-02
169	4.912E+00	1.982E+01	2.030E-01	2.054E-02	211	4.248E+00	2.906E+01	2.715E-01	2.148E-02
170	4.893E+00	2.002E+01	2.046E-01	2.057E-02	212	4.235E+00	2.929E+01	2.731E-01	2.150E-02
171	4.873E+00	2.023E+01	2.062E-01	2.059E-02	213	4.222E+00	2.953E+01	2.748E-01	2.152E-02
172	4.854E+00	2.044E+01	2.078E-01	2.062E-02	214	4.210E+00	2.976E+01	2.764E-01	2.154E-02
173	4.835E+00	2.064E+01	2.094E-01	2.064E-02	215	4.198E+00	3.000E+01	2.781E-01	2.156E-02
174	4.817E+00	2.085E+01	2.110E-01	2.067E-02	216	4.185E+00	3.024E+01	2.798E-01	2.158E-02
175	4.798E+00	2.106E+01	2.126E-01	2.069E-02	217	4.173E+00	3.048E+01	2.814E-01	2.160E-02
176	4.780E+00	2.127E+01	2.142E-01	2.072E-02	218	4.161E+00	3.072E+01	2.831E-01	2.162E-02
177	4.762E+00	2.148E+01	2.158E-01	2.074E-02	219	4.149E+00	3.096E+01	2.847E-01	2.164E-02
178	4.744E+00	2.169E+01	2.174E-01	2.076E-02	220	4.137E+00	3.120E+01	2.864E-01	2.166E-02
179	4.727E+00	2.190E+01	2.190E-01	2.079E-02	221	4.126E+00	3.144E+01	2.881E-01	2.167E-02
180	4.709E+00	2.211E+01	2.207E-01	2.081E-02	222	4.114E+00	3.169E+01	2.897E-01	2.169E-02
181	4.692E+00	2.232E+01	2.223E-01	2.083E-02	223	4.103E+00	3.193E+01	2.914E-01	2.171E-02
182	4.675E+00	2.254E+01	2.239E-01	2.086E-02	224	4.091E+00	3.217E+01	2.930E-01	2.173E-02
183	4.658E+00	2.275E+01	2.255E-01	2.088E-02	225	4.080E+00	3.242E+01	2.947E-01	2.175E-02
184	4.641E+00	2.296E+01	2.271E-01	2.090E-02	226	4.069E+00	3.267E+01	2.964E-01	2.177E-02
185	4.625E+00	2.318E+01	2.288E-01	2.093E-02	227	4.058E+00	3.291E+01	2.980E-01	2.179E-02
186	4.608E+00	2.340E+01	2.304E-01	2.095E-02	228	4.047E+00	3.316E+01	2.997E-01	2.181E-02

ENERGY	STOPPING POWER	CSDA RANGE	P_{nuc}	σ^2_{MCS}
MeV	MeV g^{-1}cm^2	g cm^{-2}		rad^2
229	4.036E+00	3.341E+01	3.014E-01	2.182E-02
230	4.025E+00	3.365E+01	3.030E-01	2.184E-02
231	4.014E+00	3.390E+01	3.047E-01	2.186E-02
232	4.003E+00	3.415E+01	3.063E-01	2.188E-02
233	3.993E+00	3.440E+01	3.080E-01	2.190E-02
234	3.982E+00	3.465E+01	3.097E-01	2.192E-02
235	3.972E+00	3.490E+01	3.113E-01	2.193E-02
236	3.962E+00	3.516E+01	3.130E-01	2.195E-02
237	3.951E+00	3.541E+01	3.147E-01	2.197E-02
238	3.941E+00	3.566E+01	3.163E-01	2.199E-02
239	3.931E+00	3.592E+01	3.180E-01	2.201E-02
240	3.921E+00	3.617E+01	3.197E-01	2.202E-02
241	3.911E+00	3.643E+01	3.213E-01	2.204E-02
242	3.902E+00	3.668E+01	3.230E-01	2.206E-02
243	3.892E+00	3.694E+01	3.246E-01	2.208E-02
244	3.882E+00	3.720E+01	3.263E-01	2.209E-02
245	3.873E+00	3.745E+01	3.280E-01	2.211E-02
246	3.863E+00	3.771E+01	3.296E-01	2.213E-02
247	3.854E+00	3.797E+01	3.313E-01	2.214E-02
248	3.844E+00	3.823E+01	3.329E-01	2.216E-02
249	3.835E+00	3.849E+01	3.346E-01	2.218E-02
250	3.826E+00	3.875E+01	3.363E-01	2.220E-02

PROTONS IN SOLID WATER

Density ρ [g cm^{-3}]:	1.066
Radiation Length X_0 [g cm^{-2}]	42.8179
Mean ionization energy I [eV]	69.87

COMPOSITION:

Element	H	C	O	Ti
Z	1	6	8	22
A	1.00794	12.01070	15.99940	47.86700
% by weight	0.075870	0.904130	0.008010	0.011990
I [eV]	19.20	81.00	106.00	263.00

ENERGY MeV	STOPPING POWER MeV g^{-1}cm^2	CSDA RANGE g cm^{-2}	P_{nuc}	σ^2_{MCS} rad^2
1	2.558E+02	2.282E-03	0.000E+00	3.866E-03
2	1.560E+02	7.483E-03	2.029E-10	5.570E-03
3	1.153E+02	1.504E-02	4.894E-09	6.657E-03
4	9.245E+01	2.480E-02	4.569E-08	7.468E-03
5	7.770E+01	3.665E-02	2.218E-07	8.120E-03
6	6.730E+01	5.053E-02	7.796E-07	8.669E-03
7	5.955E+01	6.636E-02	2.805E-05	9.144E-03
8	5.352E+01	8.410E-02	9.757E-05	9.563E-03
9	4.870E+01	1.037E-01	2.030E-04	9.940E-03
10	4.474E+01	1.252E-01	3.528E-04	1.028E-02
11	4.142E+01	1.484E-01	5.543E-04	1.060E-02
12	3.860E+01	1.734E-01	8.134E-04	1.089E-02
13	3.618E+01	2.002E-01	1.134E-03	1.116E-02
14	3.406E+01	2.287E-01	1.519E-03	1.141E-02
15	3.221E+01	2.589E-01	1.967E-03	1.164E-02
16	3.056E+01	2.908E-01	2.478E-03	1.187E-02
17	2.909E+01	3.244E-01	3.050E-03	1.208E-02
18	2.777E+01	3.596E-01	3.678E-03	1.228E-02
19	2.657E+01	3.964E-01	4.360E-03	1.247E-02
20	2.548E+01	4.348E-01	5.091E-03	1.265E-02
22	2.358E+01	5.165E-01	6.683E-03	1.300E-02
24	2.197E+01	6.045E-01	8.427E-03	1.331E-02

ENERGY MeV	STOPPING POWER MeV g^{-1}cm^2	CSDA RANGE g cm^{-2}	P_{nuc}	σ^2_{MCS} rad^2
26	2.058E+01	6.986E-01	1.029E-02	1.361E-02
28	1.938E+01	7.988E-01	1.226E-02	1.388E-02
30	1.832E+01	9.050E-01	1.430E-02	1.414E-02
35	1.617E+01	1.196E+00	1.965E-02	1.473E-02
40	1.452E+01	1.523E+00	2.524E-02	1.524E-02
45	1.321E+01	1.884E+00	3.097E-02	1.570E-02
50	1.215E+01	2.280E+00	3.681E-02	1.611E-02
55	1.126E+01	2.707E+00	4.273E-02	1.649E-02
60	1.052E+01	3.167E+00	4.873E-02	1.684E-02
65	9.877E+00	3.658E+00	5.481E-02	1.717E-02
70	9.323E+00	4.179E+00	6.098E-02	1.747E-02
75	8.839E+00	4.730E+00	6.724E-02	1.775E-02
80	8.411E+00	5.311E+00	7.360E-02	1.802E-02
90	7.691E+00	6.556E+00	8.661E-02	1.851E-02
100	7.106E+00	7.910E+00	1.000E-01	1.895E-02
110	6.623E+00	9.369E+00	1.139E-01	1.935E-02
120	6.216E+00	1.093E+01	1.281E-01	1.972E-02
130	5.868E+00	1.259E+01	1.428E-01	2.006E-02
140	5.568E+00	1.434E+01	1.578E-01	2.038E-02
150	5.306E+00	1.618E+01	1.731E-01	2.068E-02
160	5.076E+00	1.810E+01	1.887E-01	2.096E-02
180	4.689E+00	2.221E+01	2.206E-01	2.147E-02
200	4.377E+00	2.663E+01	2.533E-01	2.192E-02

PROTONS IN TECASON PMTXRO

Density ρ [g cm^{-3}]:	1.36
Radiation Length X_0 [g cm^{-2}]	25.1294
Mean ionization energy I [eV]	285.67

COMPOSITION:

Element	H	C	O	S	Ba
Z	1	6	8	16	56
A	1.00794	12.01070	15.99940	32.06600	137.32700
% by weight	0.0298	0.5322	0. .2057	0.1030	0.1293
I [eV]	19.20	81.00	106.00	203.00	555.00

ENERGY MeV	STOPPING POWER MeV g^{-1}cm^2	CSDA RANGE g cm^{-2}	P_{nuc}	σ^2_{MCS} rad^2	ENERGY MeV	STOPPING POWER MeV g^{-1}cm^2	CSDA RANGE g cm^{-2}	P_{nuc}	σ^2_{MCS} rad^2
1	2.100E+02	2.819E-03	0.000E+00	5.798E-03	28	1.697E+01	9.194E-01	1.333E-02	2.046E-02
2	1.302E+02	9.092E-03	5.707E-14	8.466E-03	30	1.606E+01	1.041E+00	1.544E-02	2.082E-02
3	9.708E+01	1.811E-02	5.368E-11	1.006E-02	35	1.420E+01	1.372E+00	2.099E-02	2.165E-02
4	7.836E+01	2.965E-02	2.643E-09	1.125E-02	40	1.277E+01	1.744E+00	2.683E-02	2.238E-02
5	6.617E+01	4.360E-02	3.466E-08	1.219E-02	45	1.163E+01	2.155E+00	3.287E-02	2.303E-02
6	5.753E+01	5.986E-02	2.216E-07	1.299E-02	50	1.071E+01	2.604E+00	3.905E-02	2.362E-02
7	5.106E+01	7.835E-02	4.143E-05	1.367E-02	55	9.935E+00	3.089E+00	4.535E-02	2.416E-02
8	4.601E+01	9.901E-02	1.479E-04	1.428E-02	60	9.284E+00	3.610E+00	5.175E-02	2.466E-02
9	4.195E+01	1.218E-01	3.056E-04	1.482E-02	65	8.725E+00	4.166E+00	5.826E-02	2.511E-02
10	3.861E+01	1.467E-01	5.184E-04	1.531E-02	70	8.241E+00	4.756E+00	6.486E-02	2.554E-02
11	3.580E+01	1.736E-01	7.884E-04	1.576E-02	75	7.818E+00	5.379E+00	7.156E-02	2.594E-02
12	3.342E+01	2.025E-01	1.119E-03	1.618E-02	80	7.443E+00	6.034E+00	7.837E-02	2.632E-02
13	3.136E+01	2.334E-01	1.511E-03	1.656E-02	90	6.812E+00	7.441E+00	9.232E-02	2.701E-02
14	2.956E+01	2.663E-01	1.964E-03	1.692E-02	100	6.299E+00	8.969E+00	1.067E-01	2.763E-02
15	2.798E+01	3.011E-01	2.478E-03	1.726E-02	110	5.874E+00	1.061E+01	1.217E-01	2.820E-02
16	2.657E+01	3.378E-01	3.049E-03	1.758E-02	120	5.516E+00	1.237E+01	1.371E-01	2.872E-02
17	2.531E+01	3.764E-01	3.676E-03	1.789E-02	130	5.211E+00	1.424E+01	1.529E-01	2.920E-02
18	2.418E+01	4.168E-01	4.355E-03	1.817E-02	140	4.947E+00	1.621E+01	1.691E-01	2.965E-02
19	2.316E+01	4.591E-01	5.084E-03	1.845E-02	150	4.716E+00	1.828E+01	1.857E-01	3.007E-02
20	2.223E+01	5.031E-01	5.858E-03	1.871E-02	160	4.513E+00	2.045E+01	2.026E-01	3.046E-02
22	2.059E+01	5.967E-01	7.531E-03	1.920E-02	180	4.172E+00	2.506E+01	2.371E-01	3.118E-02
24	1.921E+01	6.974E-01	9.349E-03	1.965E-02	200	3.897E+00	3.003E+01	2.723E-01	3.182E-02
26	1.801E+01	8.050E-01	1.129E-02	2.006E-02					

PROTONS IN WATER

Density ρ [g cm^{-3}]: 1.00
Radiation Length X_0 [g cm^{-2}] 36.083
Mean ionization energy I [eV] 78.00

COMPOSITION:

Element	H	O
Z	1	8
A	1.00794	15.99940
% by weight	0.111900	0. 888100
I [eV]	19.20	106.00

ENERGY MeV	STOPPING POWER MeV g^{-1}cm^2	CSDA RANGE g cm^{-2}	P_{nuc}	σ^2_{MCS} rad^2
1	2.575E+02	2.265E-03	0.000E+00	4.651E-03
2	1.569E+02	7.433E-03	0.000E+00	6.694E-03
3	1.160E+02	1.495E-02	0.000E+00	7.996E-03
4	9.320E+01	2.463E-02	0.000E+00	8.965E-03
5	7.843E+01	3.638E-02	0.000E+00	9.744E-03
6	6.802E+01	5.011E-02	0.000E+00	1.040E-02
7	6.023E+01	6.577E-02	5.772E-05	1.096E-02
8	5.417E+01	8.331E-02	2.105E-04	1.146E-02
9	4.931E+01	1.027E-01	4.345E-04	1.191E-02
10	4.532E+01	1.239E-01	7.202E-04	1.232E-02
11	4.199E+01	1.468E-01	1.057E-03	1.269E-02
12	3.915E+01	1.715E-01	1.441E-03	1.303E-02
13	3.670E+01	1.979E-01	1.871E-03	1.335E-02
14	3.457E+01	2.260E-01	2.344E-03	1.365E-02
15	3.269E+01	2.557E-01	2.855E-03	1.393E-02
16	3.103E+01	2.871E-01	3.400E-03	1.420E-02
17	2.954E+01	3.202E-01	3.979E-03	1.445E-02
18	2.820E+01	3.548E-01	4.590E-03	1.469E-02
19	2.699E+01	3.911E-01	5.231E-03	1.491E-02
20	2.589E+01	4.289E-01	5.903E-03	1.513E-02
21	2.489E+01	4.683E-01	6.604E-03	1.534E-02
22	2.397E+01	5.093E-01	7.333E-03	1.554E-02
23	2.312E+01	5.518E-01	8.087E-03	1.573E-02
24	2.233E+01	5.958E-01	8.866E-03	1.591E-02
25	2.161E+01	6.413E-01	9.668E-03	1.609E-02
26	2.093E+01	6.884E-01	1.049E-02	1.626E-02
27	2.030E+01	7.369E-01	1.133E-02	1.643E-02
28	1.971E+01	7.869E-01	1.218E-02	1.659E-02
29	1.916E+01	8.383E-01	1.305E-02	1.674E-02
30	1.864E+01	8.913E-01	1.393E-02	1.689E-02
31	1.815E+01	9.456E-01	1.482E-02	1.704E-02
32	1.770E+01	1.001E+00	1.573E-02	1.718E-02
33	1.726E+01	1.059E+00	1.664E-02	1.732E-02
34	1.685E+01	1.117E+00	1.756E-02	1.745E-02
35	1.646E+01	1.177E+00	1.849E-02	1.758E-02
36	1.609E+01	1.239E+00	1.944E-02	1.771E-02
37	1.574E+01	1.302E+00	2.039E-02	1.784E-02
38	1.541E+01	1.366E+00	2.136E-02	1.796E-02
39	1.509E+01	1.431E+00	2.234E-02	1.808E-02
40	1.479E+01	1.498E+00	2.332E-02	1.819E-02
41	1.450E+01	1.567E+00	2.432E-02	1.831E-02
42	1.422E+01	1.636E+00	2.532E-02	1.842E-02
43	1.396E+01	1.707E+00	2.633E-02	1.852E-02
44	1.370E+01	1.780E+00	2.735E-02	1.863E-02
45	1.346E+01	1.853E+00	2.837E-02	1.874E-02
46	1.322E+01	1.928E+00	2.940E-02	1.884E-02
47	1.300E+01	2.005E+00	3.043E-02	1.894E-02
48	1.278E+01	2.082E+00	3.147E-02	1.904E-02
49	1.258E+01	2.161E+00	3.251E-02	1.913E-02
50	1.238E+01	2.241E+00	3.356E-02	1.923E-02
51	1.218E+01	2.323E+00	3.460E-02	1.932E-02
52	1.200E+01	2.405E+00	3.566E-02	1.941E-02
53	1.182E+01	2.489E+00	3.672E-02	1.950E-02
54	1.164E+01	2.575E+00	3.778E-02	1.959E-02
55	1.148E+01	2.661E+00	3.885E-02	1.968E-02
56	1.132E+01	2.749E+00	3.992E-02	1.976E-02
57	1.116E+01	2.838E+00	4.099E-02	1.985E-02
58	1.101E+01	2.928E+00	4.207E-02	1.993E-02
59	1.086E+01	3.020E+00	4.314E-02	2.001E-02
60	1.072E+01	3.112E+00	4.422E-02	2.009E-02
61	1.058E+01	3.206E+00	4.530E-02	2.017E-02
62	1.045E+01	3.301E+00	4.638E-02	2.025E-02
63	1.032E+01	3.398E+00	4.747E-02	2.032E-02
64	1.019E+01	3.495E+00	4.856E-02	2.040E-02
65	1.007E+01	3.594E+00	4.965E-02	2.047E-02
66	9.949E+00	3.694E+00	5.075E-02	2.055E-02

ENERGY MeV	STOPPING POWER MeV g^{-1}cm^2	CSDA RANGE g cm^{-2}	P_{nuc}	σ^2_{MCS} rad^2
67	9.834E+00	3.795E+00	5.185E-02	2.062E-02
68	9.721E+00	3.897E+00	5.295E-02	2.069E-02
69	9.612E+00	4.001E+00	5.405E-02	2.076E-02
70	9.505E+00	4.105E+00	5.516E-02	2.083E-02
71	9.402E+00	4.211E+00	5.626E-02	2.090E-02
72	9.301E+00	4.318E+00	5.738E-02	2.097E-02
73	9.202E+00	4.426E+00	5.849E-02	2.103E-02
74	9.106E+00	4.535E+00	5.961E-02	2.110E-02
75	9.013E+00	4.646E+00	6.073E-02	2.117E-02
76	8.921E+00	4.757E+00	6.186E-02	2.123E-02
77	8.832E+00	4.870E+00	6.299E-02	2.129E-02
78	8.746E+00	4.984E+00	6.412E-02	2.136E-02
79	8.661E+00	5.098E+00	6.525E-02	2.142E-02
80	8.578E+00	5.215E+00	6.639E-02	2.148E-02
81	8.497E+00	5.332E+00	6.753E-02	2.154E-02
82	8.418E+00	5.450E+00	6.868E-02	2.160E-02
83	8.341E+00	5.569E+00	6.983E-02	2.166E-02
84	8.265E+00	5.690E+00	7.099E-02	2.172E-02
85	8.191E+00	5.811E+00	7.215E-02	2.178E-02
86	8.119E+00	5.934E+00	7.332E-02	2.183E-02
87	8.048E+00	6.058E+00	7.449E-02	2.189E-02
88	7.979E+00	6.182E+00	7.567E-02	2.195E-02
89	7.911E+00	6.308E+00	7.685E-02	2.200E-02
90	7.845E+00	6.435E+00	7.803E-02	2.206E-02
91	7.780E+00	6.563E+00	7.922E-02	2.211E-02
92	7.716E+00	6.692E+00	8.042E-02	2.217E-02
93	7.654E+00	6.822E+00	8.162E-02	2.222E-02
94	7.592E+00	6.954E+00	8.283E-02	2.227E-02
95	7.533E+00	7.086E+00	8.404E-02	2.233E-02
96	7.474E+00	7.219E+00	8.527E-02	2.238E-02
97	7.416E+00	7.353E+00	8.649E-02	2.243E-02
98	7.360E+00	7.489E+00	8.773E-02	2.248E-02
99	7.304E+00	7.625E+00	8.896E-02	2.253E-02
100	7.250E+00	7.763E+00	9.021E-02	2.258E-02
101	7.197E+00	7.901E+00	9.146E-02	2.263E-02
102	7.144E+00	8.040E+00	9.271E-02	2.268E-02
103	7.093E+00	8.181E+00	9.397E-02	2.273E-02
104	7.042E+00	8.322E+00	9.524E-02	2.278E-02
105	6.993E+00	8.465E+00	9.651E-02	2.282E-02
106	6.944E+00	8.608E+00	9.779E-02	2.287E-02
107	6.896E+00	8.753E+00	9.908E-02	2.292E-02
108	6.849E+00	8.898E+00	1.004E-01	2.296E-02
109	6.803E+00	9.045E+00	1.017E-01	2.301E-02
110	6.758E+00	9.192E+00	1.030E-01	2.306E-02
111	6.713E+00	9.341E+00	1.043E-01	2.310E-02
112	6.669E+00	9.490E+00	1.056E-01	2.315E-02
113	6.626E+00	9.641E+00	1.070E-01	2.319E-02
114	6.584E+00	9.792E+00	1.083E-01	2.323E-02
115	6.542E+00	9.945E+00	1.096E-01	2.328E-02
116	6.501E+00	1.010E+01	1.110E-01	2.332E-02
117	6.460E+00	1.025E+01	1.123E-01	2.336E-02
118	6.421E+00	1.041E+01	1.137E-01	2.341E-02
119	6.382E+00	1.056E+01	1.151E-01	2.345E-02
120	6.343E+00	1.072E+01	1.164E-01	2.349E-02
121	6.305E+00	1.088E+01	1.178E-01	2.353E-02
122	6.268E+00	1.104E+01	1.192E-01	2.358E-02
123	6.231E+00	1.120E+01	1.206E-01	2.362E-02
124	6.195E+00	1.136E+01	1.220E-01	2.366E-02
125	6.160E+00	1.152E+01	1.234E-01	2.370E-02
126	6.124E+00	1.168E+01	1.248E-01	2.374E-02
127	6.090E+00	1.185E+01	1.262E-01	2.378E-02
128	6.056E+00	1.201E+01	1.276E-01	2.382E-02
129	6.022E+00	1.218E+01	1.290E-01	2.386E-02
130	5.989E+00	1.234E+01	1.305E-01	2.390E-02
131	5.957E+00	1.251E+01	1.319E-01	2.393E-02
132	5.925E+00	1.268E+01	1.333E-01	2.397E-02
133	5.893E+00	1.285E+01	1.348E-01	2.401E-02
134	5.862E+00	1.302E+01	1.362E-01	2.405E-02
135	5.831E+00	1.319E+01	1.377E-01	2.409E-02
136	5.801E+00	1.336E+01	1.392E-01	2.412E-02
137	5.771E+00	1.354E+01	1.406E-01	2.416E-02
138	5.741E+00	1.371E+01	1.421E-01	2.420E-02
139	5.712E+00	1.388E+01	1.436E-01	2.423E-02
140	5.684E+00	1.406E+01	1.450E-01	2.427E-02
141	5.655E+00	1.424E+01	1.465E-01	2.431E-02
142	5.627E+00	1.441E+01	1.480E-01	2.434E-02
143	5.600E+00	1.459E+01	1.495E-01	2.438E-02
144	5.573E+00	1.477E+01	1.510E-01	2.441E-02
145	5.546E+00	1.495E+01	1.525E-01	2.445E-02
146	5.519E+00	1.513E+01	1.540E-01	2.448E-02
147	5.493E+00	1.531E+01	1.555E-01	2.452E-02
148	5.468E+00	1.549E+01	1.571E-01	2.455E-02
149	5.442E+00	1.568E+01	1.586E-01	2.459E-02
150	5.417E+00	1.586E+01	1.601E-01	2.462E-02
151	5.392E+00	1.605E+01	1.616E-01	2.465E-02
152	5.368E+00	1.623E+01	1.632E-01	2.469E-02
153	5.343E+00	1.642E+01	1.647E-01	2.472E-02
154	5.320E+00	1.661E+01	1.663E-01	2.475E-02

ENERGY MeV	STOPPING POWER MeV g^{-1}cm^2	CSDA RANGE g cm^{-2}	P_{nuc}	σ^2_{MCS} rad^2
155	5.296E+00	1.680E+01	1.678E-01	2.479E-02
156	5.273E+00	1.698E+01	1.694E-01	2.482E-02
157	5.250E+00	1.717E+01	1.709E-01	2.485E-02
158	5.227E+00	1.737E+01	1.725E-01	2.488E-02
159	5.204E+00	1.756E+01	1.740E-01	2.492E-02
160	5.182E+00	1.775E+01	1.756E-01	2.495E-02
161	5.160E+00	1.794E+01	1.772E-01	2.498E-02
162	5.139E+00	1.814E+01	1.788E-01	2.501E-02
163	5.117E+00	1.833E+01	1.803E-01	2.504E-02
164	5.096E+00	1.853E+01	1.819E-01	2.507E-02
165	5.075E+00	1.873E+01	1.835E-01	2.511E-02
166	5.054E+00	1.892E+01	1.851E-01	2.514E-02
167	5.034E+00	1.912E+01	1.867E-01	2.517E-02
168	5.014E+00	1.932E+01	1.883E-01	2.520E-02
169	4.994E+00	1.952E+01	1.899E-01	2.523E-02
170	4.974E+00	1.972E+01	1.915E-01	2.526E-02
171	4.954E+00	1.992E+01	1.931E-01	2.529E-02
172	4.935E+00	2.012E+01	1.947E-01	2.532E-02
173	4.916E+00	2.033E+01	1.963E-01	2.535E-02
174	4.897E+00	2.053E+01	1.979E-01	2.538E-02
175	4.878E+00	2.074E+01	1.995E-01	2.541E-02
176	4.860E+00	2.094E+01	2.011E-01	2.543E-02
177	4.842E+00	2.115E+01	2.028E-01	2.546E-02
178	4.824E+00	2.135E+01	2.044E-01	2.549E-02
179	4.806E+00	2.156E+01	2.060E-01	2.552E-02
180	4.788E+00	2.177E+01	2.076E-01	2.555E-02
181	4.770E+00	2.198E+01	2.093E-01	2.558E-02
182	4.753E+00	2.219E+01	2.109E-01	2.561E-02
183	4.736E+00	2.240E+01	2.126E-01	2.563E-02
184	4.719E+00	2.261E+01	2.142E-01	2.566E-02
185	4.702E+00	2.282E+01	2.158E-01	2.569E-02
186	4.686E+00	2.304E+01	2.175E-01	2.572E-02
187	4.669E+00	2.325E+01	2.191E-01	2.574E-02
188	4.653E+00	2.347E+01	2.208E-01	2.577E-02
189	4.637E+00	2.368E+01	2.224E-01	2.580E-02
190	4.621E+00	2.390E+01	2.241E-01	2.583E-02
191	4.605E+00	2.411E+01	2.257E-01	2.585E-02
192	4.589E+00	2.433E+01	2.274E-01	2.588E-02
193	4.574E+00	2.455E+01	2.291E-01	2.591E-02
194	4.559E+00	2.477E+01	2.307E-01	2.593E-02
195	4.544E+00	2.499E+01	2.324E-01	2.596E-02
196	4.529E+00	2.521E+01	2.341E-01	2.599E-02
197	4.514E+00	2.543E+01	2.357E-01	2.601E-02
198	4.499E+00	2.565E+01	2.374E-01	2.604E-02
199	4.484E+00	2.587E+01	2.391E-01	2.606E-02
200	4.470E+00	2.610E+01	2.407E-01	2.609E-02
201	4.456E+00	2.632E+01	2.424E-01	2.611E-02
202	4.441E+00	2.655E+01	2.441E-01	2.614E-02
203	4.427E+00	2.677E+01	2.458E-01	2.617E-02
204	4.414E+00	2.700E+01	2.475E-01	2.619E-02
205	4.400E+00	2.723E+01	2.491E-01	2.622E-02
206	4.386E+00	2.745E+01	2.508E-01	2.624E-02
207	4.373E+00	2.768E+01	2.525E-01	2.627E-02
208	4.359E+00	2.791E+01	2.542E-01	2.629E-02
209	4.346E+00	2.814E+01	2.559E-01	2.631E-02
210	4.333E+00	2.837E+01	2.576E-01	2.634E-02
211	4.320E+00	2.860E+01	2.593E-01	2.636E-02
212	4.307E+00	2.883E+01	2.610E-01	2.639E-02
213	4.294E+00	2.907E+01	2.627E-01	2.641E-02
214	4.282E+00	2.930E+01	2.643E-01	2.644E-02
215	4.269E+00	2.953E+01	2.660E-01	2.646E-02
216	4.257E+00	2.977E+01	2.677E-01	2.648E-02
217	4.244E+00	3.000E+01	2.694E-01	2.651E-02
218	4.232E+00	3.024E+01	2.711E-01	2.653E-02
219	4.220E+00	3.048E+01	2.728E-01	2.655E-02
220	4.208E+00	3.071E+01	2.745E-01	2.658E-02
221	4.196E+00	3.095E+01	2.762E-01	2.660E-02
222	4.184E+00	3.119E+01	2.779E-01	2.662E-02
223	4.173E+00	3.143E+01	2.796E-01	2.665E-02
224	4.161E+00	3.167E+01	2.813E-01	2.667E-02
225	4.150E+00	3.191E+01	2.830E-01	2.669E-02
226	4.138E+00	3.215E+01	2.847E-01	2.672E-02
227	4.127E+00	3.239E+01	2.864E-01	2.674E-02
228	4.116E+00	3.264E+01	2.882E-01	2.676E-02
229	4.105E+00	3.288E+01	2.899E-01	2.678E-02
230	4.094E+00	3.312E+01	2.916E-01	2.681E-02
231	4.083E+00	3.337E+01	2.933E-01	2.683E-02
232	4.072E+00	3.361E+01	2.950E-01	2.685E-02
233	4.061E+00	3.386E+01	2.967E-01	2.687E-02
234	4.051E+00	3.410E+01	2.984E-01	2.689E-02
235	4.040E+00	3.435E+01	3.001E-01	2.692E-02
236	4.030E+00	3.460E+01	3.018E-01	2.694E-02
237	4.019E+00	3.485E+01	3.035E-01	2.696E-02
238	4.009E+00	3.510E+01	3.052E-01	2.698E-02
239	3.999E+00	3.535E+01	3.069E-01	2.700E-02
240	3.989E+00	3.560E+01	3.086E-01	2.702E-02
241	3.979E+00	3.585E+01	3.104E-01	2.705E-02
242	3.969E+00	3.610E+01	3.121E-01	2.707E-02

ENERGY MeV	STOPPING POWER MeV $g^{-1}cm^2$	CSDA RANGE g cm^{-2}	P_{nuc}	σ^2_{MCS} rad^2
243	3.959E+00	3.635E+01	3.138E-01	2.709E-02
244	3.949E+00	3.661E+01	3.155E-01	2.711E-02
245	3.939E+00	3.686E+01	3.172E-01	2.713E-02
246	3.930E+00	3.711E+01	3.189E-01	2.715E-02
247	3.920E+00	3.737E+01	3.206E-01	2.717E-02
248	3.911E+00	3.762E+01	3.223E-01	2.719E-02
249	3.901E+00	3.788E+01	3.240E-01	2.721E-02
250	3.892E+00	3.814E+01	3.257E-01	2.723E-02